Inaugural-Dissertation

zur

Erlangung der Doktorwürde

der

naturwissenschaftlich-mathematischen

Gesamtfakultät

der

Ruprecht-Karls-Universität

Heidelberg

vorgelegt von

Dipl.-Math. Jan-Philip Schmidt

aus Saarbrücken - Deutschland

Betreuer: Prof. Dr. Dr. h.c. mult Willi Jäger

Tag der mündlichen Prüfung:

An analysis of age-related alterations in functional memory networks

In memory of my father

Contents

Abstract

The human brain is the most complex organ of the human body and many aspects of its functioning have not yet been understood. One of the most fascinating abilities of the human brain is the skill to store and retrieve information, which is what we refer to as memory. One attempt to get a deeper insight into the functioning of memory is to analyze the complex activity pattern of the human brain that emerges while a memory task is being processed. The understanding of memory is epistemologically very intriguing since it is this ability that enables us to collect, to store and to recall ideas, emotions and thoughts - hence, it builds our own identity. This thesis analyzes age-related changes in functional connectivity networks related to episodic and working memory processing. The data for this study were measured using fMRI technique and the sample set consisted of healthy individuals aging from 20 up to over 80 years. Based on the fMRI data we construct correlation networks by correlating pairwisely the measured voxel activity, the nodes of the network being brain voxels, the edges being correlations. These networks are thresholded, anatomically clustered and analyzed by computing statistical network measures, using spectral methods, computing network entropy and calculating persistent homology. The main findings are: elderly individuals exhibit expanded neural networks with less differentiation between episodic and working memory tasks. However, we observe compensatory mechanisms that accompany this dedifferentiaon process. Network synchronizability is higher for elderly individuals. Network entropy increases as well with age, yielding a lower network vulnerability for elderly individuals. Aging processes leave traces in the homology pattern of the networks, whereas all brain networks exhibit different persistent homology features.

Zusammenfassung

Das Gehirn ist das komplexeste Organ des menschlichen Körpers und viele funktionale Aspekte sind noch unverstanden. Eine der faszinierendsten Fähigkeiten des Gehirns ist das Vermögen, Informationen zu speichern und abzurufen. Eine Möglichkeit, tiefere Einblicke in die Funktionsweise des Gedächtnisses zu erhalten, ist die Untersuchung der Aktivitätsmuster im menschlichen Gehirn während einer Gedächtnisaufgabe. Das Verstehen der Gedächtnisleistung ist epistemologisch sehr interessant, da es genau diese Eigenschaft ist, die es uns ermöglicht, Ideen, Gefühle und Gedanken aufzunehmen, zu speichern und wieder abzurufen - folglich bestimmt sie unsere Identität. Die vorliegende Arbeit untersucht altersabhängige Veränderungen in funktionalen Konnektivitätsnetzwerken, speziell für das episodische und das Arbeitsgedächtnis. Die Daten für diese Studie wurden mittels fMRI Methode gemessen, die Stichprobe bestand aus gesunden Individuen im Alter zwischen 20 und 80 Jahren. Ausgehend von den fMRI Daten konstruieren wir Korrelationsnetzwerke mittels paarweiser Korrelation der gemessenen Voxel-Aktivitäten. Knoten im Netzwerk sind Voxel, Kanten sind Korrelationen. Für diese Korrelations-Netzwerke setzen wir einen Schwellenwert und clustern sie mittels anatomischer Information. Diese geclusterten Netzwerke charakterisieren wir durch netzwerktheoretische Parameter, verwenden spektral-theoretische Methoden und berechnen Netzwerk-Entropie sowie Homologie. Die Hauptergebnisse sind: ältere Individuen weisen größere Netzwerke auf, bei gleichzeitig reduzierter Differenzierung zwischen Arbeits- und episodischem Gedächtnis. Jedoch beobachten wir kompensatorische Mechanismen, die diesen De-Differenzierungsprozess begleiten. Die Synchronisierbarkeit der Netzwerke ist höher bei älteren Individuen. Die Netzwerk-Entropie nimmt ebenfalls mit dem Alter zu, was zur Folge hat, dass ältere Individuen eine geringere Netzwerk-Anfälligkeit aufweisen. Alterungsprozesse verändern das Homologie-Muster der Netzwerke, wobei alle Netzwerke unterschiedliche Homologie-Eigenschaften aufweisen.

Chapter 1

Introduction

Motivation and goals. The human brain is the most complex organ of the human body and many aspects of its functioning have not yet been understood. One of the most fascinating abilities of the human brain is the skill to store and retrieve information, which is what we refer to as memory. The understanding of memory is philsophically very intriguing since it is this ability that enables us to collect, to store and to recall ideas, emotions and thoughts - hence, it builds our own identity. One attempt to get a deeper insight into the functioning of memory is to analyze the complex activity pattern of the human brain that emerges while a memory task is being processed. This thesis analyzes activity patterns that are associated with memory processes. More precisely, experimental fMRI[1] data is analyzed by generating correlation networks which are then mathematically characterized. The data has been collected from young and elderly individuals and it will be a major concern how to discriminate the networks associated to young and elderly individuals, respectively.

The **primary goal** of this thesis is to obtain a deeper insight into the functioning of memory with respect to changes caused by aging. In particular, this thesis aims at mathematically characterizing functional brain correlation networks of young and elderly individuals, which are related to both short-term and long-term memory.

We hope that the results of our analysis will enrich the knowledge about age-related changes of memory processing and, in future, will be beneficial for the analysis of pathological processes such as Alzheimer disease or dementia.

[1] fMRI = functional magnetic resonance imaging

From the experimental raw data we will generate correlation networks, and a **secondary goal** of this thesis is to consider the functional brain networks as a particular representative of the general class of correlation networks. We will analyze the brain networks using persistent homology. To our knowledge, this is the first study applying this method to correlation networks.

We expect that the methods used in our analysis, that is particularly the application of persistent homology, will contribute to a better understanding of the general class of correlation networks. Moreover, we hope that the application of this method to brain networks will help to evaluate the appropriateness of this technique, in general.

State-of-the-art. It is commonly accepted that the memory processing deteriorates with age, even for otherwise healthy individuals. The underlying processes, and the changes over the lifespan, however, are frequently studied but poorly understood. Normal aging is associated with a deterioration of the cognitive functioning, and numerous studies highlight impairments especially for the working and episodic memory in elderly individuals, cf. [Gra08]. Working memory performance, reflecting the capability to simultaneously maintain and manipulate online information, cf. [Bad10], has shown to decrease with age both in terms of processing speed and accuracy.

Imaging techniques, such as fMRI, give clues as to which brain areas are involved in these processes and to the amount they are active during a given memory task in individuals of different age. Neuroimaging studies provide evidence for both over- and under-activation in brain regions that are important for memory tasks (for a review see [PNL+06]). Under-activation seems to be related to reduced performance and pathological impairment, whereas over-activation is seen as an indication for reorganization of the older brain and plays a compensatory role. Of course, the brain experiences anatomical and physiological changes during aging, see supplement chapter on biological background.

There are several network theoretic approaches to brain data, depending on how the brain data has been measured, e.g. fMRI or MEG etc. For a review on the different measurement and construction techniques, see [BS09]. A common approach is to generate models of the so-called functional connectivity: nodes of the network are defined as brain regions, an edge between two nodes is constructed if their respective

correlation pattern exceeds a predefined threshold. This is the approach presented in [ECS+05], which we will also follow, see chapter 2. Most studies about fMRI data used a seed voxel approach which is based on a hypothesis concerning a particular brain region. There have previously been studies analyzing functional connectivity, mostly using resting state data. For reference, see for example [MAB09], [SR07], [STE00] or [SJS06].

We used the network construction method presented in [ECS+05]. Our approach is explorative and completely hypotheses-free. To our knowledge, this is the first study analyzing functional connectivity related to memory experiments and age differences, simultaneously. Our results extend seed-based and BOLD-signal intensity focused studies, and support present hypotheses like compensation and dedifferentiation.

Spectral analysis of graphs has a long tradition, cf. [Chu97] or [GR01], and the application of these methods to real-world networks has been presented in [BJc], [BJa] or [Jos07]. Network entropy and network synchronizability as well have been previously studied. We will adapt these methods to our situation and compute spectral plots, network synchronizability and network entropy. Again, to our knowledge, these methods have not been applied before to brain functional networks. As we will see, these tools provide appropriate means for our purpose of characterizing the functional memory networks.

Algebraic topology has a long tradition within mathematics, but its application to real-world problems is quite novel: persistent homology has been introduced by Edelsbrunner (2002), [ELZ02] and Zomorodian (2005), [ZC05] and has been applied to networks in [HMR09]. We will embed the functional memory networks into an appropriate filtered simplicial complex. It can be shown that persistent homology of a filtered simplicial complex is equivalent to the standard homology of a particular graded module over a polynomial ring, cf. [ZC05], which makes it computational accessible. However, again to our knowledge, these topological methods have not yet been applied before to correlation networks in general, and to functional connectivity networks in particular. We will restate the methods and adapt them to our situation.

Results. The fMRI raw data was recorded for young and senior subjects during two different memory paradigms. We generated networks of functional connectivity by pair-

wise correlation of the BOLD signal for every pair of voxels, similarly to [ECS+05] and by thresholding the correlation values, we obtained binarized graphs. We analyzed the largest connected component of this graph by means of statistical network tools. This analysis revealed that senior individuals exhibit expanded functional neural networks with less differentiation between episodic and working memory demands, see chapter 4. We then clustered these networks using anatomical information provided by the MNI Talairach atlas. The clustering was performed at different anatomical levels: lobe structures, Gyri structures and Brodmann areas, see supplement chapter for a list of abbreviations and atlas information. The clustered networks were then averaged over the whole statistical sample, for the two age groups and two memory tasks, separately. These anatomically clustered and statistically averaged networks were visualized:

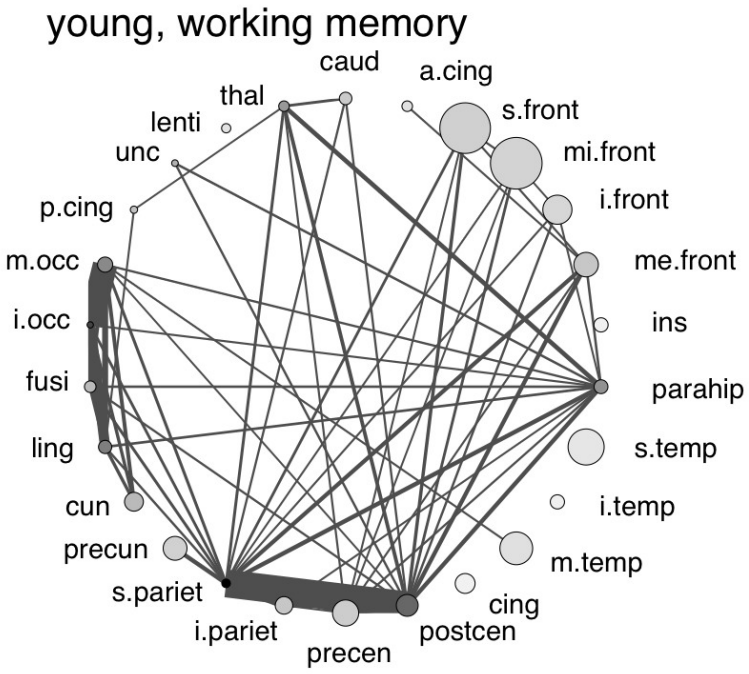

Fig. 1.1: Example of a network visualization, here: working memory network for young individuals at gyri level. Size of the nodes is proportional to the size of the anatomical region, the line thickness indicates the strength of the connection, and the shading of the nodes represents the density of the intraregional connections (dark = high intensity, bright = low intensity). See supplement chapter for a list of abbreviations.

We identified so-called hubs in the anatomically clustered networks, i.e. nodes for which the product of their degree and their betweenness is large. We observed asymmetric

compensatory mechanisms, mainly in fronto-parietal regions, see chapter 4. From now on, we will keep the anatomically clustered and averaged networks in the further analysis.

We computed the spectrum of the normalized discrete Laplacian operator

$$\Delta v(i) \;:=\; v(i) - \frac{1}{n_i} \sum_{j, i \sim j} v(j)$$

which is defined on the space $L^2(\Gamma)$ of all real-valued functions on the finite set of nodes of the network Γ, see chapter 3. This operator is the discrete analog of the well-known continuous Laplacian and can intuitively be motivated by discretizing a diffusion process defined on the network. The spectrum of this operator contains a lot of information about the underlying network structure. We used the ratio $\frac{\lambda_2}{\lambda_{max}}$ to gauge the synchronizability (w.r.t. to a broad class of functions, see chapter 3) of the networks, yielding higher synchronizability for the networks of elderly individuals. We convoluted the Dirac delta function $\sum_k \delta(\lambda, \lambda_k)$ (i.e. the spectral density of our operator) with a smooth kernel $g(x, \lambda)$ and plot the resulting density function

$$f(x) = \int g(x,) \sum_k \delta(\lambda, \lambda_k) d\lambda = \sum_k g(x, \lambda_k) \, .$$

This allows for an amenable visualization of the spectrum. This method of spectral plots has been introduced by Jost in [BJ07] and aims at being a coarse classifier of real-world networks. Our results fit well into the classification scheme presented in [BJ07], yet defining a new sub-class. We quantified the structural differences using a metric based on the Jenson-Shannon divergence measure $D(\Gamma_1, \Gamma_2) \;:=\; \sqrt{JS(f_1, f_2)}$.

We computed network entropy in order to gauge network disorder and vulnerability. To do so, we assumed the brain functional networks to be a result of a diffusive process and linked dynamical uncertainty to random walks on the network, hence allowing for a stochastic description of macroscopic properties. We adapted the entropy notion presented in [DGO04], [MDV04], i.e. based on the variational principle

$$\log \lambda = \sup_P \Big[- \sum_{i,j} \pi_i p_{ij} \log p_{ij} + \sum_{i,j} \pi_i p_{i,j} \log a_{ij} \Big]$$

with respect to all compatible stochastic processes $P = (p_{ij})$. We computed the entropy for all networks, yielding an increase of the network entropy with age:

$$H(\Gamma_{old}) > H(\Gamma_{young})$$

Together with the entropy-fluctuation theorem, cf. chapter 3, we can formulate the following statement:

Statement: We postulate that life-long learning, i.e. neural rewiring, describes a process to ever increasing entropy for the brain connectivity patterns. In other words, older networks are *noisier* than younger ones. On a physiological level, old networks are much more vulnerable in terms of cell defects (e.g. increased oxidative stress) but this vulnerability is much better accepted by high-entropy networks. Hence, neural aging can be described as an evolution to evolvability.

We computed persistent homology of the clustered networks, which provides a very sensitive method to detect topological properties. We embedded the network into an appropriate filtered simplicial complex K,

$$\emptyset = K_0 \subset K_1 \subset ... \subset K_l \subset ... \subset K_n = K\,,$$

see chapter 4 for an exact definition of our chosen filtration. The choice of the filtration algorithm remains to some extent arbitrary since there is no canonical evolution process in the context of correlation networks. However, we believe that this does not reduce the power of this method since we are interested in the global topological pattern of the networks, and the benefit of persistent homology is that it filters out topological *noise*, keeping only relevant information. Hence, it should not be important which filtration one chooses because unimportant topological information will disappear due to the method. We computed the p-persistent kth homology group of K^l

$$H_k^{l,p} := Z_k^l \Big/ \Big(B_k^{l+p} \cap Z_k^l \Big).$$

whereas $0 \leq l \leq p \leq n$. More precisely, we are interested in the rank of $H_k^{l,p}$, i.e. in the p-persistent kth Betti number:

$$\beta_k^{l+p} := \text{rank } H_k^{l,p}\,.$$

Hence, for each possible pair of parameters (l, p) one obtains a Betti number and all this information is optimally grasped visually, in so-called *homology barcodes* as suggested in [CZCG05] and [HMR09]. We used this approach and visualized the homological information, see chapter 3 for a detailed explanation and chapter 4 for the results.

Computing persistent homology is about detecting *long-lived* topological features, i.e. homology classes that survive a certain number of filtration steps. *Short-lived* topological features disappear faster and can be considered as *noise*. A persistent homology class in a higher dimension can be interpreted in such a way that, during its existence in the filtration, informational flow needs to circumvent this *obstacle* in order to reach the target. This obstacle is a higher-dimensional topological structure in the connectivity pattern of the network. All brain networks show very different persistent homology features. We formulate the most intriguing result as a statement:

Statement: aging processes leave traces in the homology pattern of the networks. For example, comparing Fig. 4.13 and Fig. 4.17, i.e. the homology barcode plot for working memory networks of elderly and young individuals, respectively, we see that young individuals already achieve a topological ***Swiss Cheese*** pattern at weak links ($\theta = 0.2$), whereas almost the same pattern appears for the seniors only at stronger links ($\theta = 0.4$). Assuming that the working memory for young individuals works better in terms of reliability and efficiency, i.e. defines a benchmark, we can deduce from the homology analysis that elderly individuals compensate this by over-activating, producing some topological noise as a side effect. We use the informal notion *Swiss Cheese* to refer to the homological pattern which exhibits non-vanishing homology up to high dimension. The non-vanishing homology can be interpreted as higher-dimensional *holes* or *voids* in the connectivity pattern.

This compelling result could not have been deduced only by means of statistical or spectral methods. Hence, we believe that persistent homology provides a very powerful tool for the analysis of functional connectivity correlation networks.

Chapter organization. This thesis is organized in five chapters and one supplementary chapter: chapter two thoroughly explains the data acquisition and the construction of the functional brain networks. Chapter three contains the mathematical methods which we used in our analysis, these comprise spectral analysis tools, network entropy as well as persistent homology. In chapter four we present our results as well as the discussion of the findings. Chapter 5 gives a short outlook on possible future research, and the supplementary chapter contains basic material on network analysis, on the biological background as well as a list of anatomical abbreviations.

Acknowledgements. First and foremost, I would like to express my gratitude to Prof. Dr. Dr. Willi Jäger for offering me the possibility to work on such a fascinating research topic, for guiding me through this project as well as for the inspiring discussions on general topics. I would like to specially thank Dr. Franziska Matthäus for mentoring this project, for fruitful discussions and for technical support as well as for always finding some time to advise me. I would also thank Dr. Carsten Diener, Dr. Traute Demirakca and their workgroup at the Central Institute for Mental Health (Mannheim) for their outstanding commitment and support. Without their experimental work this thesis would not have been possible. Moreover, I specially thank Traute, Franziska and Carsten for the very stimulating discussions about the interpretation of the results. This thesis was inspired by their concepts. I would also thank Dr. Anirban Banerjee, Dr. Milan Rajkovic, Dr. Thomas Manke and Danijela Horak for giving me advice and for fruitful discussions, which we had in Israel, Slovenia, Berlin and Leipzig. Moreover, I would like to thank Prof. Dr. Rainer Weissauer for always inspiring me and giving me advice on life in general. The financial support from the Heidelberg Academy of Sciences in the framework of the WIN-Kolleg has been acknowledged.

Heidelberg, May 2012
Jan-Philip Schmidt

Chapter 2

Experimental design and data modeling

2.1 Data acquisition and experimental paradigm

The data that was used for this thesis consisted of fMRI experiment data from a total of 20 subjects of two age groups, cf. table (2.1). All participants were healthy volunteers and showed no history of psychiatric or neurological disease. All subjects provided written informed consent for the participation in the study. The study was approved by the Ethics Committee of the Clinical Faculty of the University of Heidelberg, Germany, and the functional MRI experiments were conducted at the Central Institute for Mental Health in Mannheim, Germany.

Group	**Mean age**	**std. deviation**	**minimum**	**maximum**	**females/males**
YOUNG	26.3 yrs	±2.65	21 yrs	30 yrs	6/4
OLD	67.8 yrs	±3.99	62 yrs	77 yrs	6/4

Table 2.1: Age and gender statistics for the two age groups, see also [MSB$^+$12].

Each participant completed functional MRI scanning sessions comprising 470 scans, which were acquired using an echo planar imaging (EPI) sequence. The functional MRI was performed on a 3 Tesla TIM TRO Scanner (Siemens, Erlangen, Germany). Each volume consisted of 24 axial slices of 4 mm thickness (1 mm gap), TR 2 s, FOV

220×220mm2, 642 matrix and was angulated along the AC-PC plane. The first 5 volumes of each run were discarded to minimize T1 effects. Data pre-processing of BOLD signal was performed using SPM5 (Wellcome Department of Cognitive Neurology; `http://www.fil.ion.ucl.ac.uk/spm/software/spm5`), involving realignment to the first image which accommodates geometrical displacements due to head movements, non-brain removal and normalization to the standard template brain (Montreal Neurological Institute, MNI) using an affine transform implemented in SPM software. SPM software was further used to downscale the data volume by interpolating to a final resolution of $6 \times 6 \times 6$ mm voxel size. This resulted in three dimensional images with 27 voxel in x-direction, 33 voxel in y-direction and 23 voxel in z-direction. Spatial smoothing using a Gaussian kernel has deliberately not been done.

The stimuli were presented using a block design, involving two tasks that are supposed to address both the episodic and working memory, respectively. Two sets of 20 words representing personal, i.e. autobiographic, and non-personal events were used as visually presented stimuli, whereas the list of autobiographic events was conducted via a psychological interview and the non-personal events were selected by the subjects from a presented list of possible words. The stimuli were presented in black letters on light-gray background and all the 40 words were used as stimuli for 2 different tasks:

- The working memory task was build as a two-back-task. Subjects were asked to decide if the actual word is identical with the penultimate word. The response was conveyed through a button press, the index-finger represented the answer "yes", and the middle-finger represented the answer "no".
- The long-term memory task, i.e. the autobiographic memory task, consisted of remembering the personal event as intense as possible, for example recalling all persons which joined these events and the characteristics of the environment.

The stimuli were presented in a block design, whereas each block addressed solely the short-term and long-term memory task, respectively. Within each block, each stimulus was being presented for 2 seconds and during the inter-stimulus interval, which lasted 6 seconds, a fixation cross was presented. Each block had a length of 40 seconds and was preceded by the corresponding task instruction. During the autobiographical task 5 words per block were presented. For the two-back-task 10 words were used, implying an inter-stimulus interval of 2 seconds in this case. Each task was presented 4 times in random order.

2.2 Network construction

When dealing with networks, it is always of utmost importance that nodes and links, which are abstracted from the underlying real-world system, are precisely defined, see also supplementary chapter for reference. In this thesis, as already mentioned previously, functional connectivity networks are being investigated. These networks have been constructed using the same approach as [ECS+05].

In short, the nodes of the networks are defined as the voxels, i.e. the small cubical brain sites into which the brain volume has been subdivided, and an edge between two nodes is constructed if and only if the corresponding fMRI time series show a statistical correlation that exceeds some predefined threshold.

The remaining part of this section will explain the network construction in detail and will give a detailed account of the threshold selection.

(1.) For each participant, the fMRI time series were cut into sections according to the block-design in order to separate episodic and working memory task signal. The resulting pieces were re-concatenated in such a way that two time series were obtained, each containing purely episodic and working memory signal, respectively. Hence, for each participant two networks were constructed, based on the episodic and working memory data, respectively.

(2.) The chosen fMRI resolution yields a total amount of $27 \times 33 \times 23 = 20493$ voxels, at this stage still containing non-brain volume. By using fMRI signal intensity thresholding, non-brain volume has been removed, resulting in an amount of ~ 2000 voxels per each participant, which were then considered as the nodes of the network.

(3.) Each such set of extracted voxels defines the set of nodes of the corresponding functional network, which is still unconnected at this stage. For each pair of voxels $(\mathbf{x_1}, \mathbf{x_2})$ the Pearson correlation coefficient of the corresponding time series was computed:

$$r(\mathbf{x_1}, \mathbf{x_2}) = \frac{\langle V(\mathbf{x_1}, t) V(\mathbf{x_2}, t) \rangle - \langle V(\mathbf{x_1}, t) \rangle \langle V(\mathbf{x_2}, t) \rangle}{\sigma(V(\mathbf{x_1}))\, \sigma(V(\mathbf{x_2}))}$$

whereas $\mathbf{x_i} = (x_i, y_i, z_i)$ denotes a voxel, $\sigma^2(V((\mathbf{x})) = \langle V(\mathbf{x}, t)^2 \rangle - \langle V(\mathbf{x}, t) \rangle^2$ and $\langle \cdot \rangle$ are temporal averages, cf. [ECS+05]. This yields a square correlation matrix of size $n =\sim 2000$ for each participant and each memory task.

(4.) The resulting correlation matrices have been globally thresholded at a value $r_c = 0.85$, yielding a binary matrix for each correlation matrix. That means, if the correlation coefficient for a given pair of nodes exceeded a threshold r_c, the nodes were considered as connected. The entirety of all nodes and edges then defined a large network characterizing the functional connectivity of the brain during the given memory task. The threshold selection is being discussed subsequently.

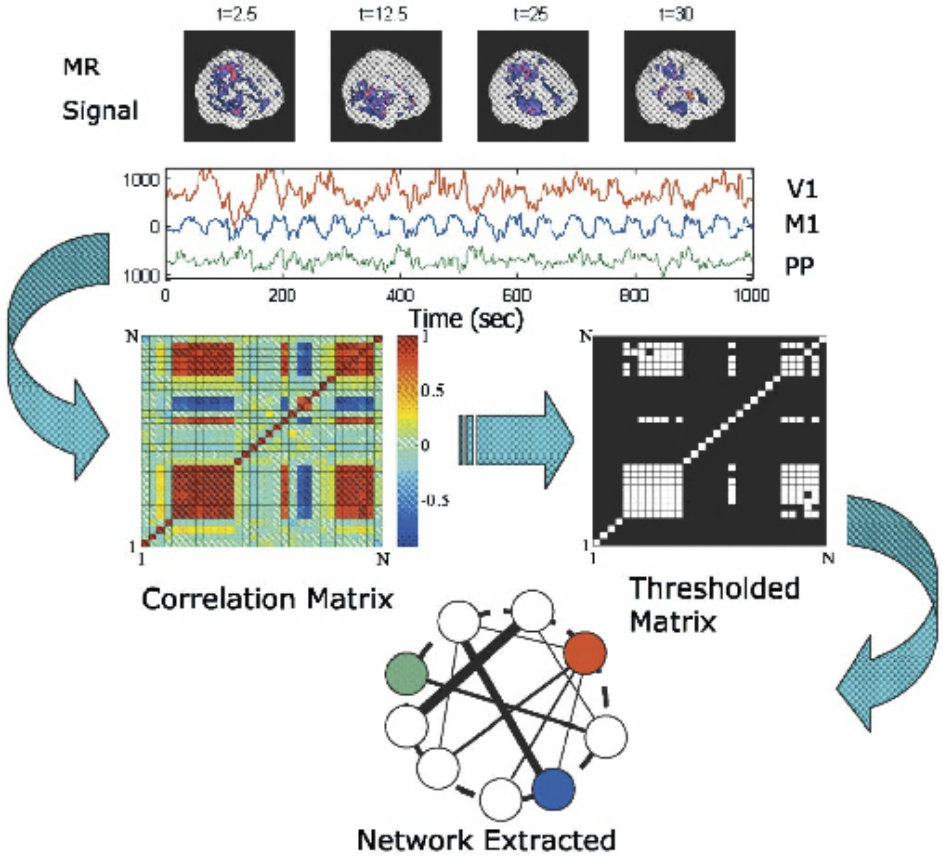

Fig. 2.1: Methodology used to extract functional networks from fMRI timeseries signal. Copyright: *Eguiluz et al.* [ECS+05]

Threshold selection. The choice of the threshold value r_c is a very important step in the generation procedure of the functional network. The correlation threshold can be considered as a filter that separates more relevant from less relevant information. A high threshold value yields a very specific network, whereas a low threshold value will eventually include too much noise.

Fig. 2.2: Schematic of functional network visualization for increasing threshold values, *Achard et al.* [ASW$^+$06].

Networks obtained for low threshold values are furthermore very dense (i.e. contain many links), which makes many statistical analyses computationally expensive. This yields a conflict of interest: the correlation threshold is required to be high enough to make computational analyses efficient, but being simultaneously low enough in order not to loose relevant structural information. This problem has been solved by systematically varying the correlation threshold in the range between 0.6 and 0.95 and computing the most important network parameters (e.g. the largest connected component, the average clustering coefficient) for these differently thresholded matrices. The result corroborates the chosen threshold $\theta_c = 0.85$: there is no phase transition for the computed pivotal network parameters, which in turn would have indicated a *natural* threshold parameter. As a consequence, any value for the threshold in the aforementioned range can be a meaningful choice, in particular $\theta_c = 0.85$. More specifically, most network parameters showed a linear or exponential increase (or decrease) with θ_c. It has been suggested that local maxima in the dependence of the clustering coefficient on the threshold can be used as a selection criterion (personal communication with Katharina Zweig, University of Heidelberg)[1]. The clustering coefficient remained roughly constant for a threshold variation between 0.65 and 0.85. After a value of 0.9 it

[1]The intuition behind this argument is as follows: since the data set is noisy, a random deletion of edges decreases the clustering argument as it is the case for a random addition of edges.

strongly decreased, and in the range between 0.85 and 0.9 local maxima were observed in most datasets. We therefore chose to generate networks with a threshold of 0.85.

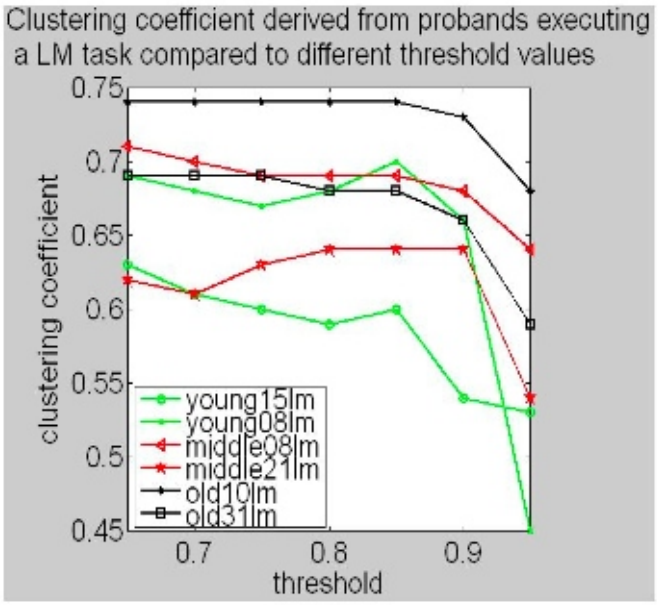

Fig. 2.3: This diagram depicts the clustering coefficient for different thresholds and age groups. This analysis has been performed in collaboration with Franziska Zickgraf.

Nota bene: The approach of this thesis is to define connectivity between brain voxels as to be high temporal correlation of the corresponding BOLD-signal time-series. This is what is referred to be as *functional connectivity*. Of course, this does not mean that the corresponding voxels are mutually connected (via chemical neuro-transmitter or anatomical paths). The simplest counter-example is the case of a common input activating both brain hemispheres, see *(Chialvo, 2004)*.

Statistical testing of significance has deliberately not been done. Of course, one could apply statistical testing methods in order to distinguish between *significant* and *insignificant* correlations. For instance, one could define the threshold in terms of the probability of the observed correlation $P(r_{ij} > R)$ under the null hypothesis that r_{ij} is less than an arbitrary value R. Hence, a functional connection between regions would not be regarded as significant unless $P(r_{ij} > R)$ was less than α, the p value for an individual test at 5% over multiple dependent tests, cf. [ASW$^+$06]. However,

this approach would entail many more hypotheses on the statistical distributions of the correlations than desired. One of the main motivations of this thesis has been to look as *"blindly"* as possible at the temporal activation patterns, i.e. in other words using as few pre-assumptions as possible. The usage of the simple Pearson correlation seemed most appropriate.

Anatomical and topological visualization of brain functional networks.

An important issue in neuroscience is the characterization of the underlying architectures of complex brain networks. This thesis analyzes functional networks in the aforementioned sense and it is, of course, a natural question if and how these networks are clustered. Classical network clustering algorithms have been applied to the constructed networks, namely the modularity approach by Mark Newman (cf. [**?**]) and the approach presented by Kertesz et al., which is able to construct overlapping clusters. Both approaches did not produce meaningful results and further network clustering techniques have not been applied. However, a meaningful clustering of the functional networks is desirable and it has been achieved by assigning anatomical information to each voxel in the network.

A standard procedure to make fMRI images comparable to each other is spatial rescaling to match the standardized MNI coordinates[1]. To retrieve anatomical information for every voxel, MNI-coordinates of the voxel centers have been transferred to the Talairach space using the open source MATLAB program `mni2tal.m` ,
see http://imaging.mrc-cbu.cam.ac.uk/imaging/MniTalairach.
The `Talairach client` has been used to access the `Talairach daemon`, a database server storing anatomical data for the Talairach brain. After having retrieved this piece of information, it has been necessary to assign the nearest gray matter to every voxel center. In particular, each voxel has been assigned a hemisphere, lobe, smaller gyri structure and, where possible, a Brodmann area.

The previously constructed functional networks have thus been clustered using anatomical information provided by the `Talairach daemon`. Finally, the resulting clustered networks have been averaged for each age group, producing so-called *consensus networks* which are considerably smaller in size.

[1] MNI = monreal neurological institute

The clustered and averaged functional networks are the main objects of interest during the further analysis. However, basic statistical parameters were also computed for the LCC[1] of the unclustered networks, see the results chapter. The small-sized consensus networks were visualized topologically and were analyzed using more intricate methods, see also later.

The reader should continuously keep in mind how the networks have been constructed and what it means for two voxels to be functionally connected when interpreting the results of the subsequent analysis. A major critique of the approach of functional connectivity is that there is yet no direct evidence for the underlying architecture of human brain anatomical networks, cf. *(Tootell et al. 2003)*, [HCE07]. Characterization of such anatomical networks would be particularly helpful to reveal intrinsic structural and organizational principles in the human brain and enhance our understanding of how functional brain states are associated with their structural substrates, [HCE07].

[1] LCC = largest connected component

Chapter 3

Mathematical methods

3.1 Spectral graph theory and network entropy

Motivation

Spectral graph theory primarily deals with the analysis of the relationship between the properties of a graph $\Gamma = (V, E)$ and the eigenvalues of underlying matrices. In particular, it is the analysis of the eigenvalues of the (normalized) graph Laplacian operator. Spectral graph theory has a long tradition in the analysis of classical graphs. It has been applied to classical graph theoretical questions, mainly in combinatorics, but recently has proven to be a helpful tool in characterizing both global and local structures of large networks. The spectrum of the normalized graph Laplacian[1]

$$\Delta v(i) \ := \ v(i) - \frac{1}{n_i} \sum_{j, i \sim j} v(j).$$

yields a very comprehensive set of invariants of the underlying network. We will use this tool

- to classify the functional brain networks by producing spectral plots
- to gauge the synchronizability of the functional brain networks

[1]The normalized Laplacian operator has the same spectrum as the operator investigated in [BJc], but it has a different spectrum as the usual (algebraic) graph Laplacian, studied in the literature, cf. [Chu97] and [GR01] for reference. Here, $v : \Gamma \to \mathbb{R}$ are real-valued functions on the set of vertices Γ, $i \sim j$ denote adjacent vertices, n_i the degree of vertex i.

- to quantify the structural difference between the networks using *Jenson-Shannon divergence measure*
- to define and calculate network entropy as a measure for network disorder

Moreover, as we will especially point out in the discussion and outlook chapter, the Laplacian spectra of the networks can give hints about their structural evolution and could eventually be used to develop hypotheses leading to a synthetic network model.

A simple but very helpful tool in the spectral analysis of networks is the visual inspection of the Laplacian spectrum, which can furthermore serve as a classifier of networks. Basically, we will convolute the spectral distribution with a smoothing kernel, e.g. a Gaussian kernel, and plot the resulting function[1]:

$$f(x) = \sum_{\lambda_j} \frac{1}{\sqrt{2\pi\sigma^2}} \exp\Big(- \frac{|x - \lambda_j|^2}{2\sigma^2} \Big) \; .$$

This has been done by [BJ07] and [BJa] for several real-world networks.

The results of this thesis may extend the list of networks that have been analyzed using this method and may help to foster the acceptance of techniques that were previously and successfully used in other domains.

Before giving the formal definitions and details of the methods it is worth stressing the importance of the spectral method. Standard statistical tools, such as average shortest path length, betweenness or transitivity, are a useful toolbox for the empirical analysis of networks. But these global statistical measures are not refined enough to gauge intricate features of networks, such as dynamic behaviour. For example, many networks have been classified as having a power-law degree distribution, cf. [BA99]. However, the power-law degree distribution fails to distinguish between systems that dynamically behave completely different. Synchronizability can be strongly influenced by small changes in the connectivity structure, whereas these small changes are not detectable by means of global statistical measures, but they leave their trace in the spectrum. This is why the Laplacian spectrum is important. Moreover, it helps unveiling processes of graph formation like motif joining or duplication since these leave traces in the

[1] The eigenvalues λ_j were convoluted with a Gaussian kernel. The variance σ^2 determines the width of the Gaussian and, hence, smaller values of σ^2 emphasize the finer details, whereas larger values bring out more the global pattern. The value of σ^2 will be once set and then kept fixed for all plots.

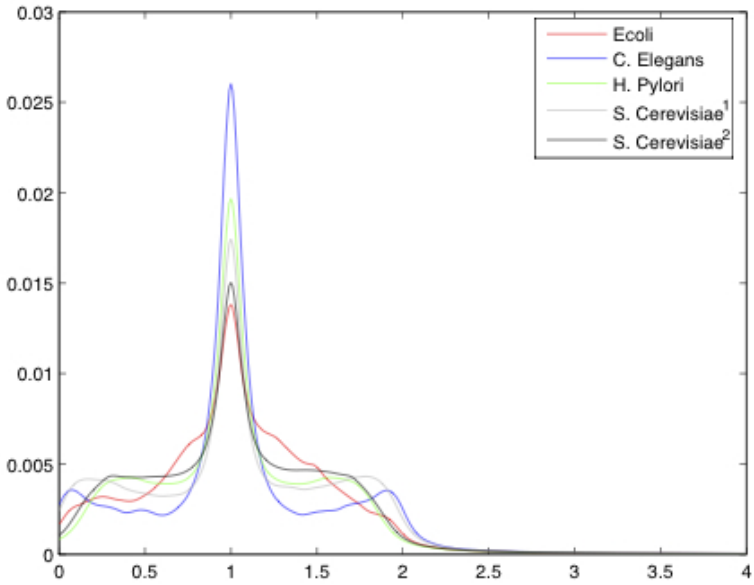

Fig. 3.1: Example of a spectral plot of different protein-protein interaction networks, convoluted with a smoothing kernel. Copyright and data source: *A. Banerjee*, [BJa].

spectrum. Last but not least, the (normalized) graph Laplacian fits well into the broader class of *Laplace-Beltrami operators*[1] $\mathcal{L}_n$, $n \geq 0$. These operators generalize the graph Laplacian and can be purely defined with the help of boundary operators acting on the simplicial *clique* complex, which can be naturally assigned to any network.

We will also make use of simplicial *clique* complexes but will rather look at their homology (cf. next section) instead of higher Laplacian spectra. For the sake of completeness, we want to mention the existence of such generalized operators, which might be useful for possible further analysis.

The methods presented in this chapter are based on [BJ08], [BJ07], [JJ02], [IM02], [BJc], [BJa], [Jos07]. Please see also [NMH03], [AJW04] and [PRK01] for further reference. Unless otherwise stated, computations have been performed using MATLAB

[1]The Laplace-Beltrami operators are defined by means of boundary and coboundary operators on the chain groups: $\mathcal{L}_n := B_{n+1}B_{n+1}^T + B_n^T B_n$. Here, B_n denotes the boundary operator on the n-th chain group, written as an incidence matrix. Clearly, $\mathcal{L}_0 = B_1 B_1^T$ is our graph Laplacian Δ. Note that $B_0 B_0^T = 0$. The incidence matrices, i.e. boundary and coboundary operators, are defined on the chain group of the associated *clique complex* to the underlying network. Please see next section for details.

software, applying the *Cholesky decomposition algorithm* for large graphs.

The normalized Laplacian operator

As we stated in chapter one, networks represent real-world systems, that is, in terms of the formal structure of a graph. The vertices of a graph represent the units in question, in our case brain cubical volumes, and an edge between vertices expresses some correlation between the corresponding units. Here, for simplicity of presentation, we only consider simple, undirected and unweighted graphs, although the methods apply and the considerations remain valid in the general situation.

First, we will give the formal definition of the version of the Laplacian which will be used in the course of the analysis, cf. [BJ09] or [Ban08a].

Definition 1. *Let Γ be a finite and connected graph with N vertices. Vertices $i, j \in \Gamma$ that are connected by an edge of Γ are called neighbours, $i \sim j$. The number of neighbors of a vertex $i \in \Gamma$ is called its degree n_i. For real-valued functions v on the vertices of Γ, i.e. $v : \Gamma \longrightarrow \mathbb{R}$, we define the (normalized) Laplacian as*

$$\Delta \; : \; L^2(\Gamma) \longrightarrow L^2(\Gamma)$$

$$\Delta v(i) \; := \; v(i) - \frac{1}{n_i} \sum_{j, i \sim j} v(j).$$

whereas $L^2(\Gamma)$ denotes the space of real-valued functions, defined on the finite set of graph vertices.

The normalized Laplacian differs from the (algebraic) Laplacian operator, which can be mostly found in the literature, but it is the natural way to discretize the operator underlying random walks on graphs, cf. [Chu97]. It also incorporates a conservation law. The material presented here can be found in [GR01], [BJc] and [BJa].

There can be found different possible normalizations of the Laplacian in the literature. The version we use here yields the following matrix form of the Laplacian $\Delta = [a_{ij}]$:

$$a_{ij} = \begin{cases} 1, & \text{if } i = j \text{ and } n_i \neq 0 \\ -\frac{1}{n_j}, & \text{if } ij \text{ is an edge} \\ 0, & \text{otherwise} \end{cases}$$

The object of interest is, of course, the spectrum of this operator since it yields important invariants of the underlying graph Γ. It is also possible, as in the case of the algebraic Laplacian, to essentially re-construct the graph from the spectral information, essentially meaning up to isospectral graphs. For the sake of better readability and unless otherwise stated, we will simply refer to the Laplacian instead of the normalized Laplacian. The following list of properties is also based on [IM02] and [BJc].

The Laplacian operator Δ is symmetric for real-valued functions u, v on the vertices and for the product

$$(u, v) := \sum_{i \in V} n_i u(i) v(i) \, .$$

Moreover, Δ is nonnegative, that is $(, u) \geq 0$ for all u. From this we can conclude the spectrum of Δ is real and nonnegative, the eigenvalue equation being

$$\Delta u - \lambda u = 0 \, .$$

A nonzero solution u is called an eigenfunction for the eigenvalue λ. The smallest eigenvalue is $\lambda_0 = 0$, which belongs to a constant eigenfunction. Since the graph Γ is assumed to be connected, the multiplicity of this eigenvalue is 1, hence

$$\lambda_k > 0$$

for $k > 0$, whereas the eigenvalues have been ordered as

$$\lambda_0 = 0 < \lambda_1 \leq ... \leq \lambda_{N-1} \leq 2$$

The eigenvalue $\lambda_{N-1} = 2$ if and only if the graph is bipartite. This is equivalent to the fact that whenever λ is an eigenvalue, then also $2 - \lambda$. Subsequently, we summarize the main results which are important for the qualitative analysis of networks.

- The normalized graph Laplacian Δ is always positive semidefinite.
- The smallest eigenvalue is $\lambda_0 = 0$ for every graph.
- The largest eigenvalue can be estimated by $\lambda_{N-1} \leq 2$ by means of the following equation:

$$\lambda_i \leq \sup_f \frac{\sum_{i \sim j} \Big(f(i) - f(j) \Big)^2}{\sum_i f^2(i) n_i} \leq 2$$

- The eigenvalues may have a multiplicity > 1.
- The number of the connected components of the graph Γ is given by the multiplicity of the eigenvalue 0.
- For the largest eigenvalue it holds true: $\lambda_{N-1} = 2$ if and only if Γ is bipartite.
- The difference $|2 - \lambda_{n-1}|$ quantifies how much the graph differs from a bipartite one.
- For a complete graph Γ with n vertices the spectrum is:

$$\lambda_0 = 0 \quad \text{and} \quad \lambda_1 = \lambda_2 = ... = \lambda_{N-1} = \frac{n}{n-1}$$

Spectral plots. The Laplacian spectrum of a graph Γ under inspection is bounded in $[0; 2]$. Though, the spectrum differs from graph to graph and hence, the number of eigenvalues varies among networks of different sizes. In order to grasp the overall structure of the spectrum, and hence of the underlying network, it is a simple but effective way to visualize the spectrum, e.g. simply by plotting a histogram with the desired numbers of bins. However, this will result in a very rough pattern. Another possibility for visualizing the pattern of spectral density is to use a smoothing kernel.[1]

Hence, one convolutes the Dirac delta function $\sum_k \delta(\lambda, \lambda_k)$ (as a spectral density) with a smooth kernel $g(x, \lambda)$ and plot the resulting density function

$$f(x) = \int g(x,) \sum_k \delta(\lambda, \lambda_k) d\lambda = \sum_k g(x, \lambda_k) \, .$$

We will use a Gaussian smoothing kernel, hence we plot the function

$$f(x) = \sum_{\lambda_j} \frac{1}{\sqrt{2\pi\sigma^2}} \exp\Big(- \frac{|x - \lambda_j|^2}{2\sigma^2} \Big) \, .$$

By varying the parameter of the kernel one can obtain a fine tuning: smaller values of σ^2 yield a more fractuation of the spectrum, i.e. one inspects finer details, whereas larger values emphasize on the global pattern. Of course, the parameter of the kernel will be set once and then kept fixed. As will be later clearly stated again, we set the parameter in accordance with the analyzed plots in [BJ08], i.e. $\sigma = 0.025$.

[1] One could use many different kernels, e.g. the Cauchy-Lorentz distribution $\frac{1}{n} \frac{\gamma}{(x-m)^2+\gamma^2}$ or the Gaussian distribution $\frac{1}{\sqrt{2\pi}\sigma} \exp\Big(- \frac{(x-m)^2}{2\sigma^2} \Big)$.

Spectral plots of a graph present an effective and visually amenable way for the classification of networks, at least to have a coarse filter at hand which helps distinguishing between different networks. This method has been used by *Banerjee and Jost* in [BJb] and [BJ08] to suggest a classification of real-world networks.

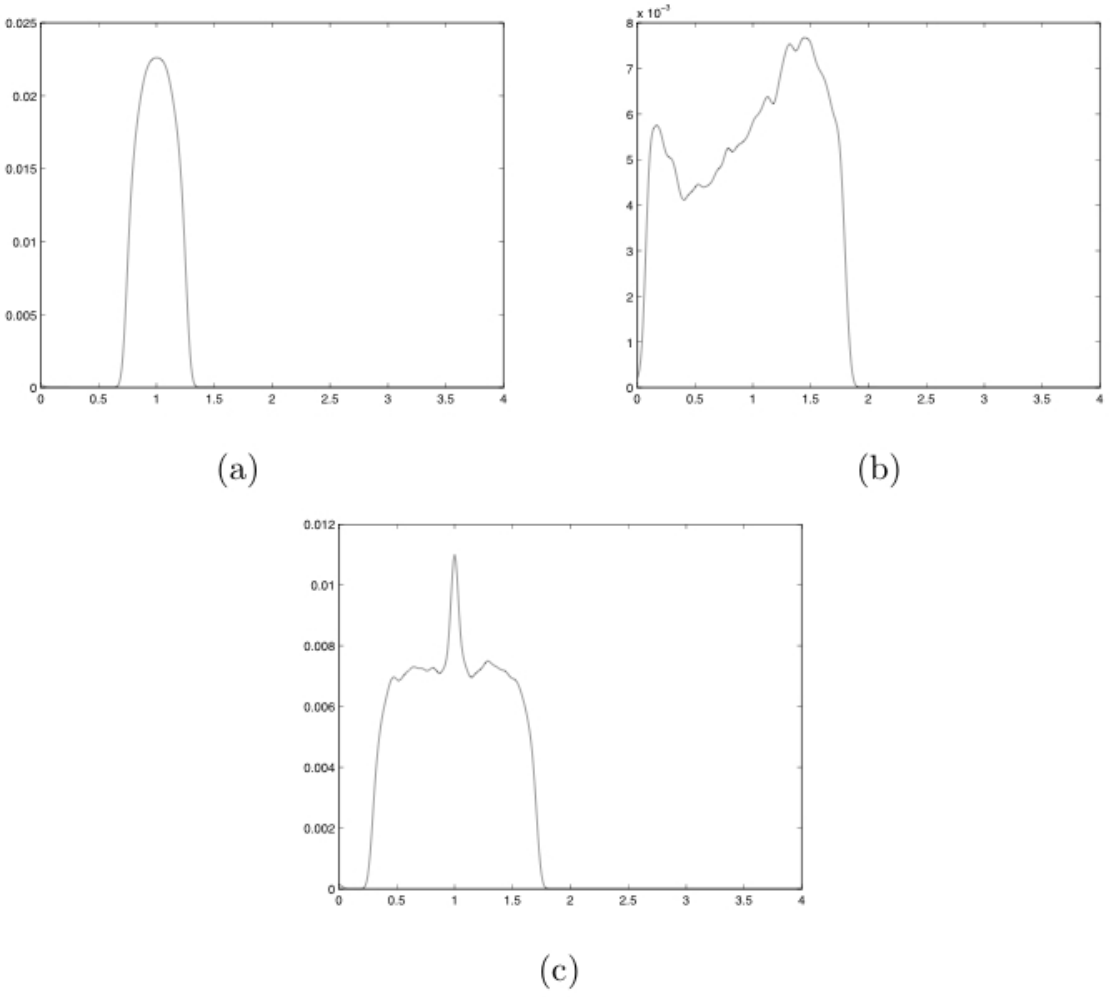

Fig. 3.2: Spectral plots of (a) a random network by the Erdös-Renyi model with $p = 0.05$, (b) a small-world network by the Watts-Strogatz model, (c) a scale-free network by the Barabasi-Albert model. Copyright: [BJ08]

Motif doubling and graph reconstruction In this last paragraph of this section we will mainly recall some facts about motif doubling in graphs and its impact on the Laplacian spectrum. This is particularly interesting if one wants to reconstruct a network from its spectrum. As we will point out in the outlook chapter at the very end of this thesis, this could be one possible direction for future research. Please see [Ban08a], [Wag01] for proofs and reference.

Of particular importance is the multiplicity m_1 of the eigenvalue 1 of Δ. m_1 is the number of linearly independent solution functions of $\Gamma v(i) = v(i)$ for all i, hence of

$$\sum_{j,j\sim i} v(j) = 0 \quad \text{for all } i$$

In other words, m_1 is the dimension of the kernel of the adjacency matrix of Γ. In view of graph (re-)construction, such functions can be created by node duplication: take any node $i_0 \in \Gamma$ and build a new graph Γ_0 by adding a new node j_0 to Γ and connecting it to all neighbors of i_0. Hence, i_0 and j_0 share the same neighbors. If one defines $v(i_0) = 1$, $v(j_0) = -1$ and $v(i) = 0$ on all other nodes, one obtains a solution function. In other words, node duplication increases m_1 by 1. Similarly, doubling an edge connecting two vertices i, j yields the eigenvalues $\lambda = 1 \pm \sqrt{\frac{1}{n_i n_j}}$ which, henceforth, are symmetric about 1, the closer to 1 the higher the degrees of the respective nodes.

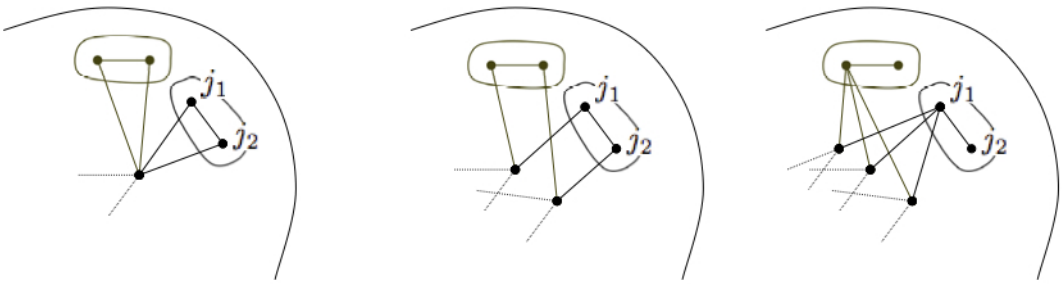

Fig. 3.3: Schematic of three different edge doubling which produce the eigenvalues $\frac{1}{2}$ and $\frac{3}{2}$. Copyright: [Ban08a]

Understanding the structural processes, e.g. motif duplication, could be translated into evolutionary processes of the underlying real-world system. For example, the structural evolution of protein-protein interaction networks (PPIN) has been modeled by means

of this method. For example, biological processes such as gene duplication or random mutation, could have been explained by structural graph formation processes such as motif duplication. Hence, one obtains a generic network model of the underlying real-world system, which can better explain system-specific properties than the standard models such as random or scale-free networks. However, the methods presented here, focus on processes that produce eigenvalues $\frac{1}{2}$, 1, $\frac{3}{2}$ and so on. It is necessary, especially in view of our functional brain networks, to explore different graph operations or conformations that produce other specific eigenvalues, which will then help to unveil the evolutionary processes. This will by far go beyond the scope of this thesis and has been purely mentioned for possible future research.

Synchronizability

This subsection is mainly based on results presented in [LAJ07], [Jos05] and [BJ09].

Many properties of dynamical processes, which are defined on networks, cannot directly be inferred from the statistical properties of the network in question. For example, small local alterations in the network structure can sensitively influence the eigenvalues relevant for synchronization, cf. [ABJ06], [BJ09].

Synchronizability is an important aspect to look at when analyzing functional brain networks: the brain voxels behave as dynamical systems evolving to certain rules and the links, i.e. high correlation values, can be considered as a proxy for inter-regional interaction.

A typical pattern for interaction is a diffusion process, which naturally gives rise to the Laplacian operator Δ, [ABJ06]. Thus it is almost obvious that dynamical properties, e.g. synchronizability, are closely linked to the spectral properties of the network. As a starting point, we look at the well-known coupled map lattice,

$$x_i(t+1) = f(x_i(t)) + \sum_{j=1}^{n} a_{ij}[f(x_j(t)) - f(x_i(t))]$$

which has been written in a slightly more general form by using individual weights $a_{ij} \geq 0$ along the links instead of a global coupling constant. This system can be

written in the obvious vector form

$$\mathtt{x}(t+1) = \Big(I - \Delta\Big) F(\mathtt{x}(t))$$

whereas $\mathtt{x} = (x_1, ..., x_n)$ and $F(\mathtt{x}) = (f(x_1), ..., f(x_n))$. By definition, the network synchronizes if $\lim_{t\to\infty} |x_i(t) - x_j(t)| = 0$ for all i, j provided that the initial conditions belong to some appropriate open set[1]. Provided that we are in this situation, then the system, asymptotically, approaches a synchronous state. By then, each node exhibits the same time evolution: $x_i(t) = s(t)$ for all i. Hence, it follows that $s(t+1) = f(s(t))$, i.e. the behaviour of the nodes for $t \longrightarrow \infty$ is identical to their behaviour in isolation. Please note that we are neglecting any coupling delays in the network. If one considers time-delay equations, then the synchronous solutions may be significantly different, cf. [LAJ07].

In the subsequent paragraph, we will state a sufficient condition for local synchronization of networks that encompasses a quite general class of functions. The presented material is mainly based on [ABJ06]. Please see also [LAJ07], [BJ09]. We focus on chaotic synchronization, that is, the case when f has a compact chaotic attractor $\mathcal{A}$ and s represents some dense (and necessarily unstable) orbit in $\mathcal{A}$, cf. [ABJ06]. We assume that f is continuously differentiable, hence small perturbations u about the solution $s(t)$ are governed by $u(t+1) = f'(s(t))u(t)$ and the solution to this looks like

$$u(t) = u(0) \prod_{k=0}^{t-1} f'(s(k)).$$

The condition to be imposed on the solution function $s(t)$ for local asymptotic stability is that

$$\lim_{t\to\infty} \prod_{k=0}^{t-1} |f'(s(k))| = 0.$$

However, this would not hold for any function s inside a chaotic attractor, but we can always find some sufficiently large number α such that

$$\lim_{t\to\infty} \prod_{k=0}^{t-1} e^{-\alpha} |f'(s(k))| = 0.$$

[1] For further details, we refer to [ABJ06] but we dare to remark that the details will not be important for the derivation which we present.

It is easy to see, that the above equation holds true for all α satisfying

$$\alpha > \mu = \lim_{t\to\infty} \frac{1}{t} \sum_{k=0}^{t-1} \log |f'(s(k))| \tag{3.1}$$

where μ denotes the Lyapunov exponent. In order to find the corresponding conditions, we consider small perturbations $\mathbf{u}(t) = \mathbf{x}(t) - \mathbf{1}s(t)$, which are governed by

$$\mathbf{u}(t+1) = f'(s(t))\Big(I - \Delta\Big)\mathbf{u}(t).$$

Since we may assume that the eigenvectors of the Laplacian operator Δ form a basis of $\mathbb{R}^n$, the perturbations $\mathbf{u}(t)$ can be taken along an eigenvector of the Laplacian operator: $\mathbf{u}(\mathrm{t}) = \mathrm{p}_i(t)\mathbf{u}_i$, where $i \geq 2$ since the perturbations along the direction $\mathbf{1}$ still yield a synchronous solution. The function $p_i(t)$, i.e. the amplitude along the ith eigenvector, behaves according to

$$p_i(t+1) = f'(s(t))(1-\lambda_i)p_i(t) = p_i(0)\prod_{k=0}^{t} f'(s(k))(1-\lambda_i).$$

Hence, the synchronizability of the system holds true

$$\lim_{t\to\infty} \prod_{k=0}^{t-1} |f'(s(k))||1-\lambda_i| = 0, \qquad i = 2, ..., n.$$

Using the above stated connection to the Lyapunov exponent one can state a sufficient condition for local synchronization as

$$\max\{\, |1-\lambda_i| \,: i = 2, ..., n\} < e^{-\mu}\,. \tag{3.2}$$

By means of this simple condition we can define:

Definition 2. *Using the above notation, we can define an appropiate synchronizability measure for the network as*

$$\sigma \;:=\; \max\{\, |1-\lambda_i| \,: i = 2, ..., n\}\,.$$

Note that smaller values of σ enlarge the class of functions f for which the system synchronizes. Hence, the Laplacian spectrum of a network characterizes its synchronizability. Since we only assumed Δ to have n linearly independent eigenvectors (which

is always true), we can use σ to compare general networks with respect to their synchronization properties. This includes directed and weighted networks, even in the case of different network sizes. In the case of undirected weighted networks the measure σ simplifies to

$$\sigma = \max\{|1 - \lambda_2|, |1 - \lambda_{max}|\}$$

whereas $\lambda_{max} = \lambda_n$. In the case of our functional brain networks we will find the eigenvalues to be in the range $\lambda_2 \leq 1 \leq \lambda_{max}$, which implies that synchronizability depends on both λ_2 and λ_{max}: higher values of λ_2 and smaller values of λ_{max} yield better synchronizability because of the condition

$$\frac{\lambda_2}{\lambda_{max}} > \frac{1 - e^{-\mu}}{1 + e^{-\mu}}$$

We will use the eigenratio $\dfrac{\lambda_2}{\lambda_{max}}$ as a quantifier of the synchronizability of our functional brain networks, larger values implying a better synchronizability.

Before closing this section we will briefly state the fact that synchronizability cannot, in general, be inferred from global statistical properties of the underlying network. Of course, it can be said that scale-free networks have poorer synchronization properties compared to other network architectures, cf. [ABJ06]. However, it is not true that a more homogeneous degree distribution always implies better synchronizability. The main reason for this (and similar examples) is that *grosso modo* small structural changes in the network, e.g. loosely adding a very small subgraph, leave their traces in the spectrum, particularly affect λ_2, but on the other hand these *small* change average out and cannot be detected by statistical measures, cf. [ABJ06].

Jenson-Shannon divergence measure

This section presents a method, cf. [Ban08b] and [Nie11], to gauge the topological distance between two networks of different size. The distance between the spectral distributions will be considered as a measurement of the structural differences and will be quantified by means of an existing divergence measure between two distributions.

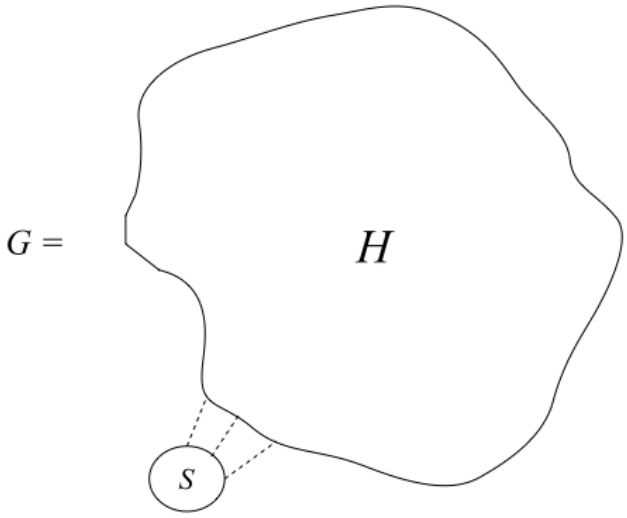

Fig. 3.4: The global statistics of the graph G are determined by H, whereas the small part S independently influences the eigenvalue λ_2. In particular, the two networks G and H are likely to share many statistical properties but may possibly differ significantly in their synchronizability. Copyright: [ABJ06]

The definition of the Jenson-Shannon divergence will be based on the *Kullback-Leibler divergence measure* (=:KL) for discrete systems. The latter is defined on two probability distributions p_1 and p_2 of a discrete random variable X as

$$KL(p_1, p_2) \;=\; \sum_{x \in X} p_1(x) \log \frac{p_1(x)}{p_2(x)}$$

Note that this divergence measure is not defined if $p_2 = 0$ and $p_1 \neq 0$ for any $x \in X$. Furthermore, KL divergence is not symmetric and does not satisfy the triangle inequality, hence cannot be a metric.
Considering the two probability distributions p_1 and p_2, the Jenson-Shannon divergence measure (=: JS) is defined as

$$JS(p_1, p_2) \;=\; \frac{1}{2} KL(p_1, p) + \frac{1}{2} KL(p_2, p)$$

where $p = \frac{1}{2}(p_1 + p_2)$. Unlike the KL divergence, Jenson-Shannon is symmetric and holds even if one of the probability measures is zero for some x. The square root of JS divergence is a metric, please see [Ban08b] for further reference. Hence, we can define our metric as:

Definition 3 (Jenson-Shannon divergence, cf. [Ban08b]). *Let Γ_1, Γ_2 be two graphs, with the spectral distribution (of graph Laplacian) f_1 and f_2 respectively. Then we define the Jenson-Shannon divergence measure between f_1 and f_2 as:*

$$D(\Gamma_1, \Gamma_2) := \sqrt{JS(f_1, f_2)}$$

One drawback of this tool is that, theoretically, there exist isospectral graphs which cannot be distinguished by this means. However, it is very unlikely that one happens to encounter two such isospectral graphs in real networks and, moreover, these would be qualitatively very similar in most respects.

Network	Γ_{Ph}	Γ_{Ec}	Γ_{Sc}	Γ_{Hp}	Γ_{Ce}	Γ_{PG}
Γ_{Ph}	0.0000	0.0904	0.0661	0.1694	0.4704	0.4704
Γ_{Ec}	0.0904	0.0000	0.0641	0.1036	0.4902	0.5074
Γ_{Sc}	0.0661	0.0641	0.0000	0.1340	0.4574	0.4738
Γ_{Hp}	0.1694	0.1036	0.1340	0.0000	0.5086	0.5380
Γ_{Ce}	0.4704	0.4902	0.4574	0.5086	0.0000	0.2429
Γ_{PG}	0.4780	0.5074	0.4738	0.5380	0.2429	0.0000

Fig. 3.5: Distance table between cellular networks of *P horikoshii* (Γ_{Ph}), *E coli* (Γ_{Ec}), *S cerevisae* (Γ_{Sc}); protein-protein interaction network of *H pylori* (Γ_{Hp}); neuronal connectivity network of *C elegans* (Γ_{Cs}) and US power-grid network (Γ_{PG}). Copyright and data source: *A. Banerjee, 2008*, [Ban08b].

Note that each network has a different size, but nevertheless we can compare their spectral distribution and gauge the structural distance. The JS divergence measure allows the quantification of the structural similarities (or differences) based on the spectral distribution which captures the qualitative properties of the underlying graph topology.

Network entropy

In this section we summarize results on how to calculate network entropy. We will cite the entropy robustness principle, which basically states that higher entropy of a network yields higher robustness. We will apply this methods to our functional brain

networks. Network entropy will be used as a tool to measure the diversity of interactions which define the system. Results for the brain networks can be found in chapter 4. The material presented here is mainly based on [DGO04], [DM04], [MDV04], [DGO04], [AGD94], [Ber93] and [Bil65].

When analyzing and characterizing networks, it is important to know the resilience of the whole system against external and internal perturbations, which amount to changes in the network parameters. One can, of course, analyze this phenomenologically, i.e. in terms of experimentally observed resilience. This has been done, for example, by Barabasi et al. in [BA99].

Here, we summarize results from a more structural approach using methods from statistical physics and ergodic theory. We will then apply these methods to our functional brain networks since we believe that the formal requirements on the system are fulfilled. The results, see next chapter, are very helpful for our intended classification of different memory networks.

The **central idea** of this approach is that biological processes typically operate at steady state, and hence, characteristic macroscopic observables do not change for relatively long times. However, this does not mean that the underlying microscopic variables are static but rather that their complex interplay results in a stable phenotype, which we can observe, cf. [MDV04].

The diverse and stochastic microscopic processes determine the resilience against perturbations. Using erdodic theory of dynamical systems, one can quantify this uncertainty by dynamical entropy (Kolmogorov-Sinai invariant). The importance for biological network analysis stems from the fact that there is a fluctuation theorem for networks, in analogy to the fluctuation-dissipation theorem in statistical mechanics, [CW51] and cf. [MDV04]. We will later restate the formal definition but the theorem says:

The **entropy-robustness principle** says that alterations in network entropy correlate positively with alterations in the resilience of the macroscopic system against microscopic perturbations, cf. [MDV04]. In other words, a higher entropy yields a greater insensitivity of an observable to perturbation of the network.

The described methods assumes that the (microscopic) processes are Markovian. We will assume this as well in the case of our functional brain networks. Hence, this will allow for a description of network entropy as a tool which gauges the diversity of interactions which define the system, in our case, this will be the weighted correlation links between small anatomical regions. The described methodology does not intend to particularly describe topological properties, but rather treats them as side-effects of an underlying functional property, which allows for a ranking of the networks according to their resilience against random changes.

We will now recall the concept of dynamical entropy, defined for a Markov process: $P = (p_{ij})$, which is given by (Billingsley, 1965), [Bil65]:

$$H = -\sum_{ij} \pi_i p_{ij} \log p_{ij} \,,$$

whereas p_{ij} denotes the Markovian transition probabilites and π_i are the components belonging to the stationary process. Before we define this stationary process in detail, we mention that there are many other possibilites to analyze complex dynmical systems by means of microscopic modelling, e.g. differential equations, cellular automata, etc.

Statement: We will assume the brain functional networks to be a result of a diffusive process. By linking dynamical uncertainty to random walks on the network, we can stochastically describe the system and derive macroscopic properties. The diversity of possible information pathways between the anatomical structures in the brain networks can be characterized by the dynamical entropy of a Markov process and, moreover, is related to the system's resilience to random changes by means of the fluctuation theorem (see below).

Now we define the technical tools and the concept of network entropy, which has been introduced in cf. [DGO04], [DM04], [Dem97], [MDV04]:

Let Γ be a (weighted) network, and $A = (a_{ij})$ its adjacency matrix. The largest eigenvalue λ of the matrix A is called Perron-Frobenius eigenvalue, we denote by v the corresponding eigenvector. This dominant eigenvalue satisfies a variational principle and is a topological invariant. The variational principle is similar to the minimization of the free energy in statistical mechanics, cf. [Cal85].

Definition 4. *A stochastic process $P = (p_{ij})$ is said to be compatible with the adjacency matrix A, if*

$$\sum_j p_{ij} = 1 \quad \text{and} \quad p_{ij} = 0 \Leftrightarrow a_{ij} = 0.$$

In the case of brain functional networks the requirement on compatibility of stochastic processes is based on the idea that microscopic variables, that is brain voxel activity, only changes in response to changes of their interaction partners. To put it differently, as a **statement:** we assume that information will primarily flow along already existing high-correlations, i.e. interacting brain voxels or gyri structures. Of course, by doing so, we ignore possible voxel modifications, such as tissue or physiological changes, which might trigger global network changes. But this is justified due to the short measurement time during the experiment.

We define the stationary distribution, π, as the eigenvector belonging to the largest eigenvalue 1 of the stochastic matrix P:

$$\pi P = \pi$$

The matrix P describes the Markov process and the long-time behaviour of which can be characterized by the stationary distribution π. Now we add to our requirements the assumptions of ergodicity, i.e. irreducibility of A and P. This implies that the components π_i satisfy $\pi_i > 0$. These components represent the relative frequency with which the node i is visited by the random walk on the network.

With respect to all compatible processes $P = (p_{ij})$ the variational principle for λ can be written as

$$\log \lambda = \sup_P \Big[-\sum_{i,j} \pi_i p_{ij} \log p_{ij} + \sum_{i,j} \pi_i p_{i,j} \log a_{ij} \Big]$$

In [AGD94] it has been shown that in the case of strongly connected networks one obtains the supremum for a unique matrix $\hat{P} = (\hat{p}_{ij})$, where

$$\hat{p}_i j = \frac{a_{ij} v_j}{\lambda v_i}$$

The functional brain networks fulfill this requirement, i.e. they are weighted and fully connected networks. Choosing the matrix P such as above, we can write the variational principle as

$$\log \lambda = -\sum_{i,j} \pi_i \hat{p}_{ij} \log \hat{p}_{ij} + \sum_{i,j} \pi_i \hat{p}_{ij} \log a_{ij}$$

Furthermore, we can write this latter equation as

$$\log \lambda = H(\hat{P}) + \Phi(\hat{P})$$

Now we have a link between the topological invariant λ on the one hand and the network entropy $H(\hat{P})$ as well as the 'potential' $\Phi(\hat{P}) = \sum_{i,j} \pi_i \hat{p}_{ij} \log a_{ij}$ on the other. The equation of the variational principle, where we started from, is completely analogous to the Gibbs variational principle in statistical mechanics, cf. [CW51].

In the equation

$$\log \lambda = H + \Phi$$

the 'potential' vanishes in the case of Boolean networks, whereas in the general case, i.e. weighted and strongly connected networks, the potential Φ describes the difference between H and the Perron-Frobenius eigenvalue.

In dynamical systems theory there are quite some theorems which link observables at steady state to relaxation properties of a perturbed system, i.e. a system that experienced perturbations and which then returns to the steady state, cf. [Bil65]. Now we restate the fluctuation theorem presented in [DGO04] and [DM04] which links the concept of entropy to the macroscopic resilience of the system. Entropy, here, is considered as a proxy measure of microscopic variability. We consider now a change of an observable from steady-state, which is seen as the result of a perturbed microscopic variable.

Fluctuation theorem, cf. [DGO04] and [MDV04]]: *Let $P_\varepsilon(t)$ be the probability that the sample mean deviates by more than ε from its unperturbed value at time t. As t increases, $P_\varepsilon(t)$ converges to zero and we defne the fluctuation decay rate, R, as*

$$R = \lim_{t\to\infty} \Big[-\frac{1}{t} \log P_\varepsilon(t) \Big] .$$

Then it holds that changes in R are positively correlated with changes in network entropy:

$$\Delta H \Delta R > 0 .$$

In this case, the entropy H is at steady state, whereas R describes the the system away from the steady state. Small values of R entail large fluctuations around the mean value, whereas large values of R correspond to small deviations of observables from the steady-state condition.

As stated in [DGO04] and [MDV04], this concept is an extension of the Gibbs formalism, which applies to equilibrium systems at steady state. But moreover, this formalism can also be applied to non-equilibrium systems at steady-state, cf. [Dem97]. This is assumed for many biological systems. The good thing for our analysis of brain networks is that we can use this tool to describe resilience of the system at a macroscopic level, regardless of our ignorance about the microscopic processes.

3.2 Persistent homology

The **basic idea** of persistent homology of networks is to embed a network into a simplicial complex via a filtration process, and, while doing so, calculating the (simplicial) homology relative to all previous filtration steps. This allows for the detection of *long-lived* topological features, i.e. homology classes which *survive* several filtration steps.

Consequently, *short-lived* topological features are considered as noise, thus being irrelevant for the structural understanding of the network. Persistent homology will be denoted as a parametrized version of a Betti number, being visually presented in a very amenable way, so-called homology barcode plots.

This section is mainly based on [CZCG05], [ZC05], [HMR09] and [CCdS06]. Please see also [ELZ02], [CSEH07], [Hat02], [May92] and [Bre97] for further reference. Computations, see chapter 4 for the results, have been performed with MATLAB, using the free software package PLEX, provided at

`http://comptop.stanford.edu/u/programs/jplex/`. Regarding computational aspects, please see also the Computational HOmology Project, CHOMP, `http://www.math/gatech/edu/~chomp` , as well as [ZC05].

From a general viewpoint, algebraic topology provides methods to gauge *qualitative* or *global* properties of a topological[1] space X. The basic idea is to assign a collection of algebraic objects to the space X which algebraically encode the geometrical information contained in X and, moreover, which are topological invariants with respect to certain classes of functions defined on X. Having assigned the set of algebraic objects to X one uses algebraic techniques to analyze these objects and, hence, obtains insight into the geometric information about the space X, please see for a general overview of the field [Bre97], [Hat02].

Basically there are two methods which are prominent in the field of algebraic topology: homotopy and homology. The first technique assigns so-called homotopy groups π_i, $i \in \mathbb{N}$, to the space X. These groups contain information about the number and variety of mappings from the k-dimensional sphere into X, whereas two spheres in X are considered equivalent if they belong to the same equivalence class, i.e. are *homotopic* to each other, cf. [HMR09]. Please see also [Bre97] for the exact definition. This approach is very powerful regarding the amount of information which one obtains about the space X. However, the computational demands are in general extremely high. Homology, on the other hand, is computationally much more approachable. There are very deep theoretical links between these two concepts, homotopy and homology, cf. [Bre97], [Hat02]. The homological approach also assigns a set of invariants to the space X, the so-called homology groups $H_i(X)$. There are different homology theories, all of which fulfill the same theoretical properties imposed by the Eilenberg-Steenrod axioms. We will only make use of simplicial homology. For the sake of better readability and unless otherwise stated, we will only refer to homology instead of simplicial homology.

The homology groups, that is $H_k(X)$ for $k \in \mathbb{N}$, contain structural information about so-called *chains*, which are formed from simple and oriented objects, called simplices. The homology groups consist of *cycles*, i.e. chains with vanishing boundary, and any two k-cycles are considered equivalent if their difference is the boundary of a $(k+1)$-chain. To put it differently, the homology groups $H_k(X)$ provide information about the number of $k-$dimensional subspaces of X which do not have a boundary *in* X

[1] from the Greek $\tau o \pi o \sigma$, which means *place*, and $\lambda o \gamma o \sigma$, which means *study*

and which are themselves not a boundary of some $(k+1)$-dimensional subspace of X. Contrary to homotopy groups, the computation of homology groups is much more feasible and can be done by means of methods from linear algebra. However, the ease in computation is to the detriment of topological insight. Nevertheless, as can be seen in chapter 4, the results obtained from this method allow for a better discrimination between our functional brain networks associated to memory.

Homology groups are computationally amenable and provide valuable information about topological spaces.

Complex networks can be embedded into simplicial complexes (see below). While a network is purely a one-dimensional object, the embedding into a simplicial complex unveils much more structural information which was before, i.e. without the higher-dimensional simplices attached, covertly encapsulated.

However, by computing the (simplicial) homology just for the final complex, in which the network has been embedded, one does not account for the fact that there might be topological *noise* contained in the network, i.e. one does not know whether some homological property is reliable or has just been produced by some *unimportant* link in the underlying network. Persistent homology is a means by which one can discern relevant topological information from noise. Homological information is mainly about the number and type of voids, i.e. abstract and higher-dimensional holes, and the subject of persistent homology is to extract those voids that are *persistent*, i.e. long-living, and, hence, are relevant. This is done by filtrating the simplicial complex and by computing the homology at each filtration step, relative to all previous filtration steps.

The concept of persistent homology has been introduced by Edelsbrunner, Letscher and Zomorodian, cf. [ELZ02], [ZC05]. It has been first applied to point-cloud data, analyzing the persistence of topological features over a long range of parameters. In the rest of this section we present and summarize the concept and state the formal definitions.

This section is mainly based on [HMR09], where the concept of persistence has been applied to networks but only in a general case. We will use this method,

see chapter 4, to analyze the functional brain networks as a special instance of general correlation networks. To our knowledge, this is the first time that persistent homology has been applied to correlation networks.

One can show that the concept of persistent homology can be formulated in the framework of standard algebraic topology. More precisely, as is shown in [ELZ02], [ZC05], the persistent homology of a filtered $d-$dimensional simplicial complex is simply the standard homology of a particular graded module over a polynomial ring. However, we will not present the material from this bird perspective and in this generality since we believe that this would be to the detriment of readability. Our presentation follows [HMR09].

The definition of a simplex, i.e. a *simple* geometrical unit which can be used to dismantle a more complex geometical space, can of course be given in terms of geometry: an n-simplex Δ^n is an n-dimensional polytope in $\mathbb{R}$ with $n+1$ vertices. However, one also give a purely algebraic definition, circumventing any ambiguities arising from the surrounding space. Moreover, it is only the algebraic approach which makes the concept applicable to the coordinate-free concept of a network.

Definition 5 (cf. [Bre97])**.** *An (abstract) simplicial complex is a set* $V = \{v_0, v_1, ..., v_n\}$ *whose elements are called* vertices*, and a collection* K *of finite subsets of* V*, called* simplices*, such that*

$$\sigma \in K\,,\ \emptyset \neq \tau \subset \sigma \Rightarrow \tau \in K$$
$$v \in V \Rightarrow \{v\} \in K$$

A simplicial complex K *is called a simplicial* $n-$*complex if its largest simplex has at most* $n+1$ *vertices.*

The requirements imposed on K can be also read as follows: (i) the intersection of two simplices is a simplex, (ii) the sub-simplices (=faces) of each simplex in K are also in K. Moreover, we have the uniqueness property, i.e. each pair of simplices has a distinct set of faces implying that each simplex is unique. It is possible, cf. [May92], to assign a topological space $|K|$ to such an abstract simplicial complex, which, for finite complexes, is equivalent to a geometrical simplicial complex, cf. [Bre97].

Note that for a sub-complex K' of a simplicial complex K, we have a canonical inclusion map $\iota : K' \to K$, which induces a map between the respective homology groups (see below for the definition): $H_*(K') \to H_*(K)$.

A filtration of a simplicial complex K is a collection of subcomplexes $\{K_i\}$ such that

$$\emptyset = K_0 \subset K_1 \subset ... \subset K_n = K$$

Two simplices σ and ρ are called $q-$connected if there is a sequence of simplices $\sigma, \sigma_1, \sigma_2, ..., \sigma_n, \rho$, such that any two consecutive ones share a $q-$face, implying that they have at least $q+1$ vertices in common, cf. [HMR09]. Such a chain is called a $q-$chain. The complex K is $q-$connected if any two simplices in K of dimensionality greater or equal to q are $q-$connected. A convenient way to represent a simplicial complex is via a so called incidence matrix, whose columns are labeled by its vertices and whose rows are labeled by its simplices. Please see [HMR09] for reference.

In the simplicial framework one has the two notions of chains and cycles, which are completely analogous to the notions of paths and loops in the continous domain. The set of all $k-$chains can be equipped with a group structure, the group operation being the (formal) addition of chains. Formally, one generates the free abelian group on the set of all $k-$chains. This group is denoted as C_k. Hence, for all $k \in \mathbb{N}$ one obtains a group C_k. This family of groups is endowed with a family of *boundary operators*, linking subsequently indexed chain groups:

$$\delta_k \, : \, C_k \longrightarrow C_{k-1}$$

whereas $k = 0, 1, 2, ...$ The boundary operator δ_k assigns to any $k-$chain σ its boundary $\delta_k(\sigma)$, which is a collection of $(k-1)$-dimensional faces of σ, hence being itself a $(k-1)$-chain. The family of boundary operators endows the chain groups into a chain complex,

$$\emptyset \longrightarrow C_n \xrightarrow{\delta_n} C_{n-1} \xrightarrow{\delta_{n-1}} ... \longrightarrow C_1 \xrightarrow{\delta_1} C_0 \xrightarrow{\delta_0} \longrightarrow \emptyset$$

with $\delta_k \delta_{k+1} = 0$ for all k. The chain groups $\{C_k\}_{k \in \mathbb{N}}$ have been defined as the free abelian group C_k generated by the the k-chains, respectively in each dimension k. This algebraic structure can be naturally considered as a $\mathbb{Z}$-module. Hence, the boundary operators δ_k are $\mathbb{Z}$-linear maps and one has the notion of kernel and image: the kernel of δ_k is the set of all k-chains with vanishing boundary . Please see [HMR09] as well as [Bre97] and [Hat02] for reference.

These two subspaces play an important role:

$$k\text{-cycles}: \quad Z_K := \ker \delta_k = \{z \in C_k \ : \ \delta_k(z) = \emptyset\}$$

$$k\text{-boundaries}: \quad B_k := \text{im } \delta_k = \{b \in C_{k-1} \ : \ \exists b \in C_k \ : \ b = \delta_{k+1}(z)\}$$

Hence, we define the kth homology group as

$$H_k := \ker \delta_k \,/\, \text{im } \delta_{k+1} = Z_k / B_k$$

The kth Betti number of a simplicial complex K is defined as the rank of the k homology group:

$$\beta_k := \text{rank } H_k = \text{rank } \ \ker \delta_k - \text{im } \delta_{k+1}$$

The Betti number β_k can intuitively be interpreted as the number of k-dimensional holes, the Betti number $beta_0$ reflects the number of component. Unless otherwise stated we will always consider homology over $\mathbb{Z}$.

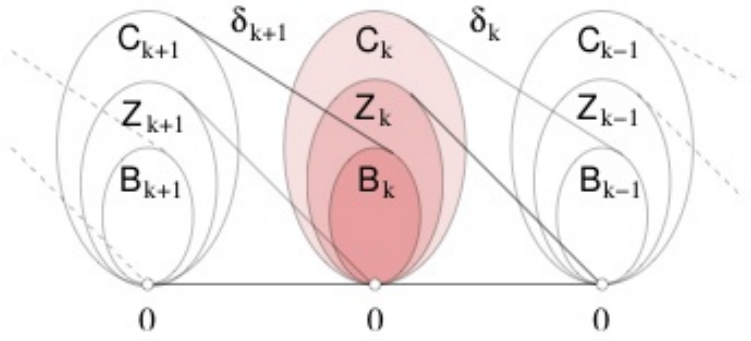

Fig. 3.6: Schematic diagram of the boundary homomophism. Here, Z_* denotes the kernel, B_* the image, respectively. Copyright: [ZC05].

Construction of simplicial complexes from graphs. Before we can precisely define persistent homology, we need to clearly state how we embed the network into a simplicial complex. This is, by far, not unique, however, there are several natural ways to do this. Two possible methods are the so-called neighborhood complex and the clique complex, cf. [HMR09]. Roughly summarized, the neighborhood complex $N(\Gamma)$ is constructed as follows: for each vertex v of the graph G there is a simplex containing the vertex v, along with all vertices w corresponding to directed edges $v \to w$. This is,

obviously, only possible for directed networks. The clique complex $C(\Gamma)$ is constructed by means of all complete subgraphs as simplices and the vertices of Γ as its vertices, hence it is the complete subgraph complex. For further reference on these definitions, cf. [Jon07] and [HMR09].

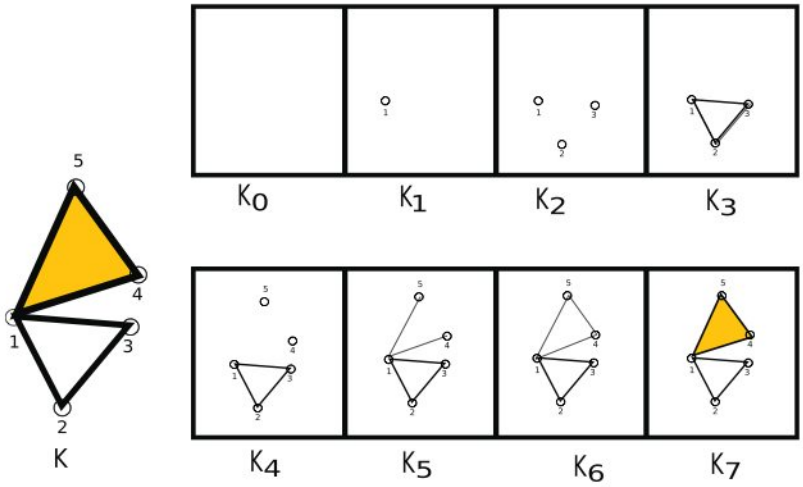

Fig. 3.7: Example: the simplicical complex K and its one possible filtration. Copyright: [HMR09].

The **choice of filtration** can be seen as a proxy measure for the evolution of the network as it evolves from the most simple case (just nodes) to the most complicated one containing faces of the highest possible dimension. This filtration process is, however, not unique. For the brain functional networks we will use the following filtration algorithm in order to embed the network into a simplicial complex:

(1.) all nodes exist already at the beginning of the filtration, being 0-simplices.

(2.) we pick a start node v_0, the choice of this *seed* node remains arbitrary but we keep this choice fixed for all networks.

(3.) 1-dimensional simplex is added to this node, then 2-dim, 3-dim, etc. (up to the highest possible dimension at this step).

(4.) at each filtration step we add one more node, once we have three nodes we may add the face of a triangle, similarly in higher dimensions.

(5.) these steps are iterated until all 0-simplices have been included and all simplices have been added up to the highest possible dimension.

Note that this is not the only possible filtration, however, we believe that it is the most appropriate one since it reflects well the possible dynamics of the network. Ideally, one would like to know the exact sequence how the network was built but this certainly does not apply since out network was obtained from correlations of time series. However, this method can be seen as a proxy to detect the (dynamic) evolution of the network. Persistent homology then captures the long-living topological properties and distinguishes *relevant* information from *noise*.

Definition of persistent homology. For a given network, we choose a filtration into a simplicial complex, i.e.

$$\emptyset = K_0 \subset K_1 \subset \cdots \subset K_n = K$$

Each such K_i is a subcomplex and persistent homology is about the *topological history* when this filtration is being constructed. In other words, we look at the homology at *each* stage of the filtration with respect to the previous steps of the filtration. In [ELZ02] and [ZC05], persistence is defined with respect to cycle and boundary groups of complexes in the filtration. As we already mentioned, the definiton of persistence can be set in the much more general frame of spectral sequences, which we will not follow for the sake of a better intuition. Homology is about capturing equivalent classes of cycles by factoring out the boundary cycles. In other words: the main focus is on *counting* the non-bounding cycles whose *lifespan* is longer than a chosen threshold, i.e. longer than a certain number of *next* filtration steps, cf. [HMR09]. Hence, persistent homology is all about detecting long-lasting topological properties of the complex, hence, of the underlying network. Those cycles, which *survive* through a number of filtration steps, are important. To make this mathematically precise, let Z_k^l and B_k^l represent the kth cycle group and the kth boundary group, respectively, of the lth (sub-)complex K^l in the filtration sequence. See [HMR09] and [ZC05] for further details. Since we are interested in the long-lasting *non*-bounding cycles, we factor the kth cycle group by the kth boundary group p complexes *later* in the filtration, i.e. by K^{l+p}. Formally, we define the p-persistent kth homology group of K^l as

$$H_k^{l,p} = Z_k^l \Big/ \left(B_k^{l+p} \cap Z_k^l \right).$$

This is, of course, well-defined since $B_k^{l+p} \cap Z_k^l$ is a group itself since it is the intersection of two subgroups of C_k^{l+p}. Hence, we can easily define the p-persistent kth Betti number β_k^{l+p}:

$$\beta_k^{l+p} := \text{rank } H_k^{l,p}$$

Note that superscripts indicate the filtration index and are not related to cohomology, cf. [ZC05]. Again, this can be intuitively interpreted as the number of homology classes in the complex K^p which came into existence in the complex K^l or earlier. For each p and for each pair (k, p), $0 \leq k \leq p \leq n$ there is a Betti number. Intuitively, for p large (i.e. long enough), the topological noise may vanish and only pertinent information remains. For further reference on formal aspects, please be referred to [ZC05], [HMR09] and [ELZ02].

Visualization of persistence homology. In order to capture this amount of information it is helpful to visualize the parameterized Betti numbers in an accessible way, see example below. One way to do this is to consider the state of the filtration as time, hence the x-axis depicts the actual filtration step. The y-axis represents the number of non-vanishing simplices, hence the Betti number. The whole diagram represents the evolution of voids (0-dim, 1-dim, 2-dim, 3-dim, etc.) in the simplicial complex as it evolves from the most simple case (only nodes) to the most complicated one, which contains faces of the highest possible dimension.

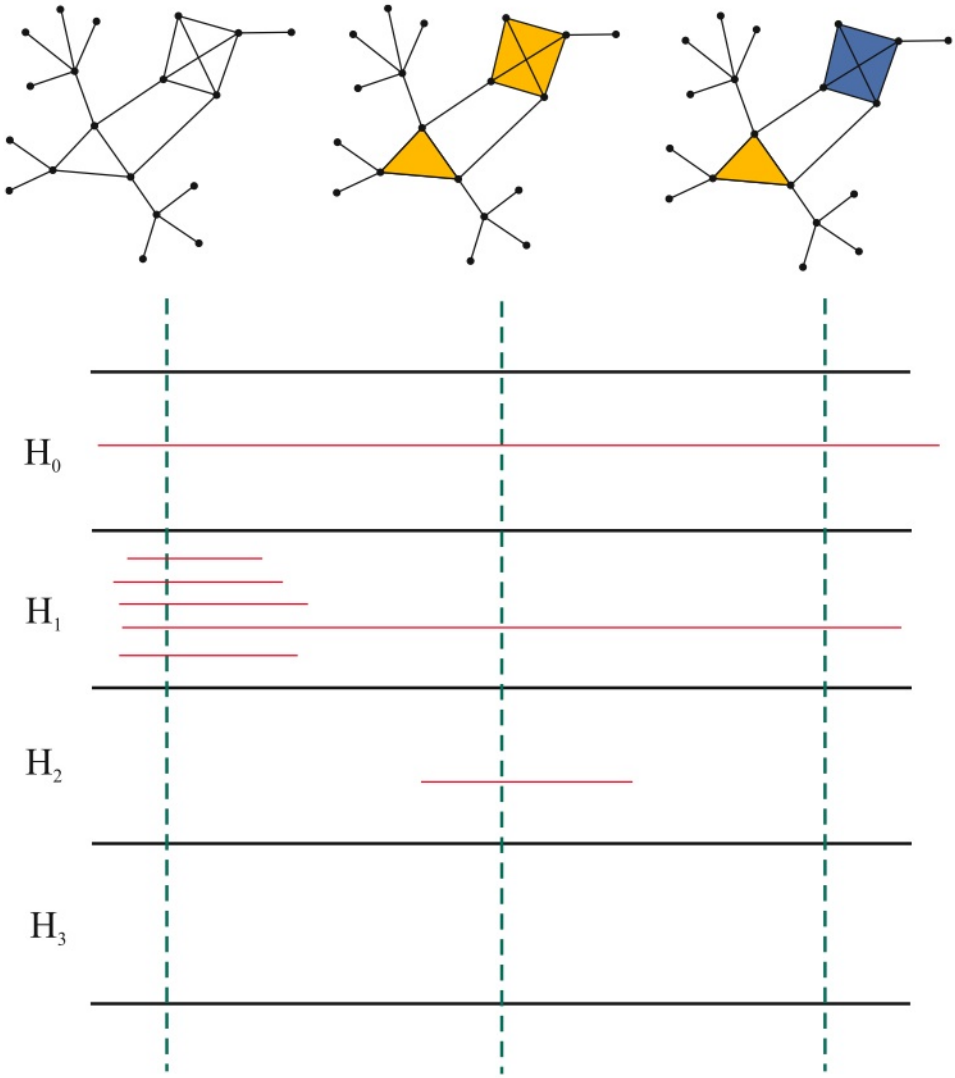

Fig. 3.8: An example of a barcode diagram for some arbitrary simplicial compley, shown above. The rank of H_k equals the number of parameter intervals (=red barcode line). For the sake of simplicity and better readability, the shown filtration deviates from the more complex one which we will use for the brain networks. In step one, we already consider the given network, which by definition is a one-dimensional simplicial complex. Then all possible 2-dim simplices are added at once, leaving a 1-dim void that cannot be filled. The blue tetrahedron is filled in the last filtration step, closing the previously generated 2-dim void. Hence, *this* void should be considered *short*-lived, whereas the remaining 1-dim void is *persistent*. In the context of brain networks we will interpret this as an *obstacle* for informational flow. The only persistent homologies are H_0 and H_1. Copyright: [HMR09].

Chapter 4

Results and Discussion

Statistical network analysis

First we will present the statistical properties of the functional brain networks. These will allow for a global characterization of the network topology, furthermore we will be able to gauge the importance of specific regions, as well as find a shift in local connectivity. Most of the resutls presented here have been included into a joined research paper, cf. [MSB+12] (*under review*).

Please recall the construction process of the functional brain networks, which has been presented in chapter 2. First we analyzed the thresholded, but still anatomically unclustered, networks. For these networks, we computed the largest connected component (LCC). The restriction to the LCC has been deliberately made since the second largest connected component of the networks showed to be negligibly small compared to the LCC. Compared to young individuals, seniors showed a strong increase in the size of the LCC, as well as increased network density and increased transitivity. The following boxplots and table present the statistical parameters, which were computed for the LCC, see Fig. 4.1 and Table 4.1.

By inspection of the parameters, one observes differences in all characterizing statistical parameters. One interesting observation concerns the small-worldness parameter. It is significantly highest for young individuals during working memory processes, being much lower for the episodic memory task, and also much lower for older individuals, independent of the task. The small-worldness parameter quantifies wiring efficiency, i.e. high clustering but short average path length. The largest connected component (LCC)

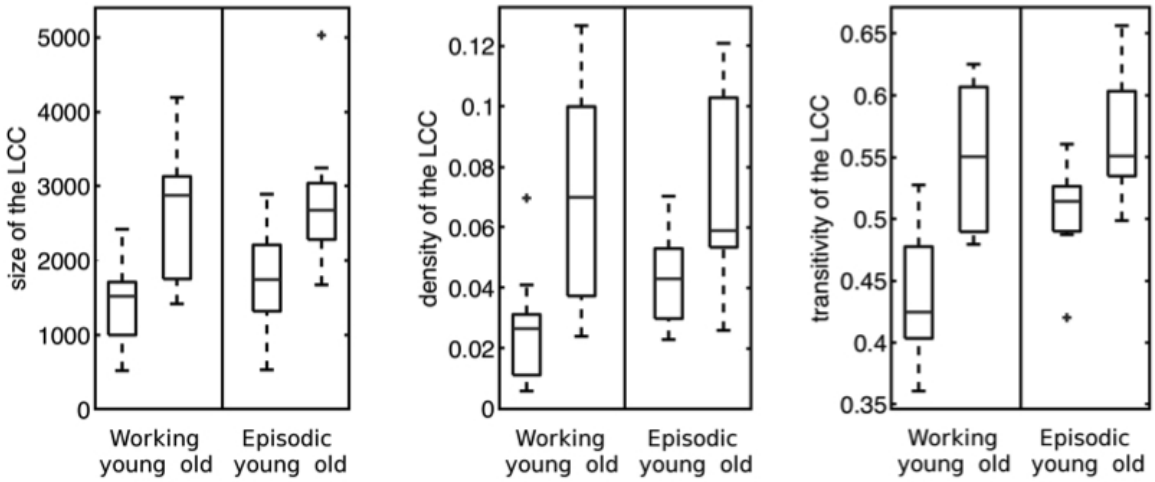

Fig. 4.1: Boxplot of different network parameters: size of the LCC (left), network density (middle) and transitivity (right). See also [MSB+12].

Table 4.1: Statistical parameters for the functional connectivity networks. Shown are the size of the LCC, the density, the average shortest path (asp), transitivity, cost efficiency and small-worldness. Standard deviation is shown in brackets. See also [MSB+12].

	YOUNG	
	working	episodic
size of LCC	1429.80 (± 597.19)	1751.60 (± 675.96)
density	0.03 (± 0.02)	0.04 (± 0.01)
asp	4.41 (± 1.53)	3.41 (± 0.48)
transitivity	0.44 (± 0.06)	0.51 (± 0.04)
cost efficiency	0.42 (± 0.14)	0.32 (± 0.05)
small-worldness	20.58 (± 15.81)	9.29 (± 2.45)
	OLD	
	working	episodic
size of LCC	2642.60 (± 909.49)	2824.10 (± 904.06)
density	0.07 (± 0.04)	0.07 (± 0.03)
asp	3.19 (± 0.62)	3.06 (± 0.51)
transitivity	0.55 (± 0.06)	0.57 (± 0.05)
cost efficiency	0.29 (± 0.06)	0.29 (± 0.05)
small-worldness	7.29 (± 3.44)	6.59 (± 2.47)

of the young individuals' networks is smaller, as well as the young individuals' network density, comparing working and episodic memory tasks. For elderly subjects, there was no such difference observed between the two different memory tasks. Remarkably, the networks of the older individuals exhibit a much larger variability than it is the case for the younger group.

A natural question is how to evaluate the importance of an anatomical structure for the memory processing. From now on, we will consider the anatomically clustered networks. Please see chapter 3 for the clustering process. Briefly restated, we used the Talairach atlas to retrieve anatomical information for each voxel, and each voxel has been assigned to a hemisphere, lobe, smaller gyri structure and, where possible, a Brodmann area. In order to answer the aforementioned question, we computed for every anatomical region its relative hubness, degree and betweenness. We chose to represent the results as bar plots, see Fig. 4.2, 4.3 and 4.4. Due to the different size of the anatomical structures, the resulting values had to be compared to the *expected* value, that is, the value which would result if the parameter distribution were random throughout the entire brain. These expected values are indicated by the solid line. Hence, an anatomical structure is considered important if the parameter, i.e. the line of the bar, is larger than the average, i.e. the bar exceeds the solid line. Naturally, one has to be careful about statements concerning smaller anatomical regions, since these are less reliable due to the fact that a smaller number of voxels enters the statistics. We will therefore focus on the analysis of the medium and large structures.

We defined hubness not only on the basis of the node degree alone, we adapted this measure in as much as to include also the betweenness of the node. This measure was applied to identify important brain areas on the level of lobes and smaller structures.

Fig. 4.2 depicts the relative hubness of the different lobes, both for the left and right brain hemisphere. One can observe that for younger subjects the hubness is rather symmetrically distributed over the two hemispheres, whereas for elderly individuals the left hemisphere exhibits higher relative hubness. In particular, the parietal and the occipital lobes show exceeding hubness, whereas it is less in the limbic lobe.

Fig. 4.3 and Fig. 4.4 depict the relative hubness, the relative degree and the relative betweenness of the smaller structures (gyri) and Brodmann areas. For both age groups and for both memory tasks, the hubs are localized in the parahippocampal, postcentral and middle occipital gyrus. By inspection, one can observe that the working memory

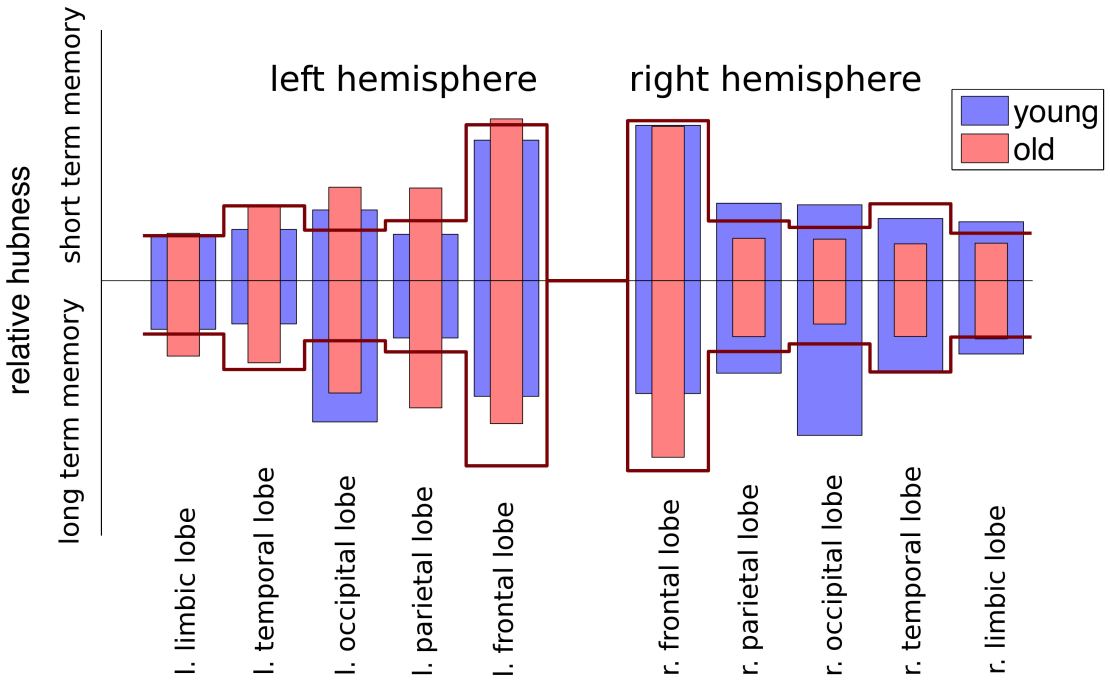

Fig. 4.2: Relative hubness of the different lobes, for the left and right brain hemisphere. The bar plots depict the number of voxels which contain LCC in the given lobes. The solid lines show the *expected*[1] value, relative to the size of the structure. An anatomical region is the more involved into the processing of the memory task the more the bar exceeds the solid line. In collaboration with Franziska Matthäus, see also [MSB+12].

task involves frontal areas, among which are the inferior and medial frontal gyrus, as well as parietal/occipital areas, especially the cuneus and the middle occipital gyrus. For the episodic memory task, it can be seen that a large number of parietal and occipital areas are involved, e.g. the cuneus, the precuneus (old), and fusiform gyrus (young). Moreover, the thalamus exhibits increased hubness, in particular for young individuals.

The diagrams also allow for a classification of the different regions regarding their role in memory processing. The postcentral gyrus, in particular for the young individuals during the working memory task, clearly plays the role of a regulator / effector.[1] This

[1]A node is called regulator / effector if it has a high degree because its activity correlates with a large number of other nodes. One reason for this can be that this node regulates the activity of other regions (regulator), or is dependant on the activity of many other nodes (effector). Nodes possessing a high degree often also exhibit a high betweenness.

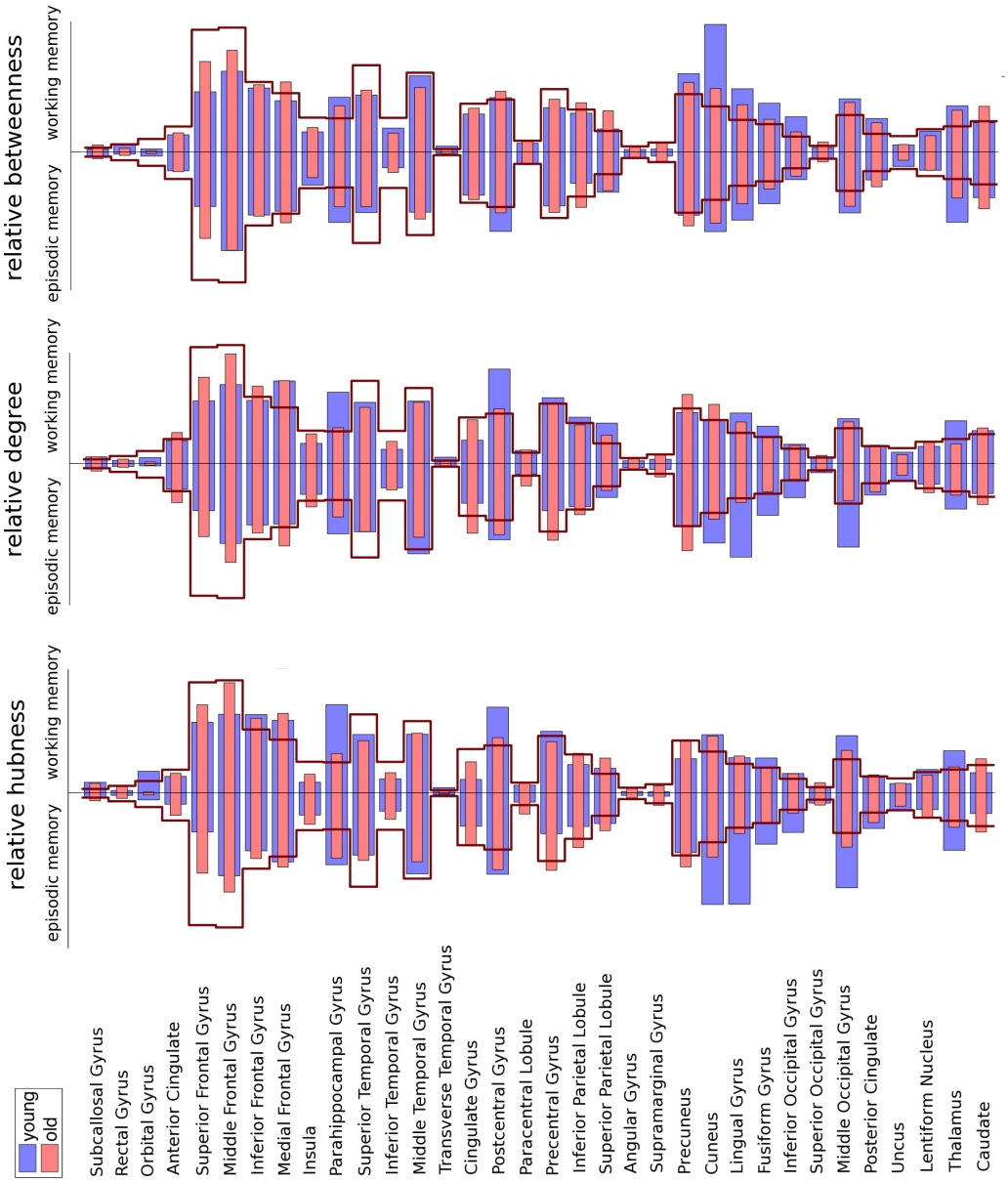

Fig. 4.3: Relative hubness (left), relative degree (middle) and relative betweenness (right) of the different gyri structures, for both working and episodic memory. The bar plots depict the number of voxels which contain LCC in the given lobes. The solid lines show the *expected* value, relative to the size of the structure. An anatomical region is the more involved into the processing of the memory task the more the bar exceeds the solid line. In collaboration with Franziska Matthäus, see also [MSB+12].

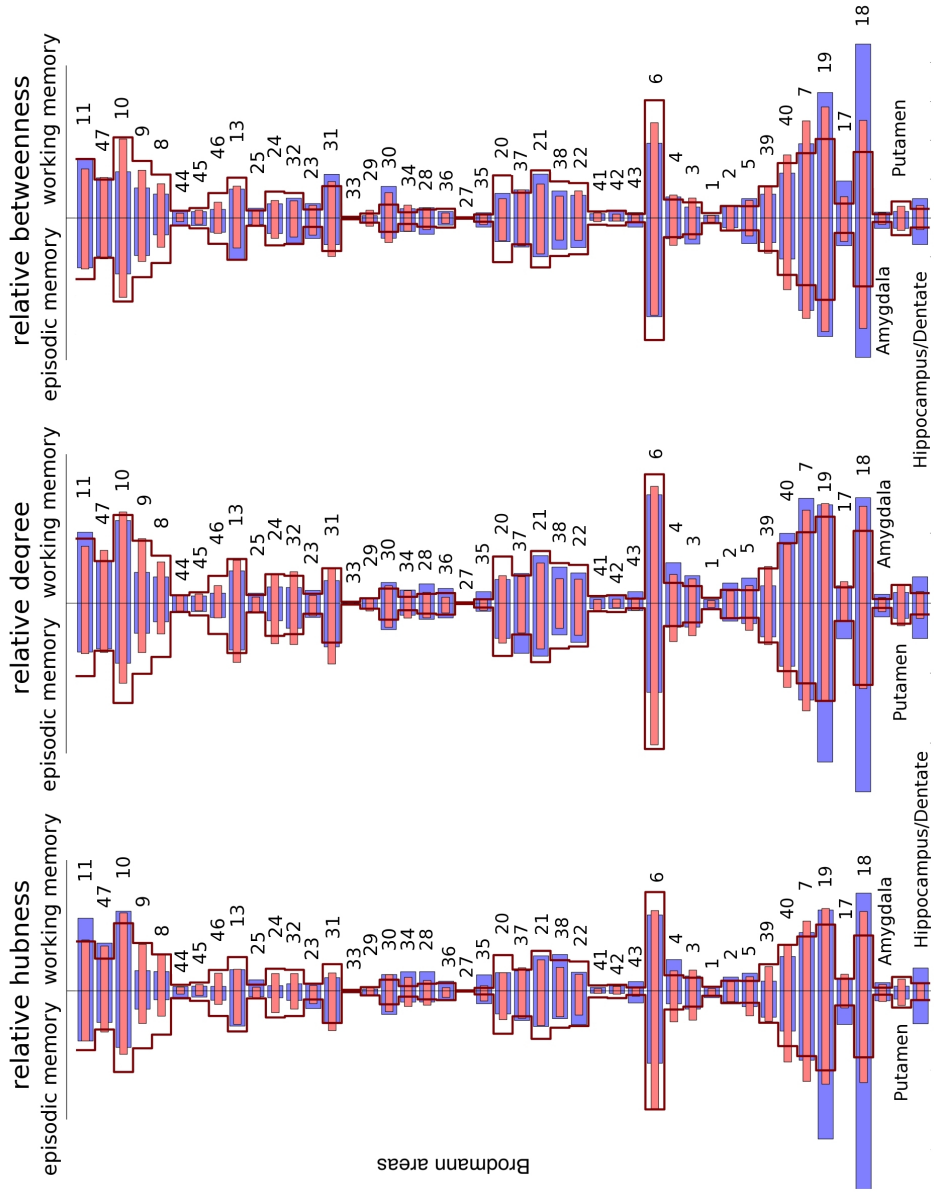

Fig. 4.4: Relative hubness (left), relative degree (middle) and relative betweenness (right) of the different Brodmann structures, for both working and episodic memory. The bar plots depict the number of voxels which contain LCC in the given lobes. The solid lines show the *expected* value, relative to the size of the structure. An anatomical region is the more involved into the processing of the memory task the more the bar exceeds the solid line. In collaboration with Franziska Matthäus, see also [MSB+12].

is indicated by the higher degree. On the other hand the cuneus (BA 19) and the precuneus (also for young subjects during working memory task) can be classified as betweenness hubs.[2]

In order to visualize the network structure we proceeded as follows: the number of links was counted within and between all anatomical regions and for all networks, i.e. for all networks of the same age group and memory task. Then we normalized the inter- and intraregional connectivites by the expected number of links for random wiring, i.e. we used the following normalization factor: let p be the probability to find an edge between two nodes in a random network, then the expected number of intraregional links is given by $pN(N-1)/2$, for a region of size N. Hence, the expected number of edges between two regions of size N and M, respectively, is given as pMN.

Fig. 4.4, 4.5 and 4.6 display the network visualization on the lobe, gyri and Brodmann level, respectively. By inspection, one can clearly observe large differences between the network structures of the two age groups, but, moreover, there are also differences between the two memory tasks within an age group. On the lobe level, young subjects show rather intense connections between the left and right occipital lobes, and between the left and right parietal lobes. However, the network structure in this age group is very symmetric. For elderly individuals we also observe these connections but they are dominated by a very strong connection beween the left parietal lobe and other lobes in the left hemisphere. Moreover, the left parietal and left occipital lobe exhibit a much stronger internal connectivity than their counterparts in the right hemisphere.

On the gyri stucture level we observe a strong connection of the parahippocampus with many other, particularly occipital, areas. The strongest connection can be found between the postcentral gyrus and the superior parietal lobule (young, working memory), middle and inferior occipital gyrus (both age groups), superior parietal lobule and precuneus. For both age groups and both memory tasks there is a strong parietal and an occipital cluster to be found. In addition, the frontal gyri in elderly subjects' networks show a much stronger internal connectivity.

[2]A betweenness hub is characterized by a high betweenness but not necessarily by a high degree. It can be considered as a connector / relay since it itself is not connected to many other nodes, but it controls a large portion of paths travelling through this node.

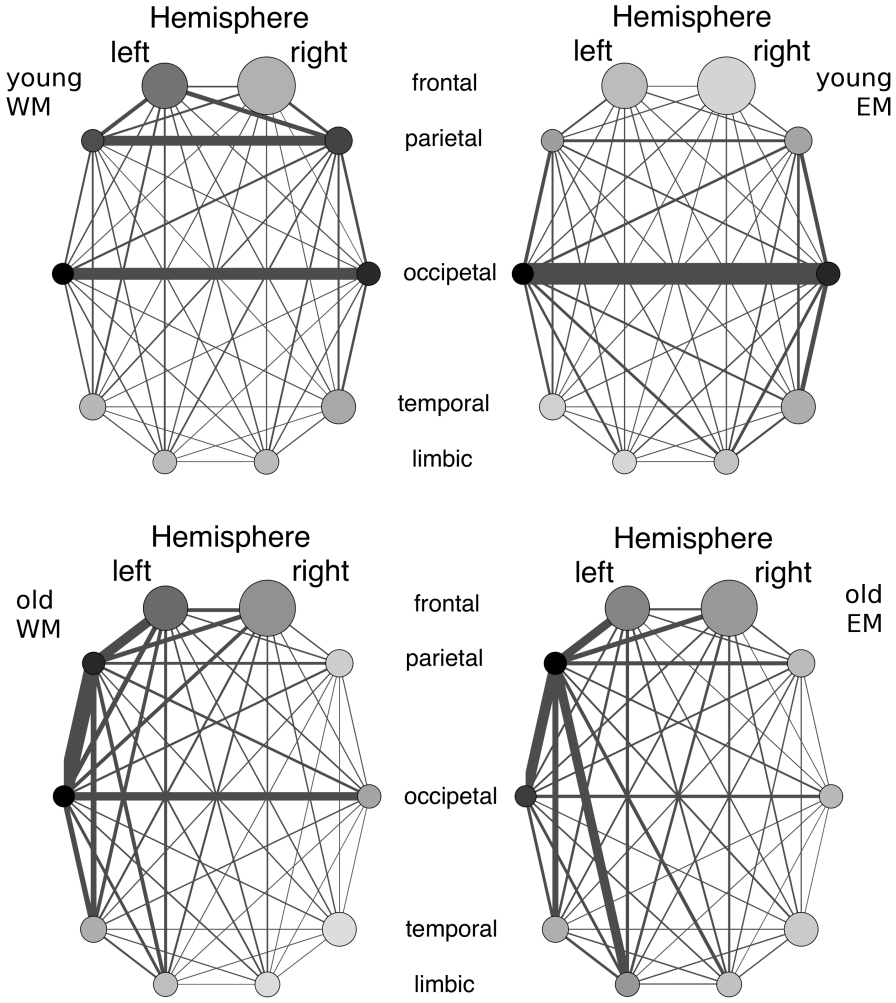

Fig. 4.5: Network visualization on the lobe level. Size of the nodes is proportional to the size of the anatomical region, the line thickness indicates the strength of the connection, and the shading of the nodes represents the density of the intraregional connections (dark = high intensity, bright = low intensity). Moreover, WM = working memory and EM = episodic memory. In collaboration with Franziska Matthäus, see also [MSB+12].

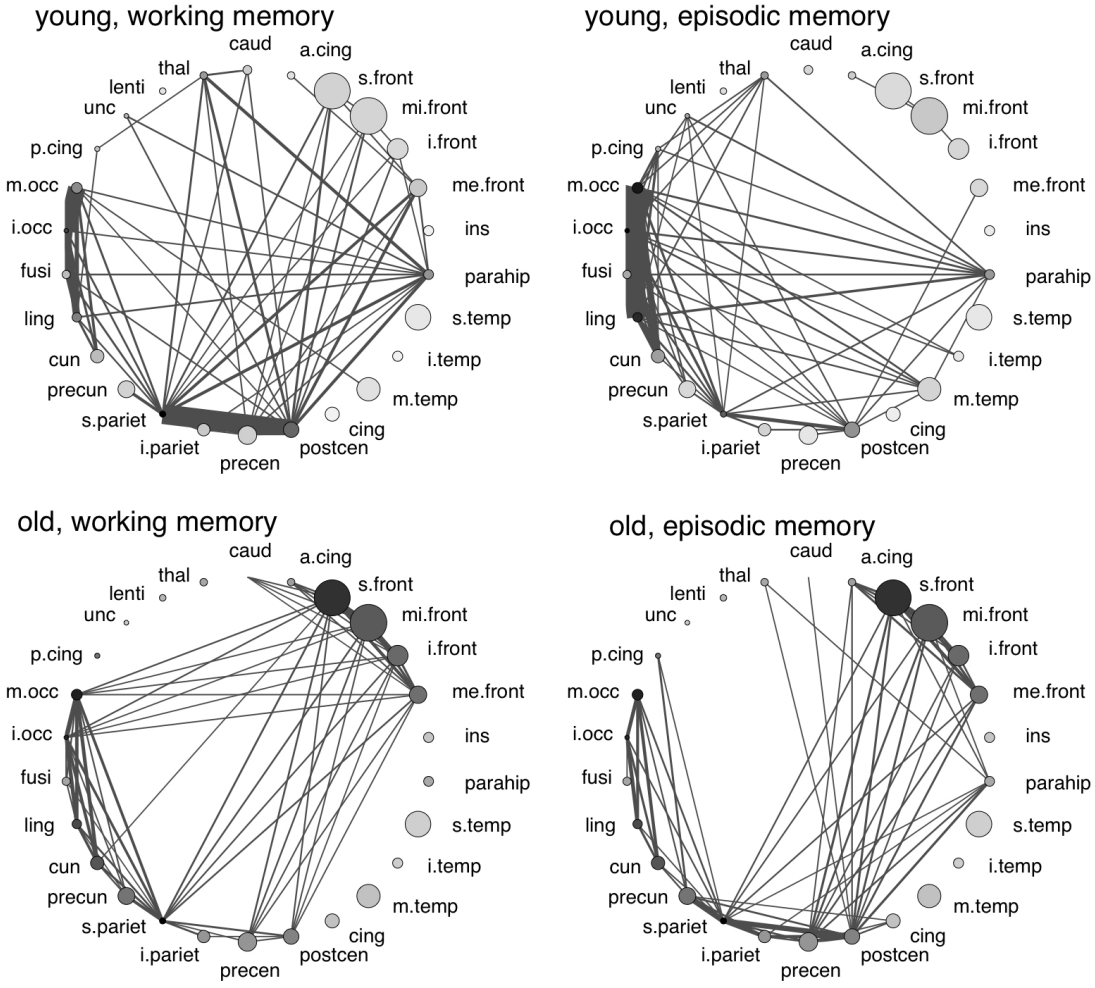

Fig. 4.6: Network visualizaion on the gyri level, whereas only the strongest links are displayed. All networks exhibit parietal and occipital clusters. For the elderly subjects, we additionally observe a frontal cluster. Size of the nodes is proportional to the size of the anatomical region, the line thickness indicates the strength of the connection, and the shading of the nodes represents the density of the intraregional connections (dark = high intensity, bright = low intensity). For elderly subjects, the pattern is more symmetric, having strong inter- and intra-connected clusters at *a. cing* , *s. front*, *mi. front* and *i. front*. Please find a list of abbreviations in the supplement. Younger individuals show a much more heterogenous pattern, having a focus in the parietal /postcentral region for the working memory and similarly in the occipital / fusiform region for the episodic memory. In collaboration with Franziska Matthäus, see also [MSB+12].

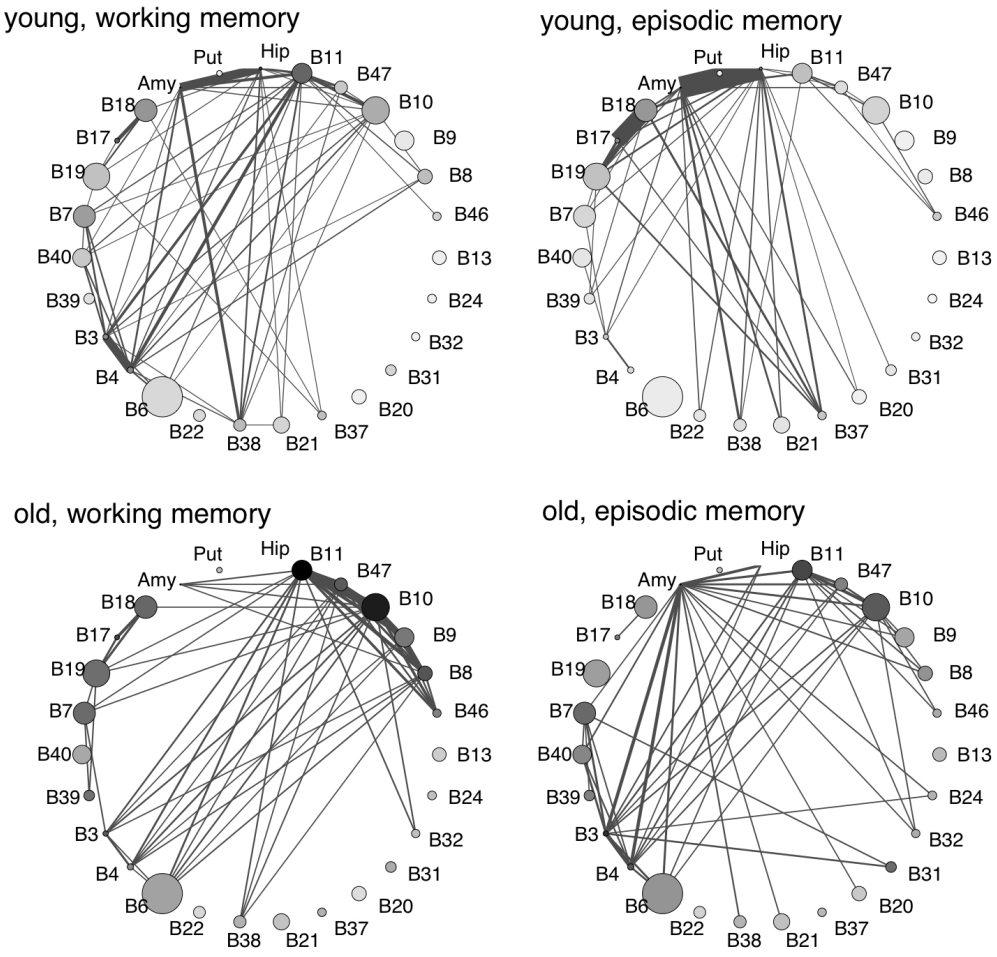

Fig. 4.7: Network visualizaion on the Brodmann level, whereas only the strongest links are displayed. All networks exhibit clusters in BA 10, BA 11, BA 47 as well as BA 6. The region BA 10 is more prominent in the networks of older subjects, with respect to both inter- and intraregional connectivity. Moreover, the difference between the two age groups are bigger for the episodic memory task. One observes that for younger individuals there are more interregional connections between BA 17−19 and BA 37, whereas for elderly subjects there is a shift towards interregional connections, BA 3−4 and BA 6 and BA 10−11 and BA 47. In particular, the region BA 6 is much more interregionally involved in the networks of older individuals than this is the case for younger subjects, independent of the memory task. In collaboration with Franziska Matthäus, see also [MSB+12].

Summary and discussion of key results, see also [MSB$^+$12]:

- Age-related differences in the statistical network properties:

  Networks of older individuals were characterized for both memory tasks by a larger LCC, in size and density. Transitivity was also increased, whereas the average shortest path length was lower compared to the young individuals. The structural changes were evident for both memory task, but more apparent for the working memory task. The greater size of the LCC for the elderly subjects can be explained by an extended activity pattern. Many studies have reported that elderly individuals recruit more brain areas during working memory tasks (and similar findings are available for episodic memory). Studies with transcranial magnetic stimulation suggest that over-activation is related to compensatory mechanisms, and a better performance is correlated with the extent of over-activation. On the other hand, the extended activation also accompanies pathological changes. Another, maybe complementary process, is believed to be a progressive dedifferentiation, where brain areas become less specialized with age and start to engage in new functions. Small-worldness is a measure for effective information processing and we found it to be largest for the young subjects under working memory demand. In general, small-worldness and cost-efficiency were reduced in elderly individuals, which is in agreement with previous results for resting state networks. Hence, we can generalize this result to working memory networks.

- Age-related differences in the hub structure of the functional connectivity:

  Concerning the lobes, cf. Fig. 4.5, we found hubs for the young subjects in the occipital, parietal and limbic lobe. Here, the distribution of the hubness was very symmetric for both memory tasks. Seniors showed the largest hubness in the occipital and parietal lobe, with a very strong asymmetry towards the left hemisphere. For the episodic memory task also the left limbic lobe exhibited hubness. In the young subjects hubness concentrated in frontal and less in occipital areas for the working memory task. For the episodic memory task the frontal areas were less, and the occipital areas much stronger involved. Seniors showed additional hubness centers in parietal areas, and decreased hubness in occipital areas, especially for the episodic memory task. Our

hubness pattern is in good agreement with most findings recent studies, see [MSB+12] for details.

- Age-related differences in the network connectivity structure:

  Very symmetric connection patterns have been found between the two hemispheres for young individuals, the strongest links being between the left and right occipital, and the left and right parietal lobes. The occipital lobes play a crucial role in the processing of visual information, which is the form in which the memory tasks are presented. The involvement of parietal areas in memory processing, especially in elderly individuals, has been shown before, and is hypothesized to relate to attention processes, see also [MSB+12]. The networks of elderly individuals exhibited a strong asymmetry, particularly focused on the left parietal lobe. Our results are in good agreement with previous findings, reporting a higher connectivity in frontal, and a reduced connectivity in posterior areas for seniors compared to young subjects, see [MSB+12] for references.

Statement: Our findings about the age-related reorganization can be explained by two different hypotheses: *overactivation* and *dedifferentiation*. Over-activation implies that additional structures are being involved in brain memory processes as a result of compensatory purpose. Dedifferentiation means that brain areas loose their specific task with ageing and engage in new and different tasks. We found that the hubness of the "young" networks was specific, in contrast to that of elderly individuals, which was distributed over a larger area. Moreover, networks for elderly individuals showed additional regions with increased hubness, which very well agrees with previous studies, see [MSB+12] for further reference.

Spectral analysis

In this section we present the results from the spectral graph analysis. Again, as stated already in the previous section we will consider the anatomically clustered networks for this analysis: the lobe network (size n=10), the gyri network (n=26) and the Brodmann network (n=27). First we will show the spectral plots for these networks, for each age group and both memory tasks. These plots will allow for a classification of the functional brain networks, in particular with respect to structural differences of networks from other domains and, for future research, to structural networks coming from tensor imaging analysis. Please recall the spectral methods presented in chapter 4. We will use a Gaussian kernel for smoothing the spectral distributions, hence we plot

$$f(x) = \sum_{\lambda_j} \frac{1}{\sqrt{2\pi\sigma^2}} \exp\Big(- \frac{|x - \lambda_j|^2}{2\sigma^2} \Big) \, .$$

whereas we set $\sigma = 0.01$ for all plots.

The spectral plots for the anatomically clustered networks, i.e. Lobe, Gyri and Brodmann level, are depicted in Fig 4.8, 4.9 and 4.10. One observes that on all levels, the spectra become more homogenous for the older age group, independent of the memory task. Moreover, the networks of both age groups and both memory tasks do not exhibit symmetry around 1, as it is the case, for example, for protein-protein interaction networks, see [BJ07]. The networks for older subjects do exhibit a higher peak around 1 as it is the case for younger individuals, independent of the memory task. The most prominent property of all networks, next to the non-existing symmetry, is the shift to the left. As we will point out in the discussion and outlook chapter, this could be a starting point for further analysis.

The spectral plots have been computed because they allow an easy *visual* distinction. They should be thought of as a coarse *fingerprint* of the networks. This method has been introduced by *Jürgen Jost* in [BJ07] and [BJ08]. To our knowledge, this method has not been applied to functional brain networks before and our findings fit very well into the classification zoo, which has been suggested by Jost and Banerjee, see also [BJ07], [BJ08] and [Ban08a]. As we can deduce from there, the spectral plots of the functional brain networks exhibit general similarities with biological networks, e.g. the high and prominent peak around the eigenvalue 1. However, they are distinct enough to build their own class. Future research should analyze the structural distinctions in

detail.

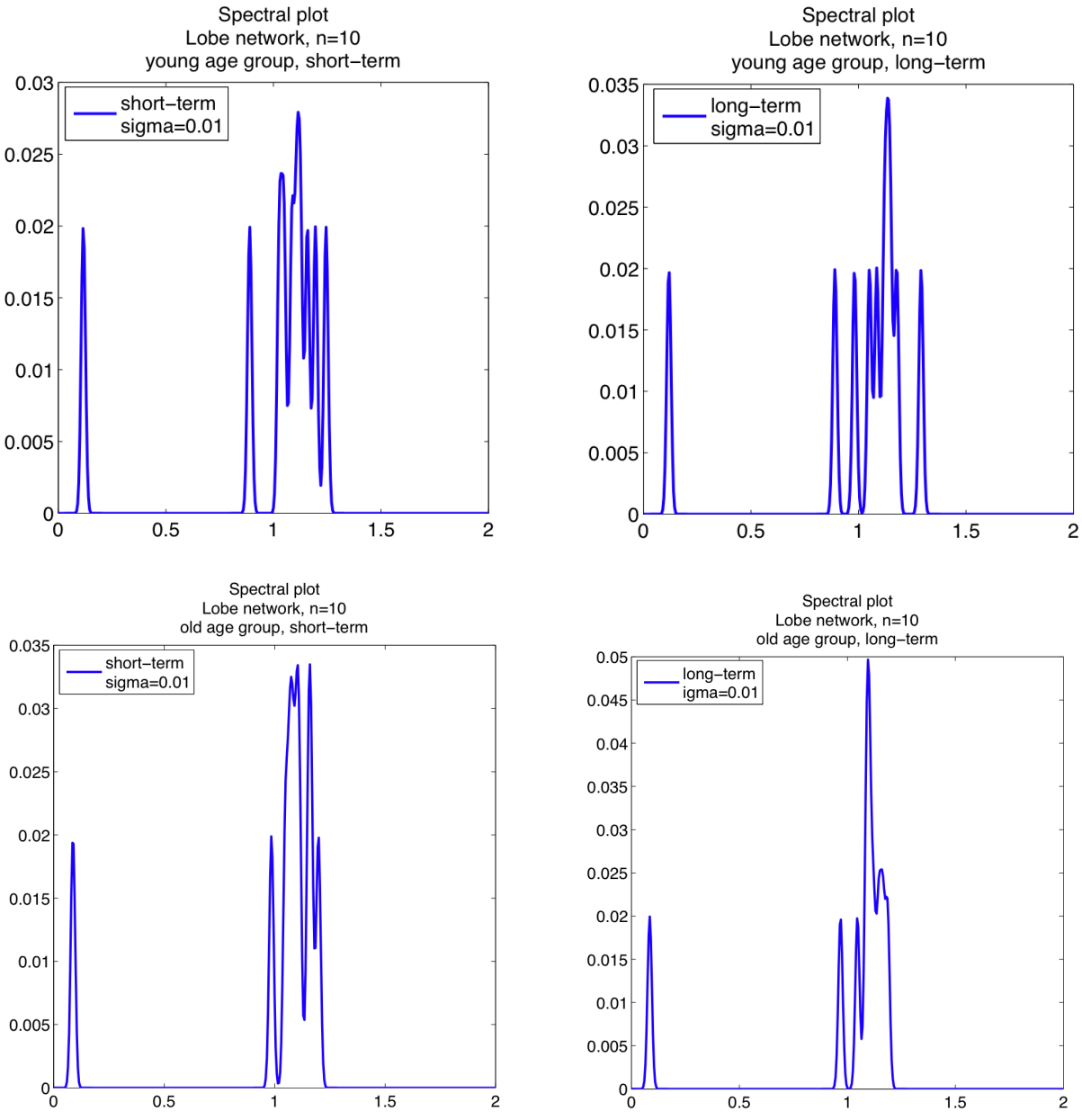

Fig. 4.8: Spectral plots of Lobe level networks, n=10. We used $\sigma = 0.01$ in all network plots as parameter for the Gaussian kernel. Comparing the two age groups and two memory tasks, the most distinguishing facts are the more homogenous spectra for elder individuals and, in particular, the high peak in the old age group, long-term memory. Moreover, all spectral plots do not exhibit symmetry around 1. Instead, one observes a shift to the left.

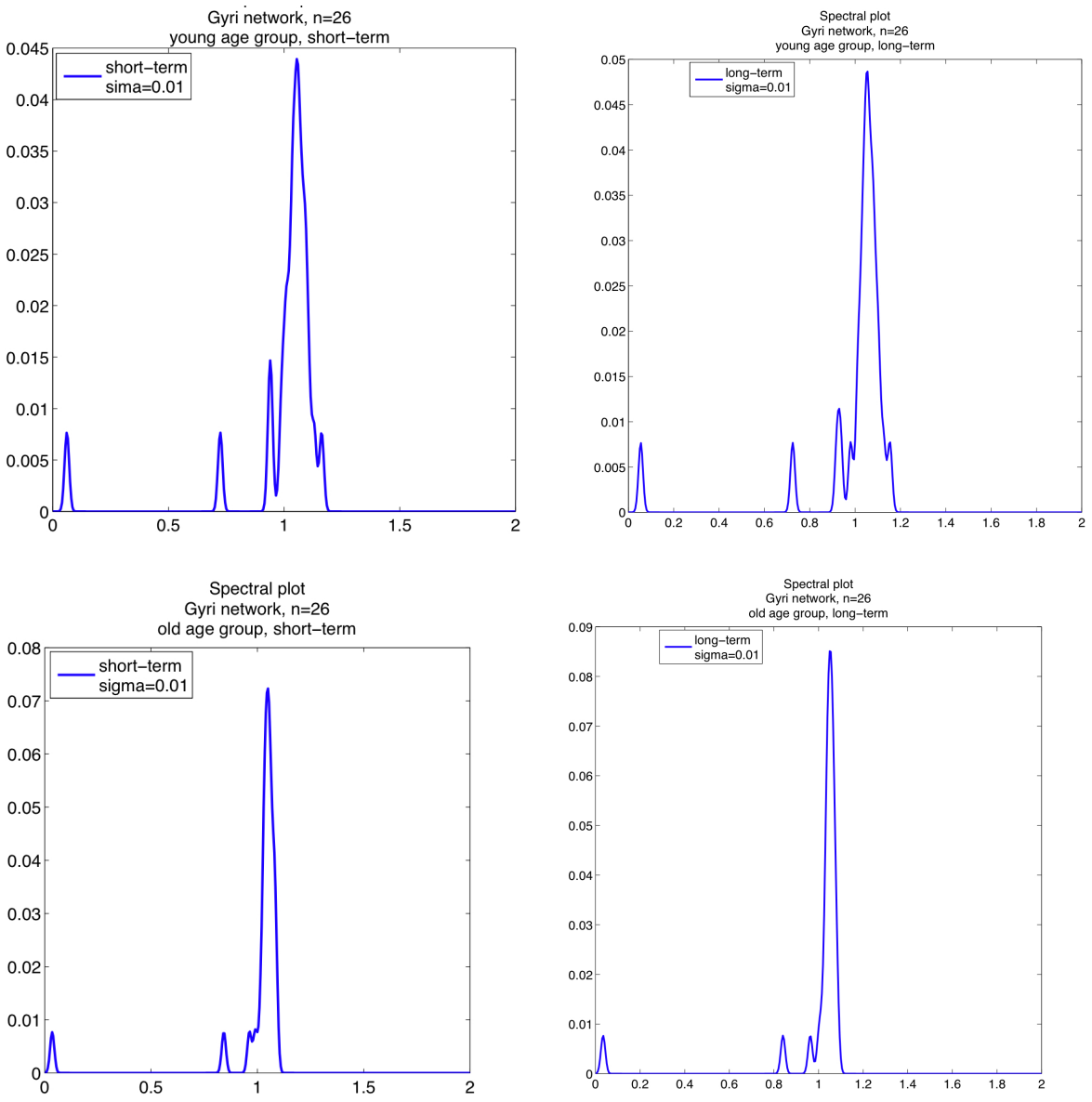

Fig. 4.9: Spectral plots of Gyri level networks, n=26. We used $\sigma = 0.01$ in all network plots as parameter for the Gaussian kernel. Compared to the Lobe level spectra, the Gyri spectra are more homogenous, in particular for the older individuals, independent of the memory task. Moreover, all spectral plots do not exhibit symmetry around 1. Instead, one observes a shift to the left, as it is the case for the Lobe level spectra. The high peak around 1 now appears for both memory tasks in the elderly subjects' networks.

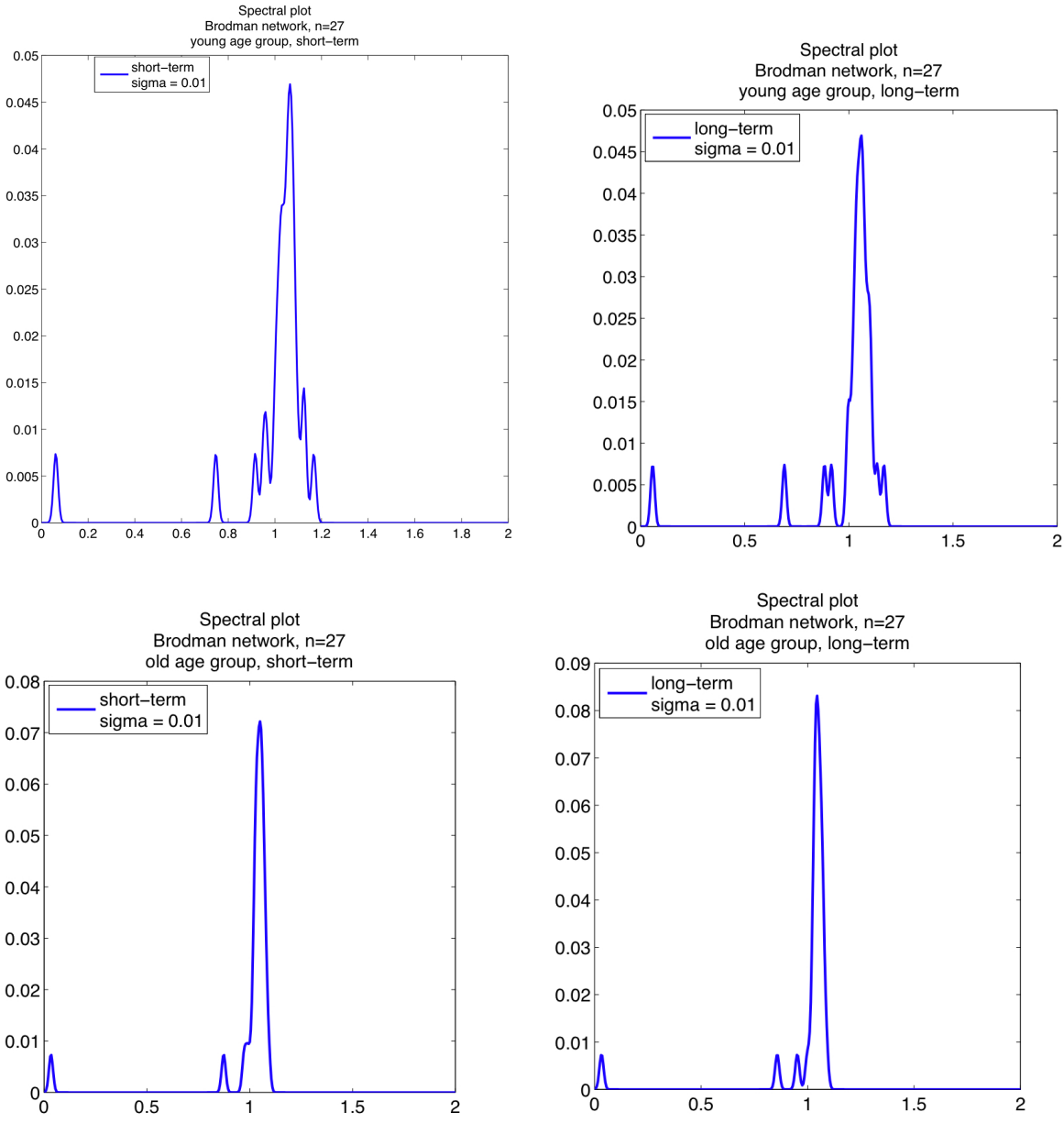

Fig. 4.10: Spectral plots of Brodmann level networks, n=27. We used $\sigma = 0.01$ in all network plots as parameter for the Gaussian kernel. Similarly to the Gyri level spectra, the Brodmann spectra for the older individuals are more homogenous, independent of the memory task. Moreover, all spectral plots do not exhibit symmetry around 1. Instead, one observes a shift to the left, as it is the case for the Lobe level spectra. As it is the case for the Gyri spectra, the high peak around 1 now appears for both memory tasks in the elderly subjects' networks.

We used Jenson-Shannon divergence (JS) in order to quantify the distance between the networks, in particular:

$$D(\Gamma_1, \Gamma_2) = \sqrt{JS(f_1, f_2)}$$

Please see chapter 3 for the exact definition of the JS metric. Of course, it makes only sense to compare the networks of one coarse-graining level with each other, i.e. Lobe, Gyri and Brodman networks seperately. The results are shown in Table 4.2, 4.3 and 4.4.

Network	$\Gamma_{Lobe,WM,young}$	$\Gamma_{Lobe,WM,old}$	$\Gamma_{Lobe,EM,young}$	$\Gamma_{Lobe,EM,old}$
$\Gamma_{Lobe,WM,young}$	0.0000	0.4438	0.3952	0.4474
$\Gamma_{Lobe,WM,old}$	0.4438	0.0000	0.4354	0.2567
$\Gamma_{Lobe,EM,young}$	0.3952	0.4354	0.0000	0.4257
$\Gamma_{Lobe,EM,old}$	0.4474	0.2567	0.4257	0.0000

Table 4.2: Jensen-Shannon divergence measure for the networks at Lobe level, whereas WM = working memory, EM = episodic memory.

Network	$\Gamma_{Gyri,WM,young}$	$\Gamma_{Gyri,WM,old}$	$\Gamma_{Gyri,EM,young}$	$\Gamma_{Gyri,EM,old}$
$\Gamma_{Gyri,WM,young}$	0.0000	0.3495	0.1324	0.3791
$\Gamma_{Gyri,WM,old}$	0.3495	0.0000	0.3345	0.0897
$\Gamma_{Gyri,EM,young}$	0.1324	0.3345	0.0000	0.3629
$\Gamma_{Gyri,EM,old}$	0.3791	0.0897	0.3629	0.0000

Table 4.3: Jensen-Shannon divergence measure for the networks at Gyri level, whereas WM = working memory, EM = episodic memory.

Network	$\Gamma_{Brod,WM,young}$	$\Gamma_{Brod,WM,old}$	$\Gamma_{Brod,EM,young}$	$\Gamma_{Brod,EM,old}$
$\Gamma_{Brod,WM,young}$	0.0000	0.3531	0.2584	0.3593
$\Gamma_{Brod,WM,old}$	0.3531	0.0000	0.3358	0.1556
$\Gamma_{Brod,EM,young}$	0.2584	0.3358	0.0000	0.3715
$\Gamma_{Brod,EM,old}$	0.3593	0.1556	0.3715	0.0000

Table 4.4: Jensen-Shannon divergence measure for the networks at Brodman level, whereas WM = working memory, EM = episodic memory.

The most intriguing fact we observe from the tables is that the structural distance between the networks for different memory tasks (within the same age group) becomes much smaller with age, in particular:

$$D(\Gamma_{Gyri,WM,young}, \Gamma_{Gyri,EM,young}) = 0.1324 \; > \; 0.0897 = D(\Gamma_{Gyri,WM,old}, \Gamma_{Gyri,EM,old})$$

The relation holds true for Lobe level and Brodmann level networks as well. Hence, this means that the networks not only change their structure with age, but also converge together structurally. In other words, the functional networks for senior individuals are much more similar to each other than this is the case for young subjects. Of course, when interpreting these results we have to bear in mind that the data, which we base our analysis on, come from a cross-sectional study. Hence, theoretically, it could be the case that the structural changes are due to a bias in the population sample. However, there is no evidence for such a bias and we (globally) assume our methods are applicable.

Synchronizability analysis. We evaluated the synchronizability of the clustered functional brain networks, i.e. we computed the eigenratio $\frac{\lambda_2}{\lambda_{N-1}}$. This ratio is a proxy for the synchronizability of networks and holds for a large class of functions. The only assumptions needed are continuous differentiability for the dynamics applied to the nodes, as well as a compact chaotic attractor. Please see chapter 3 for details. The results of this analysis are shown in Table 4.5, 4.6 and 4.7. We can read from the tables that synchronizability of the networks increase with age, independent of the memory task. This holds true for all levels: Lobe, Gyri and Brodmann. Hence we can state that the functional networks for senior individuals allow for a much faster synchronization than it is the case for younger individuals.

Network	$\Gamma_{Lobe,WM,young}$	$\Gamma_{Lobe,WM,old}$	$\Gamma_{Lobe,EM,young}$	$\Gamma_{Lobe,EM,old}$
Synchronizability	0.7147	0.8225	0.6899	0.8162

Table 4.5: Synchronizability measure for the networks at Lobe level, whereas WM = working memory, EM = episodic memory.

Network	$\Gamma_{Gyri,WM,young}$	$\Gamma_{Gyri,WM,old}$	$\Gamma_{Gyri,EM,young}$	$\Gamma_{Gyri,EM,old}$
Synchronizability	0.6231	0.7738	0.6281	0.7757

Table 4.6: Synchronizability measure for the networks at Gyri level, whereas WM = working memory, EM = episodic memory.

Network	$\Gamma_{Brod,WM,young}$	$\Gamma_{Brod,WM,old}$	$\Gamma_{Brod,EM,young}$	$\Gamma_{Brod,EM,old}$
Synchronizability	0.6402	0.8012	0.5906	0.7881

Table 4.7: Synchronizability measure for the networks at Brodmann level, whereas WM = working memory, EM = episodic memory.

Entropy analysis. We computed the Shannon entropy for the clustered functional brain networks. Please recall that we defined the entropy as

$$H(\hat{P}) = -\sum_{i,j} \pi_i \hat{p}_{ij} \log \hat{p_{ij}} = \sum_i \pi_i H_i$$

whereas H_i is the standard Shannon entropy defined for each node i and π_i are the components of the stationary distribution, see [MDV04] or chapter 3 for a formal definition. The results for the different networks are listed in table 4.8:

Network Γ	Entropy H
Brodmann, old, episodic	$H = 4.5514$
Brodman, old, working	$H = 4.505$
Brodman, young, episodic	$H = 4.0010$
Brodman, young, working	$H = 4.1212$
Gyri, old, episodic	$H = 4.5960$
Gyri, old, working	$H = 4.4644$
Gyri, young, episodic	$H = 3.7790$
Gyri, young, working	$H = 4.1111$
Lobe, old, episodic	$H = 3.0994$
Lobe, old, working	$H = 3.038$
Lobe, young, episodic	$H = 2.7695$
Lobe, young, working	$H = 3.114$

Table 4.8: Entropy values of the different networks. The potential Φ has been normalized in order to allow for a comparison.

From these results we can see that

$$H(\Gamma_{episodic,old}) \approx H(\Gamma_{working,old})$$

$$H(\Gamma_{episodic,young}) < H(\Gamma_{working,young})$$

whereas we denote by $H(\Gamma)$ Shannon entropy measure for the networks, accordingly. The two relations above hold true for all levels: Lobe, Gyri, Brodman. Besides this result we have in general:

$$H(\Gamma_{old}) > H(\Gamma_{young})$$

whereas only lobe level (and only for working memory) is an exception, which might be considered as an outlier due to the very coarse structure at this anatomical level ($n = 10$).

The results of the entropy analysis can be interpreted as follows: the networks of older individuals are more *noisy* than the networks of younger subjects. However, we can tell from the entropy-robustness principle that older networks are more robust, i.e. they exhibit a faster approach to steady state. This result is very intuitive since, in general, we can think of a brain state as a certain activity pattern which arises after some input signal and/or processing. This is then the steady state, and older people are capable of reaching this steady faster than younger people. Hence, this can be read as follows: during ageing the brain builds certain *well trotten trails*, which are easier to reach for older people after there has been some input signal. On the other hand, the network of younger people might be more flexible and can more easily deviate from these *paths*.

Summary and discussion of key results:

- The spectral plots of all networks are asymmetric about 1 and exhibit a shift to the left. Spectral plots of older individuals become more homogenous, independent of the memory task. The spectral plots fit well into the classification scheme of network spectra, suggested by *Jürgen Jost* in [BJ07], [BJ08]. The brain functional networks exhibit a similar spectral plot as other biological networks, e.g. high peak around the eigenvalue 1, but there are sufficiently distinct and network generation principles should be examined in future research.
- The Jenson-Shannon divergence measure quantifies the structural distance and reveils that the networks of both memory tasks become structurally similar with age, i.e. the working and episodic memory networks converge in their structure, from young age to older age.

- The networks of senior individuals allow for a much better synchronizability than it is the case for younger subjects. Synchronizability can be gauged by two important eigenvalues from the Laplacian spectrum, and as we showed in the theoretical part (chapter 3), applies to a broad class of possible functions governing the dynamics. However, synchronizability is not easy to interpret in the case of functional brain networks since these networks arise from correlation networks. In order to interpret synchronizability, we consider the edges in the correlation network, i.e. the high-correlation links as *static* and as the only possible way for informational flow between the network nodes. The result is in good agreement with the entropy result since older networks, i.e. *well trotten trails* should be faster to synchronize.

- The networks of older people exhibit a higher entropy, i.e. older networks are more *noisy* than younger ones. This corroborates very well our hypothesis of over-activation, since these *noisier* networks exhibit more redundancy. On the other hand, from the entropy-robustness principle we can tell that older networks are more robust, i.e. they exhibit a faster approach to steady state.

Statement: We postulate that life-long learning, i.e. neural rewiring, describes a process to ever increasing entropy for the brain connectivity patterns. In other words, older networks are *noisier* than younger ones. On a physiological level, old networks are much more vulnerable in terms of cell defects (e.g. increased oxidative stress) but this vulnerability is much better accepted by high-entropy networks, see entropy-fluctuation theorem in chapter 3. Hence, neural ageing can be described as an evolution to evolvability.

Persistent homology

In this section we will present the results obtained by the algebraic topological method. We use persistent homology to analyse the networks, please see chapter 3 for the definition. We will consider the anatomically clustered networks at lobe, Gyri and Brodmann level. Please recall that these networks are represented by weighted and normalized networks, see also the visualizations in Fig. 4.5, 4.6 and 4.7.

Computing persistent homology requires a filtration and we use the following algorithm, which we already stated in chapter 3:

(1.) all nodes exist already at the beginning of the filtration, being 0-simplices.

(2.) we pick a start node v_0, the choice of this *seed* node remains arbitrary but we keep this choice fixed for all networks.

(3.) 1-dimensional simplex is added to this node, then 2-dim, 3-dim, etc. (up to the highest possible dimension at this step).

(4.) at each filtration step we add one more node, once we have three nodes we may add the face of a triangle, similarly in higher dimensions.

(5.) these steps are iterated until all 0-simplices have been included and all simplices have been added up to the highest possible dimension.

Note that the choice of the seed node remains arbitrary but keeping the choice of this node fixed for all networks allows for a comparison. Moreover, the actual choice is rather unimportant since we are only interested in qualitative features of the networks. As the results show this method is very fine and detects subtle changes in the structure while distinguishing from noise at the same time. Since we will restrict ourselves on presenting the results for the Gyri level networks, we will give a detailed interpretation for these results, bearing in mind that it is completely analogous for the other networks.

We chose as seed node v_0 the first node in the clustered connectivity matrix of the network. The visualization of this network is shown in Fig. 4.6, starting at top and going clockwise. Of course, this is not the only possible filtration, however, we believe that it is appropriate since it reflects well the possible dynamics of the network. Ideally, one would like to know the exact sequence how the network was built but this certainly

does not apply to our case where the network was obtained from correlations of time series. However, this method can be seen as a proxy to detect the (dynamic) evolution of the network. As explained in chapter 3, persistent homology detects long-living topological properties.

The graph of the persistent homolgy (PH), which is also called homology barcode, consists of the time (x-axis) which quantifies the state of the simplicial complex (SC). The y-axis represents the simplices whose number may be read off the digram. Hence, the whole diagram represents the evolution of voids (0-dim, 1-dim and so on) in the simplicial complex, as it evolves from the most simple case (just nodes) to the most comlicated one containing faces of the highest possible dimension.

Computation was performed with MATLAB, using the JPLEX package, provided as free software from `http://comptop.stanford.edu/u/programs/jplex/`, see also the theoretical section on this in chapter 3. It can be shown that the persistent homology of a filtered simplicial complex is simply the standard homology of a particular graded module over a polynomial ring, cf. [ZC05]. At the end of this section we include the complete list containing the number of the simplices of different dimensions that appear in the filtration.

When reading the homology plots one has to bear in mind that we analyse the anatomically clustered and weighted networks. Hence, in order to do the homology computations we need to binarize the networks again. However, since we do not want to loose the information given by the weights, we used four slicing parameters in a wide range: $\theta = 0.2$, $\theta = 0.4$, $\theta = 0.6$ and $\theta = 0.8$. However, we will not account for the weights given at the nodes, which are the intraregional connections in the respective anatomical structure. These weights on the nodes will be globally normalized to 1.

Hence, we will only analyse the spatial organization of the correlations *between* the individual regions. Nevertheless, we believe that this is not a drawback of the method since we are primarily interested in the interplay of the regions. We computed the homology for each of the three anatomical levels: Lobes, Gyri, Brodmann. However, since we believe that the Gyri level contains most information, which is relevant for our purposes, we will only present the plots for the Gyri level networks, see Fig. 4.11 until Fig. 4.18. Hence, we obtain four times four diagrams: each configuration, e.g. episodic memory network for younger individuals, yields four diagrams, one per slicing

parameter. However, as already mentioned, we include a comprehensive list, covering all three anatomical clustering levels and containing the number of simplices of different dimensions that appear in the filtration.

When looking at the plots for one possible configuration, one should look at them all together *at once* and read them as they were kind of an evolution. By doing the slicing from 0.2 to 0.8, one starts by forgetting the *weakest* interregional connections and then finally only considering the *strongest* links.

Our first observation is that for all possible configurations (old/young, working/episodic) the topological complexity first increases, i.e. when moving from slicing parameter 0.2 to 0.4 or 0.6 and then decreases again since by restricting to the strongest links the networks strongly shrinks in size and, thus, reduces its complexity. Moreover, we observe from the diagrams that all networks show very different persistence features, which indicates that the method is very sensitive in detecting topological changes of the networks. The x-axis represents time, which in our case means the different steps of the filtration process: moving from the most simple case (just nodes) to the most complicated one containing faces of the highest possible dimension. The y-axis represents the number of the (generating) simplices in a particular dimension, hence it is the dimension, or more precisely rank, of the free chain groups.

Topologically, we can interpret the different Betti numbers: the zeroth Betti number reflects the number connected components. The 1-dimensional voids are calculated by the first Betti number. In a certain way, the 1-dimensional voids reflect that informational flow needs to be re-directed in order to reach the target nodes. The same applies in a similar way to higher dimensions: a persistent homology class in a higher dimension can be interpreted in such a way that, during its existence in the filtration, informational flow needs to circumvent this *obstacle*. This obstacle is a higher-dimensional topological structure in the connectivity pattern of the network.

It is also important to pay attention to the maximal Betti numbers, i.e. the maximal dimension of voids present in the network and their duration. Some networks have clearly longer lasting voids than others: for example, comparing Fig. 4.11 / 4.12 with Fig. 4.15 / 4.16 , that is: episodic network of older individuals with that of younger ones, we can see that

(1.) The episodic network of older individuals, i.e. Fig. 4.11 / 4.12, exhibits only one (long-lasting) component for slicing parameter 0.2 and 0.4, which we can tell from the first barcode plot. This single component is being generated by one node, and the network only starts falling apart when restricting to very strong links, that is, i.e. for slicing parameter 0.6 and higher there are more than one component that last over longer period of time. Interestingly, for slicing parameter 0.2 there are several long-lasting voids of dimension 2, in other words two-dimensional holes which persist over a longer period of filtration steps. These, however, do not appear in dimension 1, and they become fewer when moving to slicing parameter 0.3.

(2.) The episodic network of younger individuals, i.e. Fig. 4.15 / 4.16, already exhibits several (long-lasting) components at slicing parameter 0.2. This means, in turn, that the weighted, clustered and connected Gyri network, which we started from, is only held together by very weak links. This is contrary to the case of older subjects' network, for the same memory task. For the younger individuals, there is a similar pattern but this is shifted to lower slicing parameters, i.e. the appearance of higher-dimensional voids already takes place at slicing level 0.2. Moreover, for youger individuals there are long-lasting voids of dimension 2, which do appear for older people but only at slicing parameter 0.6.

A very intriguing observation concerns the homology barcode plots for young and elderly individuals, working memory: from entropy analysis we know that the networks get noisier with age which corroborates the over-activation hypothesis. The topological analysis of the networks helps to refine this statement: if we look at the homology barcode plots for the working memory network of the elderly individuals (Fig. 4.13) we see that at slicing parameter $\theta = 0.2$ the homology pattern ends up at dimension 2. Now, if we remove these *weak* links from the network, i.e. going to slicing parameter $\theta = 0.4$, we see that the homology structure is almost identical to that one for young individuals but at slicing level $\theta = 0.2$. There are holes up to dimension 5 and 6, respectively. This ***Swiss Cheese*** pattern is already achieved by very weak links ($\theta = 0.2$) for the young individuals (Fig. 4.17), whereas the seniors need to strengthen these links ($\theta = 0.4$) in order to achieve the same pattern. We use the informal notion *Swiss Cheese* to refer to the homological pattern which exhibits non-vanishing homology up to high dimension.

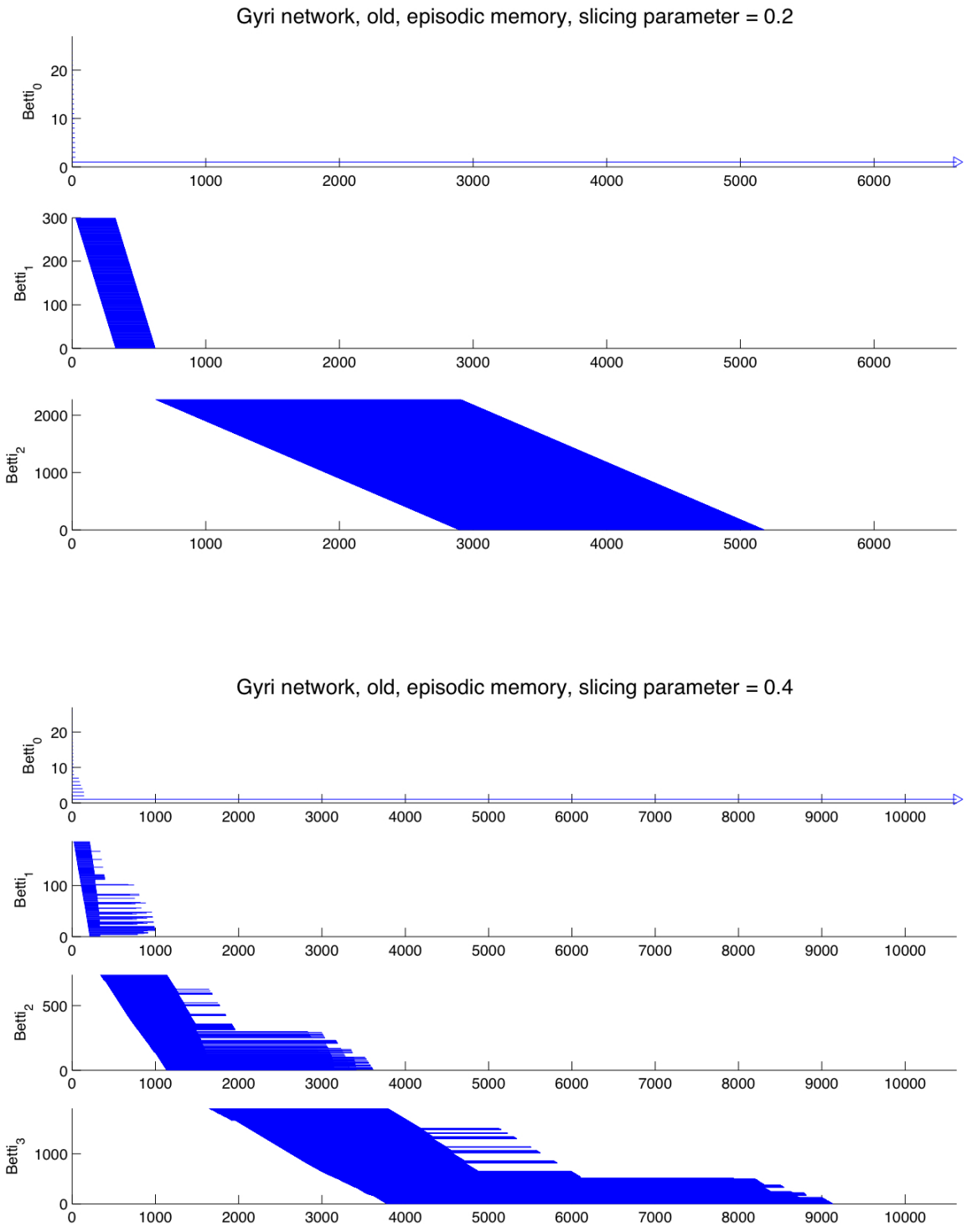

Fig. 4.11: Homology bar code for the episodic memory network at Gyri level and for older individuals, slicing parameter 0.2 and 0.4, cf. [SHR12].

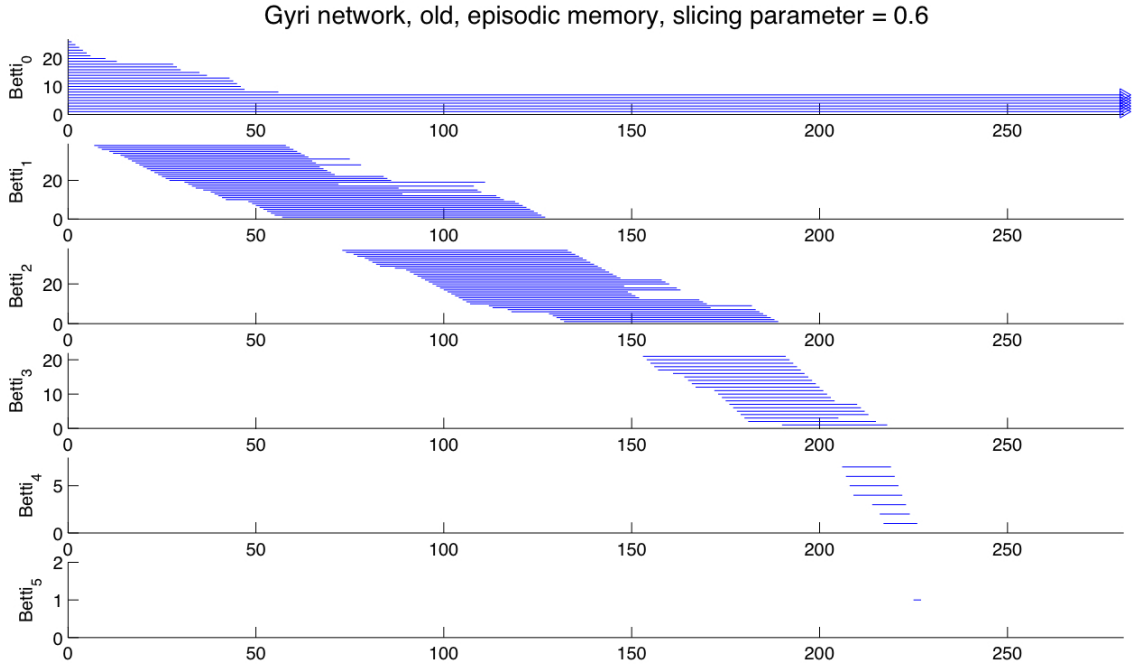

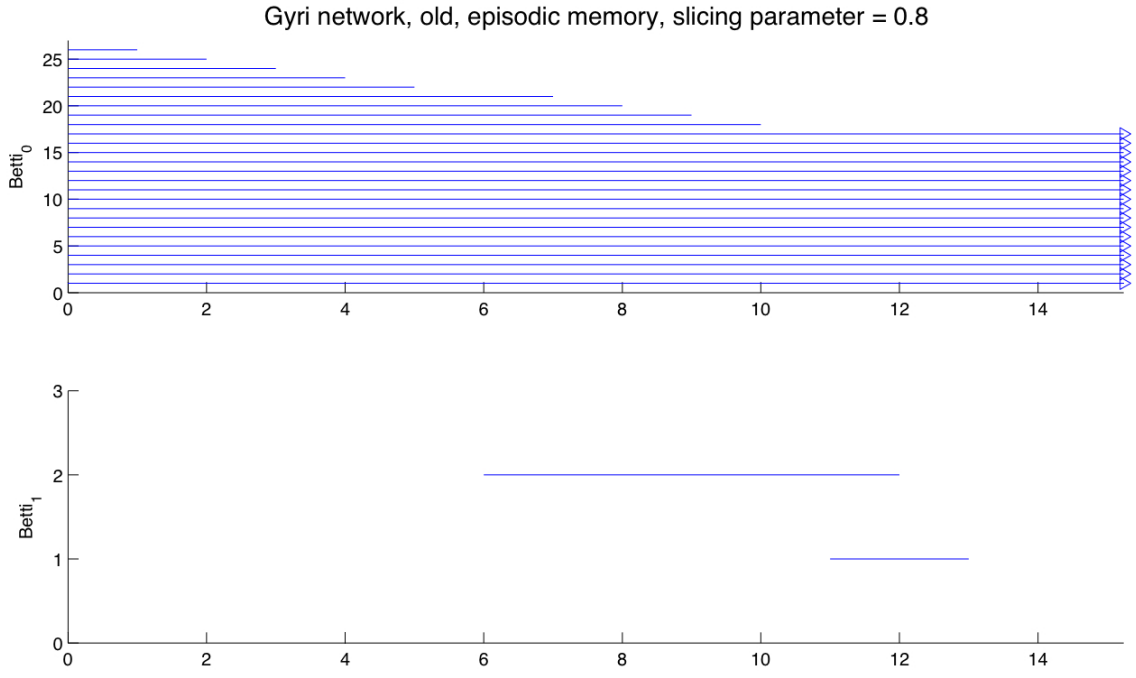

Fig. 4.12: Homology bar code for the episodic memory network at Gyri level and for older individuals, slicing parameter 0.6 and 0.8, cf. [SHR12].

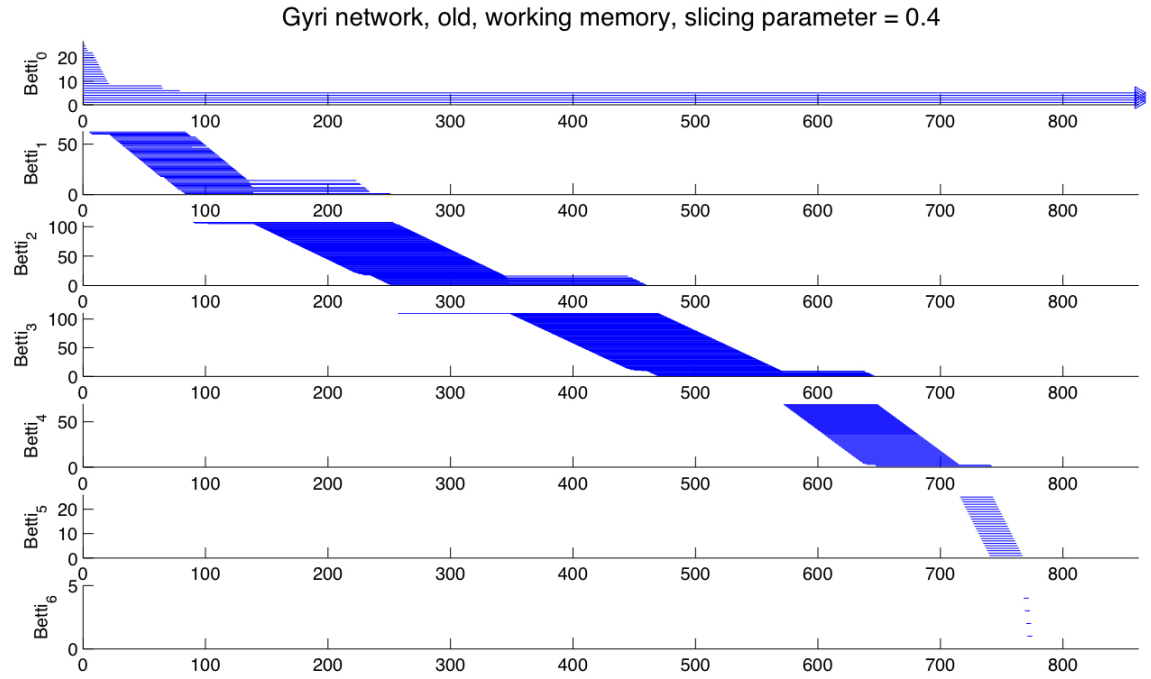

Fig. 4.13: Homology bar code for the working memory network at Gyri level and for older individuals, slicing parameter 0.2 and 0.4, cf. [SHR12].

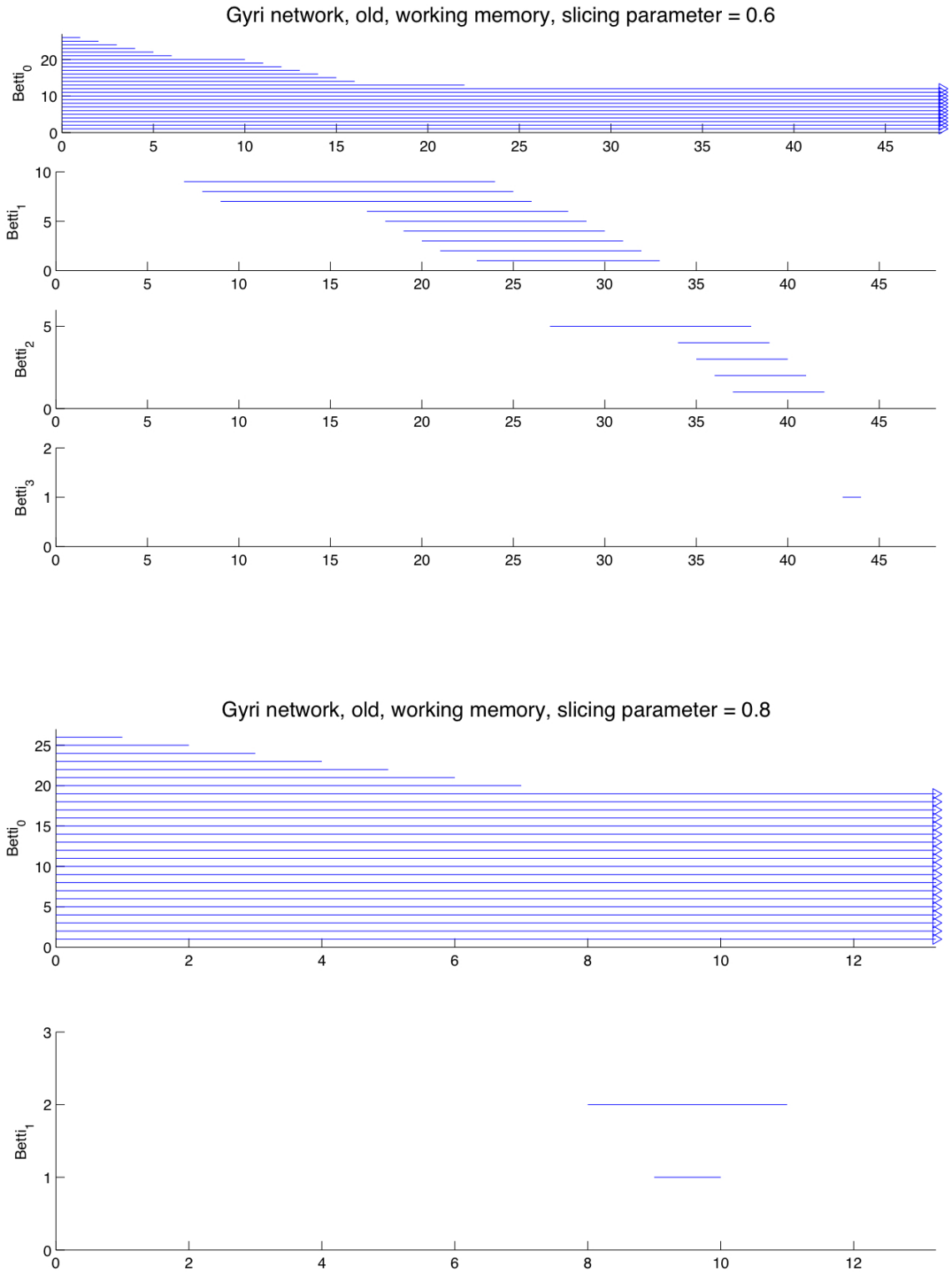

Fig. 4.14: Homology bar code for the working memory network at Gyri level and for older individuals, slicing parameter 0.6 and 0.8, cf. [SHR12].

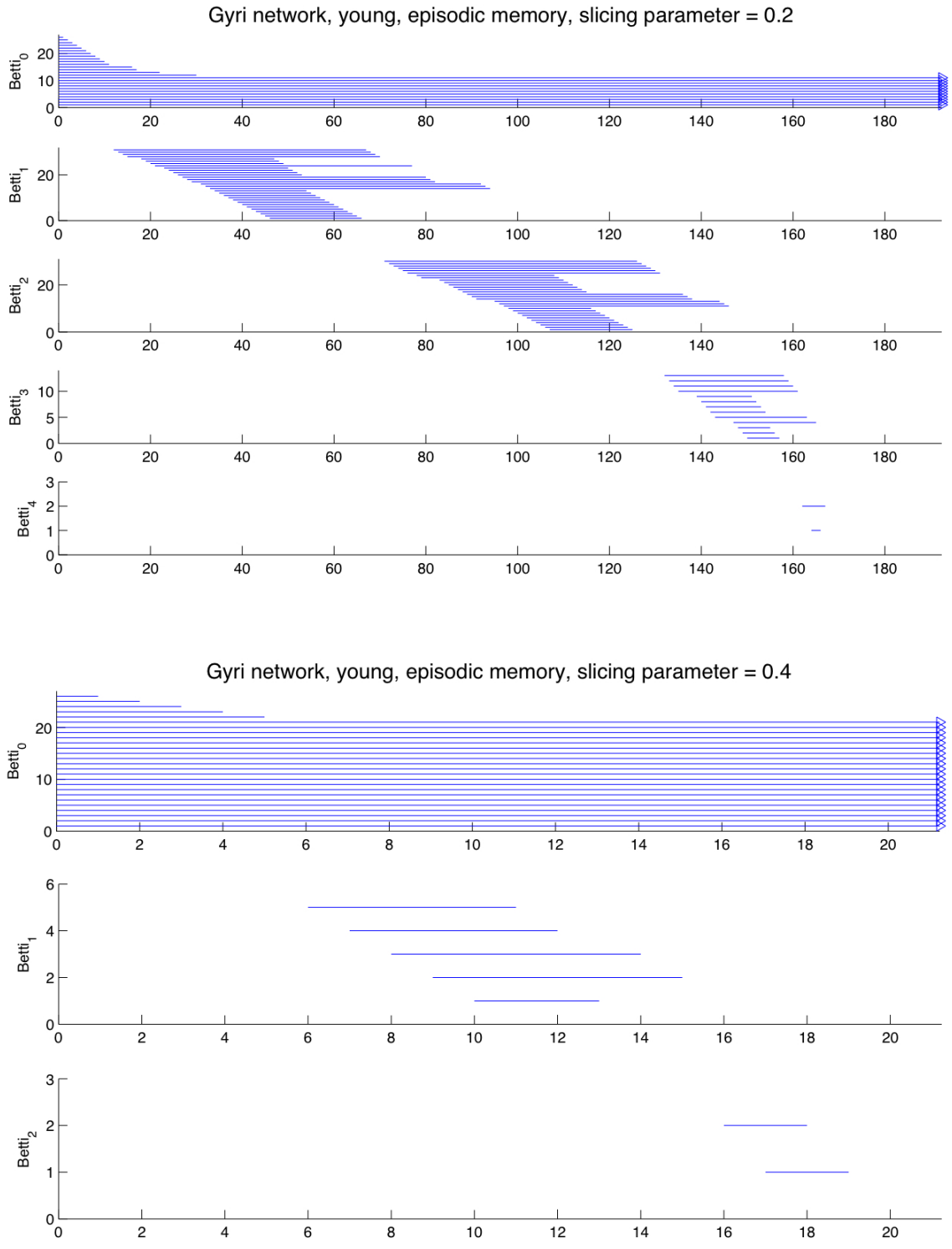

Fig. 4.15: Homology bar code for the episodic memory network at Gyri level and for younger individuals, slicing parameter 0.2 and 0.4, cf. [SHR12].

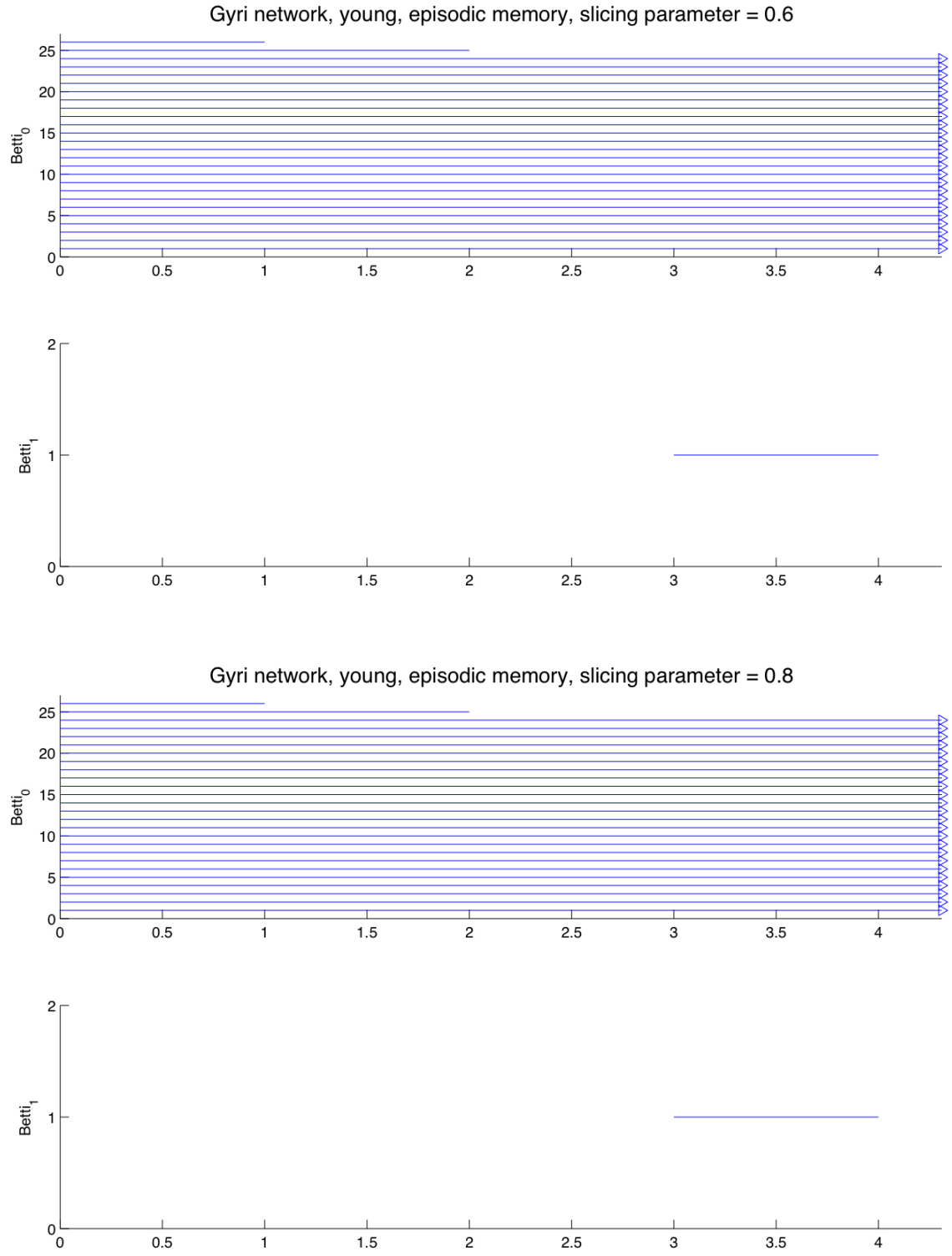

Fig. 4.16: Homology bar code for the episodic memory network at Gyri level and for younger individuals, slicing parameter 0.6 and 0.8, cf. [SHR12].

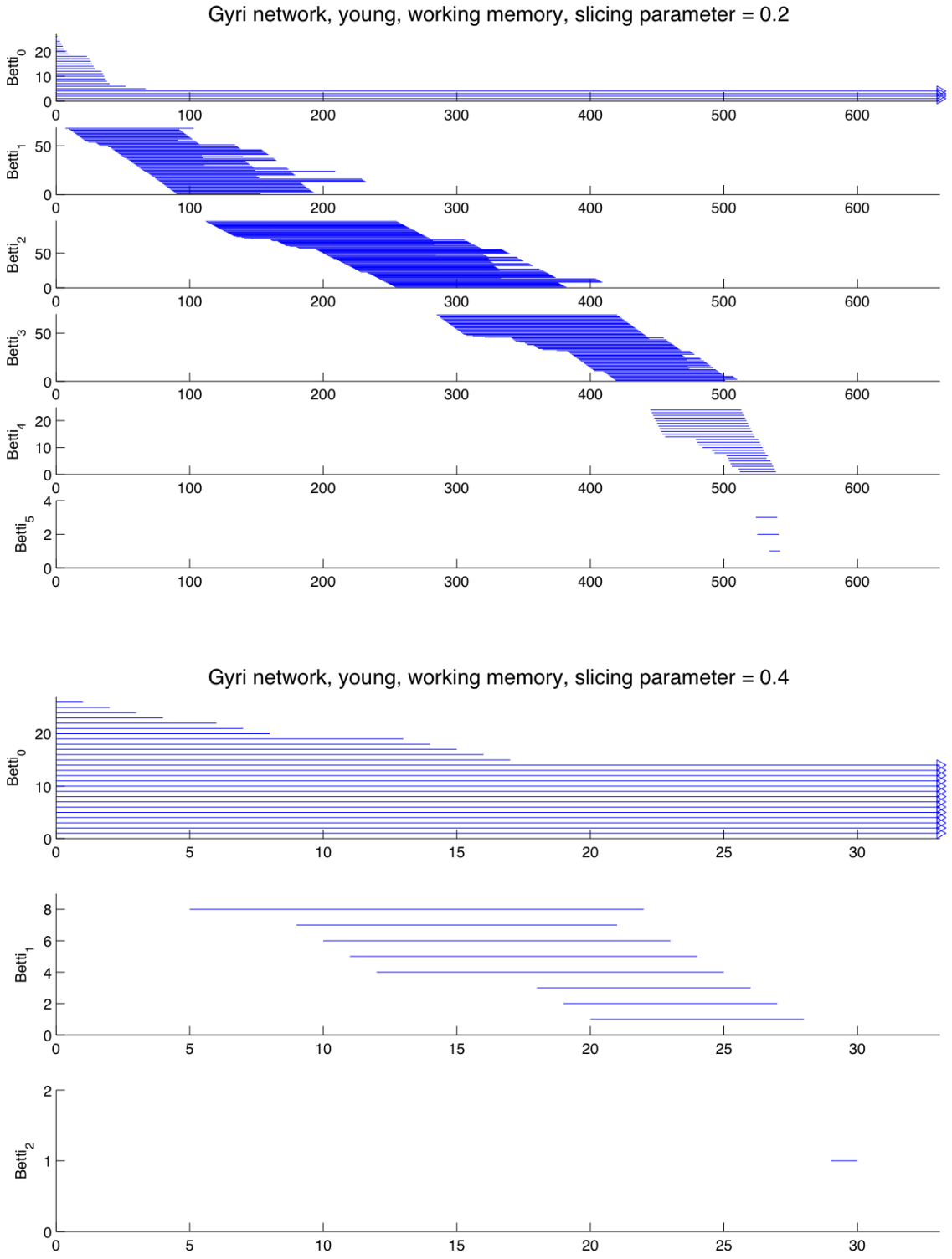

Fig. 4.17: Homology bar code for the working memory network at Gyri level and for younger individuals, slicing parameter 0.2 and 0.4, cf. [SHR12].

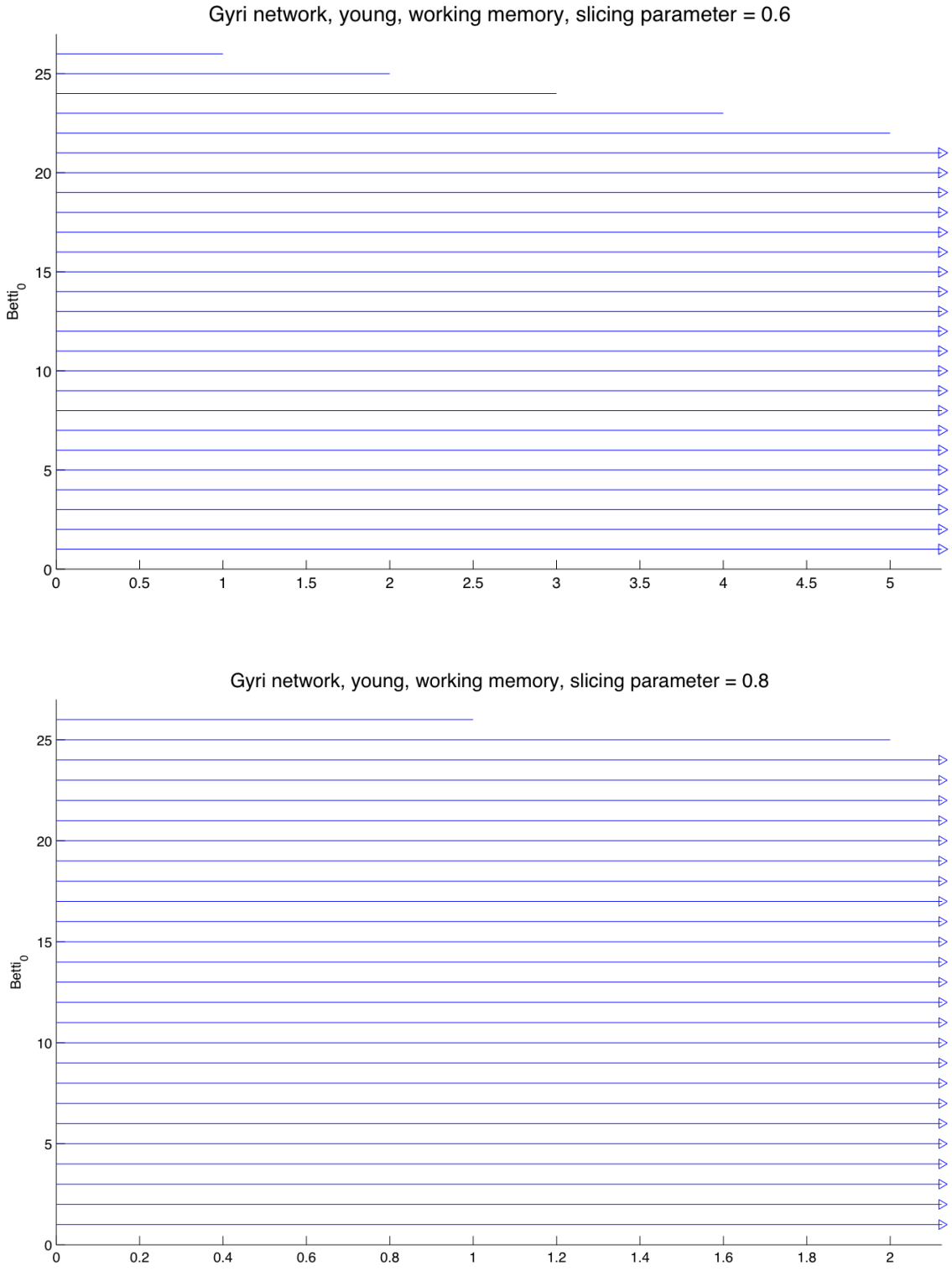

Fig. 4.18: Homology bar code for the working memory network at Gyri level and for younger individuals, slicing parameter 0.6 and 0.8, cf. [SHR12].

LOBE OLD LONGTERM										
Slicing	0-dim	1-dim	2-dim	3-dim	4-dim	5-dim	6-dim	7-dim	8-dim	9-dim
0.2	10	43	105	161	161	105	43	10	1	
0.4	10	27	35	26	11	2				
0.6	10	10	2							
0.8	10	4								

LOBE OLD SHORTTERM										
Slicing	0-dim	1-dim	2-dim	3-dim	4-dim	5-dim	6-dim	7-dim	8-dim	9-dim
0.2	10	40	86	110	86	40	10	1		
0.4	10	19	22	15	6	1				
0.6	10	8	3							
0.8	10	3								

LOBE YOUNG LONGTERM										
Slicing	0-dim	1-dim	2-dim	3-dim	4-dim	5-dim	6-dim	7-dim	8-dim	9-dim
0.2	10	18	14	6	1					
0.4	10	2								
0.6	10	2								
0.8	10	2								

LOBE YOUNG SHORTTERM										
Slicing	0-dim	1-dim	2-dim	3-dim	4-dim	5-dim	6-dim	7-dim	8-dim	9-dim
0.2	10	44	112	182	196	140	64	17	2	
0.4	10	18	10	1						
0.6	10	5	1							
0.8	10	2								

Fig. 4.19: Number of simplices of different dimensions that appear in the filtration, cf. [SHR12].

GYRI OLD LONGTERM								
Slicing	0-dim	1-dim	2-dim	3-dim	4-dim	5-dim	6-dim	7-dim
0.2	26	324	2576	14674				
0.4	26	211	924	2648	5480			
0.6	26	57	75	58	28	81		
0.8	26	11	2					

GYRI OLD SHORTTERM								
Slicing	0-dim	1-dim	2-dim	3-dim	4-dim	5-dim	6-dim	7-dim
0.2	26	278	1735	7291				
0.4	26	83	169	217	179	94	29	4
0.6	26	23	14	6	1			
0.8	26	9	2					

GYRI YOUNG LONGTERM								
Slicing	0-dim	1-dim	2-dim	3-dim	4-dim	5-dim	6-dim	7-dim
0.2	26	46	61	43	15	2		
0.4	26	10	7	2				
0.6	26	3	1					
0.8	26	3	1					

GYRI YOUNG SHORTTERM								
Slicing	0-dim	1-dim	2-dim	3-dim	4-dim	5-dim	6-dim	7-dim
0.2	26	90	164	165	93	27	3	
0.4	26	20	9	1				
0.6	26	5						
0.8	26	2						

Fig. 4.20: Number of simplices of different dimensions that appear in the filtration, cf. [SHR12].

BRODMAN OLD LONGTERM										
Slicing	0-dim	1-dim	2-dim	3-dim	4-dim	5-dim	6-dim	7-dim	8-dim	9-dim
0.2	27	323	2374	12263						
0.4	27	126	320	533	608	480	260	93	20	2
0.6	27	30	23	8	1					
0.8	27	6	1							

BRODMAN OLD SHORTTERM										
Slicing	0-dim	1-dim	2-dim	3-dim	4-dim	5-dim	6-dim	7-dim	8-dim	9-dim
0.2	27	265	1476	5465						
0.4	27	66	310	213	76	34	9	1		
0.6	27	14	8	2						
0.8	27	2								

BRODMAN YOUNG LONGTERM										
Slicing	0-dim	1-dim	2-dim	3-dim	4-dim	5-dim	6-dim	7-dim	8-dim	9-dim
0.2	27	50	43	20	6	1				
0.4	27	8	2							
0.6	27	2								
0.8	27	2								

BRODMAN YOUNG SHORTTERM										
Slicing	0-dim	1-dim	2-dim	3-dim	4-dim	5-dim	6-dim	7-dim	8-dim	9-dim
0.2	27	101	232	341	331	212	86	20	2	
0.4	27	23	13	2						
0.6	27	7								
0.8	27	2								

Fig. 4.21: Number of simplices of dfferent dimensions that appear in the filtration, cf. [SHR12].

Summary of key results:

- All networks show very different persistent homology features. The homology method is more sensitive than statistical or spectral methods regarding the detection of structural changes.
- Episodic memory networks of older individuals exhibit only one connected component up to slicing 0.6. Then it starts falling apart. At slicing level 0.4 there are long-lasting 3-dimensional voids. Episodic memory networks of younger individuals already has several connected components at slicing level 0.2. Compared to older subjects' episodic network there are long-lasting 1-dim. and 2-dim. voids, at slicing level 0.2.
- Working memory networks of older individuals show only one connected component compared to several ones for younger subjects, at slicing level 2. However, compared to the same age group and to the episodic memory task, there are now several long-lasting voids in dimension 2, more prominent for older subjects than for younger ones.

Statement: Ageing processes leave traces in the homology pattern of the networks. For example, comparing Fig. 4.13 and Fig. 4.17, i.e. the homology barcode plot for working memory networks of elderly and young individuals, respectively, we see that young individuals already achieve a homological *Swiss Cheese* pattern at weak links ($\theta = 0.2$), whereas almost the same pattern appears for the seniors only at stronger links ($\theta = 0.4$). Assuming that the working memory for young individuals works better in terms of reliability and efficiency, i.e. defines a benchmark, we can deduce from the homology analysis that elderly individuals compensate this by over-activating, producing some topological noise as a side effect. We use the informal notion *Swiss Cheese* to refer to a high-dimensional homological pattern which exhibits non-vanishing homology up to high dimension. The non-vanishing homology can be interpreted as higher-dimensional *holes* or *voids* in the connectivity pattern.

Chapter 5

Outlook

The results of this thesis attempt to contribute to an enhanced understanding of the functional connectivity networks during episodic and working memory. The main result, *grosso modo*, is that senior individuals exhibit expanded functional neural networks with less differentiation between episodic and working memory demands. We observed asymmetric compensatory mechanisms, mainly in fronto-parietal regions. Moreover, our findings show that older networks exhibit a higher entropy as well as a higher synchronizability. Ageing processes leave traces in the topological structure, which can be deduced from the homology analysis. However, there are many open questions that could be addressed in future research on this topic. We would like to mention some possible future research threads:

- Concerning the experimental data acquisition, we would like to suggest to extend and apply the network approach to resting state data in order to analyze the dynamical interplay of network changes between active and resting states, respectively. Future studies should, moreover, focus on regional changes in BOLD responsitivity, which would allow for a further distinction between compensation mechanisms and neural dedifferentiation. In addition, we would like to suggest accompanying studies focusing on anatomical networks, using MNI tensor imaging analysis.

- Concerning the functional brain networks, one should try to extend the spectral analysis and persistent homology analysis to the unclustered networks, which we considered in the very first part of the statistical analysis. However, this would be computationally very cost-intense and was beyond the computational means

we had at hand for this work. Moreover, one could also look in detail at the different lobe structures and analyze their *internal* connectivity pattern by using the spectral method and persistent homology.

- On the theoretical side, we would like to suggest further theoretical research on (generic) network models, which would re-produce networks with a pre-defined spectral pattern. For the time being, there are only very few network processes known, e.g. random deletion, motif doubling, preferential attachment etc., but these do not suffice to explain the spectral patterns which we obtained from our analysis. Such models would then help to explain biological processes which govern the connecvity patterns. Moreover, we would like to suggest further theoretical research on simplicial complexes of networks: on the one hand, one should try to link higher-order Laplacian operators, e.g. Laplace-Beltrami, to properties of the underlying network structure. Additionally, one could work on appropriate entropy measures that can be defined on simplicial complexes. On the other hand, it seems very interesting to link the persistent homology approach with the dynamics of a network.

Supplement

Foundations of network analysis

This chapter provides the basics of network theory. The experienced reader is kindly asked to skip this section, referring back if necessary. For reference on the material presented here see, for example, [New03], [BA99] or [DM03].

Motivation

The historical origin of graph theory is rooted in the the physical world. In 1735 the legendary Swiss born mathematician Leonhard Euler ($1707 - 1783$) solved the so-called *Königsberg bridge problem*: he showed that it was impossible to traverse the seven bridges across the Pregel river exactly once in a single trip, while starting and returning at the same point. In his proof of the conjecture, Leonhard Euler represented the problem as a small and undirected graph with multiple links, cf. [Har69].

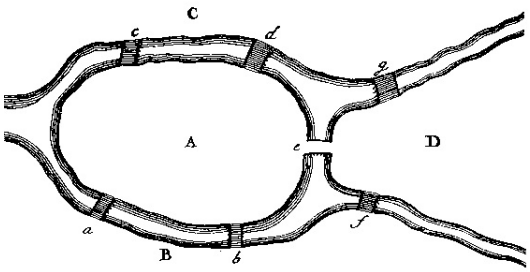

Fig. 5.1: Original schematic diagram drawn by Leonhard Euler in 1735.

Leonhard Euler's approach is today regarded as the birth of a new branch in mathematics: graph theory. In the middle of the nineteenth century, graph theory had been enriched by many theoretical concepts, being inspired both from real-world problems

such as the analysis of electrical circuits and the exploration of chemical isomers as well as from inner-mathematical problems, cf. [Har69] and [Wes96].

Significant progress in network theory had been made in the course of the study of social networks, cf. [WF94]. In 1967, the social psychologist Stanley Milgram ($1933 - 1984$) conducted a prominent experiment, cf. [Mil67]. He monitored paths of acquaintanceship across a large social network in the United States and discovered the impressive smallness of the world of social relations. But the origins of this *small-world* phenomenon remained obscure until in 1998 Duncan J. Watts and Steven Strogatz associated it with specific types of connectivity, cf. [WS98]. Almost at the same time, in 1999, the Hungarian physicists Albert-László Barabasi and Réka Albert unveiled the scale-free structure of many real-world networks, cf. [BA99]. Both discoveries launched a new era of network theory, first and foremost driven by insights from statistical physics. Today, network theory pervades many areas of science and networks are widely used to represent technological, biological and social systems, cf. [New03], [BLM$^+$06], [DM03] and [AO04]. Neural systems have long been described as sets of discrete elements linked by connections. Nonetheless, network theory has essentially only been applied to neuroscience roughly in the past 15 years, cf. [BS09] and [Bre95].

Although in most of the literature the two notions *graph* and *network* are used interchangeably, we dare to give a *semi-formal* definition of what is nowadays understood as being a network rather than a graph.

Definition 6. A network is a real-world system that is being represented as a mathematical graph $\mathcal{G} = (\mathcal{V}, \mathcal{E})$ in which each *element* of the real-world system is represented by a node $i \in \mathcal{V}$ and a *relationship* or *interaction* between two elements is represented by an edge $e_{ij} \in \mathcal{E}$ between the corresponding nodes in the graph.

By abuse of notation, we will continue using both notions, network and graph, interchangeably but reminding ourselves of the possible distinction whenever it will be necessary.

Basic network formalism According to definition (2.1), the representation of a real-world system as a network requires the precise specification of nodes and edges.

Two nodes are said to be *neighbors* if they are connected by an edge, and the *degree* k_i of node i is the number of neighbors it has. The complete description of a particular graph is provided by its adjacency matrix $(A)_{ij}$. An unweighted graph of N vertices has an $N \times N$ adjacency matrix, having entry $A_{ij} = 1$ if node i is connected to node j, being 0 otherwise. Possibly, the boolean entries of A are replaced by values in $[0; 1]$, representing *weights* of the edges.

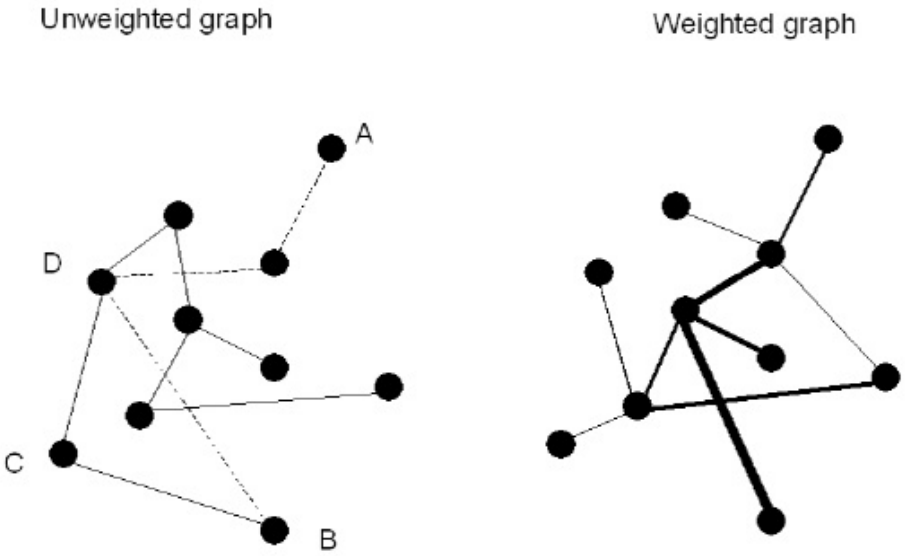

Fig. 5.2: Representation of a network as a graph, unweighted and weighted case. Copyright: *Stam and Reijneveld (2007)*, [SR07].

Graph topology can be quantitatively described by a wide variety of statistical measures, some of which are discussed here. It is not yet established which measures are most appropriate for the analysis of brain networks. We will later see that spectral methods as well as methods using algebraic topology can give much more insight into networks, especially into the global dynamics of networks.

Characteristic network measures

In the remaining part of the chapter we introduce some fundamental quantitative-statistical network characteristics, which will be used in the course of the analysis. For

further reference, please see, for example, [BA99], [SR07] .

Degree and degree distribution The simplest local characteristic of a vertex is its degree k_i: the total number of edges attached to a vertex. The degree is the most fundamental network measure and most other measures are ultimately linked to this concept. Hence, it appears to be obvious to look at the distribution of the degrees in a particular network: the degree distribution $P(k)$ is the probability that a randomly chosen node in a random network has degree k:

$$P(k) = \frac{\langle N(k) \rangle}{N}$$

Here, $\langle N(k) \rangle$ is the average number of nodes of degree k in the network, whereas the averaging is over the entire statistical ensemble. Of course, we assume that the total number of nodes N stays the same. When doing empirical network research, i.e. looking at one particular graph G, then one measures the frequency of occurence of nodes with degree k in this graph: $P_G(k) = N_G(k)/N$. Here, $N_G(k)$ is the number of nodes of degree k in graph G. This is also usually called *degree distribution*. In random networks all connections are equally probable, resulting in a Gaussian and symmetrically centred degree distribution, cf. [BS09]. Complex networks generally have non-Gaussian degree distributions, often with a long tail towards high degrees. For example, the degree distributions of scale-free networks follow a power law, cf. [BA99]: that is, the probability that a node has degree k is given as $P(k) \sim k^{-\lambda}$. In biological systems, the degree exponent λ often ranges between 2 and 3, and the very gradual (*heavy-tail*) power law decay of the degree distribution implies that the network lacks a characteristic scale - hence such networks are called *scale-free* networks, cf. [BS09]. However, due to physical constraints, physically embedded networks, in which nodes have limited capacity for making connections, often do not have pure power law degree distributions. When analyzing these kind of networks one often experiences exponentially truncated, or so-called *cut-off* power law degree distributions. This will also be the case for the the fMRI[1] networks which we analyze in this work.

Density The *density* of a network is the ratio between the number of existing edges and the total number of theoretically possible links in a network of the same size, which is, for a network of size N: $\frac{N(N-1)}{2}$.

[1] fMRI = functional magnetic resonance imaging

Clustering coefficient The notion of *clustering coefficient* of a network is a pivotal concept which measures the extent to which the neighbors of a node are also connected. Watts and Strogatz [WS98] defined the clustering coefficient of node i by

$$c_i^{ws} = \frac{2E_i}{k_i(k_i - 1)} \tag{5.1}$$

where E_i is the number of edges between the neighbors of i. Usually, the arithmetic mean of c_i^{ws} over all nodes is defined as the clustering coefficient C_p of the whole network. C_p is a measure of the extent of local cluster or *cliquishness* of the network. Clearly, $0 \leq C_p \leq 1$; and $C_p = 1$ if and only if the network is fully connected, that is, each node is connected to all other nodes.
An alternative measure for network clustering is given by [NMW00], also called *transitivity*. It is expressed by:

$$C^{\Delta} = \frac{3 \times \text{number of triangles}}{\text{number of paths of length 2}} \tag{5.2}$$

where a triangle is a set of three nodes in which each contacts the other two. Both notions of clustering are quite intuitive and are often in good agreement. For computational reasons and for the sake of consistency with the existing literature, we will mainly consider C^{Δ} here, unless otherwise indicated. For further reference, see also [New03], [BS09] and [HG08].

Average shortest path length Another important measure is the *average shortest path length*. In the case of an unweighted graph the path length or distance $d_{i,j}$ between two vertices i and j is the minimal number of edges that have to be travelled to go from i to j. This is also called the *geodesic path* between i and j. The average shortest path length L of a graph is the mean of the path lengths between all possible pairs of vertices:

$$L = \frac{1}{N(N-1)} \sum_{i,j \in \mathbb{N},\, i \neq j} d_{i,j}$$

The average shortest path length is a global characteristic; it indicates how well integrated a graph is, and how easy it is to transport information or other entities in the network. This definition has been taken from [SR07].

The degree distribution, clustering coefficient and path length are the core statistical measures of graphs. On the basis of these measures four different types of graphs can be distinguished: (i) ordered, (ii) small-world, (iii) random and (iv) scale-free. A further sub-division is described in Amaral et al. [ASBS00]. Here, we will only briefly describe random networks and the important concept of small worldness.

Random network This paragraph is based on [Dor09], please see also [NSW01] for further reference. In terms of statistical physics, a *random network* is not a single graph but a statistical ensemble. This ensemble is defined as a set of its members, i.e. particular graphs, where each member has its own given probability of realization. By this definition, a given random network is some graph with one probability, another graph with another probability, and so on. To obtain a characterizing quantity of a random network, one should, in principle, collect the full statistics for all members of the statistical ensemble, or at least, and in practice, averaging over a large number of realizations. The simplest random networks are so-called classical random graphs. There are two main versions of classical random graphs: the *Gilbert model* and the *Erdös-Renyi model*, we shall only make use of the latter one. The Erdös-Renyi model is a statistical ensemble of all possible graphs of precisely N vertices and precisely E edges, where each member of the ensemble has equal probability of realization. To put it in a nutshell, an edge in this model is being put between each pair of nodes with equal probability, independently of the other edges.
Random networks have low average clustering whereas complex networks have high clustering, which is associated with high local efficiency of information transfer and robustness.

Small-worldness The notion of *small-worldness* has been introduced by Watts and Strogatz in [WS98] and is, intuitively, defined as follows: a network G is called a small-world network if it has a similar average shortest path length but has a greater clustering coefficient than an equivalent Erdös-Renyi random graph with the same number of nodes and edges, whereas an Erdös-Renyi random graph is constructed by uniquely assigning each edge to a node pair with uniform probability, cf. [Bol01] and cf. [HG08].

Many real-world networks fall into the broad class of small-world networks: tightly interconnected clusters of nodes and an average shortest path length that is similar

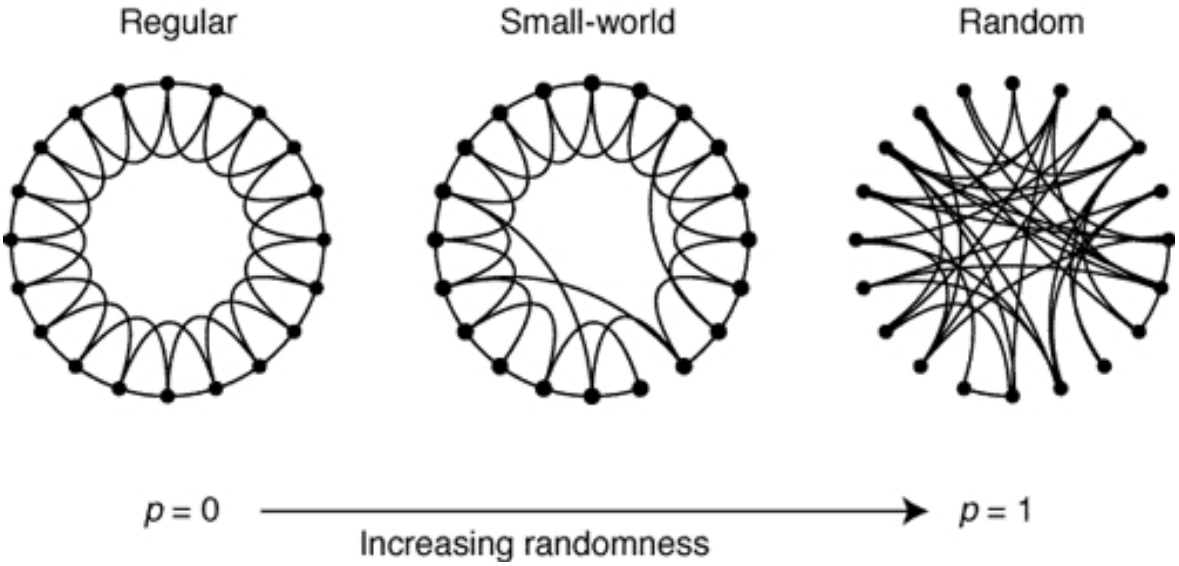

Fig. 5.3: Schematic visualization of small-worldness, see Watts and Strogatz, [WS98].

to an equivalent random graph, cf. [HG08]. This definition of small-worldness is semi-quantitative and yields a categorical distinction between networks, but it is unsatisfactory that there remains uncertainty about the extent of a network's small-world status.

In order to give a quantitative definition of small-worldness we will adopt the approach of [Spo06] and [HG08], see also [BMLA$^+$06], [ASW$^+$06] for further reference. The trade-off between local *cliquishness*, i.e. high local clustering, and average shortest path length can be used to quantify the notion of small-worldness. This will enable us to compute and statistically determine the small-worldness of a given network.

Let G be a network with n nodes and m edges. Let L_g be the average shortest path length of G and let C_G^Δ be its clustering coefficient, using definition (3.2). Let L_{rand} and C_{rand} be the respective quantities for the corresponding Erdös-Renyi random graph. The intuitive notion of small-worldness implies that a network is said to be small-world if $L_g \geq L_{rand}$ and $C_g^\Delta \gg C_{rand}^\Delta$. Now we put

$$\gamma_g^\Delta = \frac{C_g^\Delta}{C_{rand}^\Delta} \quad \text{and} \quad \lambda_g = \frac{L_g}{L_{rand}} \tag{5.3}$$

Definition 7. A network G is said to be a *small-world* network if

$$S^{\Delta} := \frac{\gamma_g^{\Delta}}{\lambda_g^{\Delta}} > 1 \,. \tag{5.4}$$

Of course, a complete analogous definition can be given for S^{ws}. However, due to convenient computational properties of the notion of transitivity and as already stated before, we will be mainly using C^{Δ}, hence S^{Δ}. For example, one can show analytically that, under the conditions such as a constant rewiring parameter, the small-worldness S^{Δ} scales linearly with network size n. For further reference, see also [HG08] and [Spo06].

Betweenness The *betweenness* of a node quantifies *grosso modo* the importance of this node regarding the number of shortest paths passing through this node. In particular, the betweenness of a node m is defined as the probability that a shortest path between a pair of vertices of a network passes through this node. Let the total number of the shortest paths between node i and node j be $B(i, j)$, and $B(i, m, j)$ be the number of them passing through node m. Then we define:

$$b(m) = \sum_{i \neq j} \frac{B(i, m, j)}{B(i, j)}$$

Unlike the degree, the value of the betweenness of a node reflects the topology of the entire graph, nodes with a high betweenness play an important role in a network and can be thought of as *central bridges*. This definition has been taken from [Dor09], please see for further reference.

Cost-efficiency The *cost efficiency* of a network, see Achard and Bullmore [AB07], is defined as the difference between the global efficiency E_global and the density, whereby the global efficiency of a network is defined as the inverse of the harmonic mean of the minimal path lengths,

$$E_{global} = \frac{1}{N(N-1)} \sum_{i \neq j \in G} \frac{1}{L_{i,j}} \,,$$

normalized by the global efficiency of a fully connected graph of the same number of nodes.

Modularity and clustering For the sake of completeness, we shall mention the notion of modularity when it comes to community detection in networks. The basic concept is an optimization task over all possible partitions of the given network subject to the maximization of a so-called modularity function. However, we will deliberately not pursue this approach since at this stage we shall make intensive use of the anatomical information that is contained in the raw data. This does not contradict the completely blind, i.e. hypothesis-free, approach that we initially mentioned. To the contrary, as we will see, we have not made use of any hypotheses up to that stage. We will use the anatomical coordinates of the nodes in order to anatomically cluster instead of using Newman's modularity approach. Our strategy will be described in detail at the end of the next chapter. For further reference on Newman's modularity, please see [New03].

Biological background

In the appendix, we give a short summary of the biological background, including neurophysiology, neuroanatomy and memory processing. This chapter, though relevant and necessary, can be skipped and considered as a reference for later use.

Neurophysiology and neuroanatomy

This thesis analyses functional brain networks, and thus focuses on the large-scale processing of memory related information. Nevertheless, we considered it necessary to summarize the basics of neurophysiology as well as neuroanatomy. This section primarily addresses the medically unexperienced reader and is based on [KSea09], [DSH05] and [JW94].

Cytoarchitecture of neural cells

A neuron basically consists of a cell body *(soma* or *perikaryon)* and one or more cellular projections. These projections can be further subdivided into dendrites and axons. Dendrites receive the excitation signal which is triggered by a variation of voltage-gated ion conductances. Axons serve as the connection to other neurons and muscle cells, cf. Fig. (5.1).

The terminal split-up of the axons *(telodendron)* together with the neighboring cell and the interjacent gap constitute the synapse, where the excitation transfer from one neuron to the other takes place. In the central and peripheral neural system the neuronal structures are enclosed by glial cells. Some glial cells primarily have

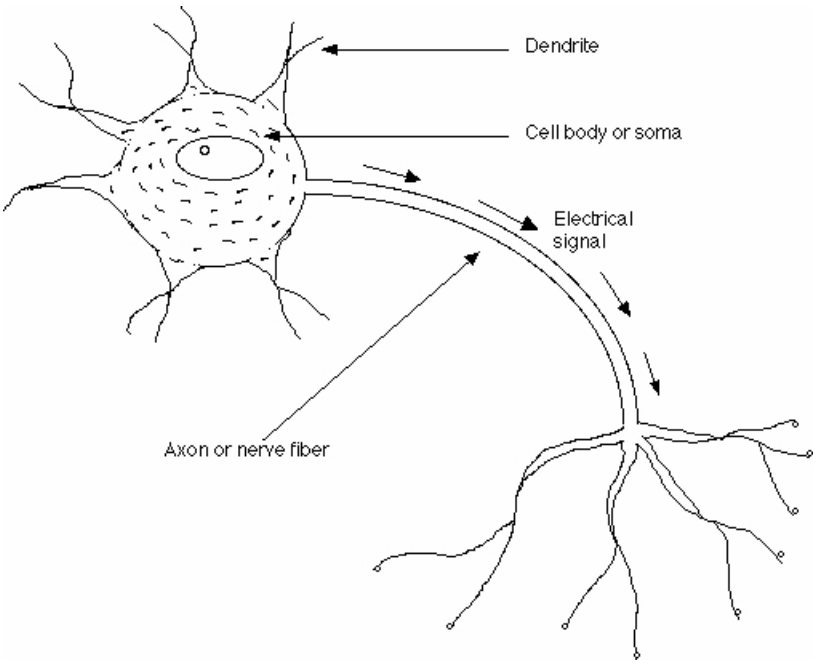

Fig. 5.4: Schematic of a neural cell. Copyright: `http://www.cns.nyu.edu/~david/courses/perception/lecturenotes/brain/ brain-slides/neuron.gif`, Date: Sep 15th, 2011.

a supporting function, others control the internal environment of the brain, i.e. the surrounding fluid of the neurons and the nutrifying of the neurons.

Action potential

Neurons are capable of triggering and transmitting informational signals by means of changing the transmembrane potential difference. These changes are processed by ionic currents (Na^+ and K^+) alongside the nerve fibre membrane. These local variations in the transmembrane potential are called action potential and are used for informational coding. The action potential itself is based on voltage-controlled ionic channels, which become permeable for Na^+ and K^+, and is triggered by a depolarization (between the interior and exterior of the cell) of the so-called resting potential, which is roughly between -80 and -90 mV. The neurophysiological cycle of an action potential consists of the following chronological chain of processes: the increasing depolarization, the overshooting (i.e. reversal of the membrane potential) and the repolarisation phase with hyperpolarization. The complete cycle lasts just about 1 ms.

Transmission of excitation

Action potentials are transmitted alongside the nerve fiber and are conveyed to neighboring neurons (so-called *effector cells*) via the synapses. This process is carried out by transmitters which are emitted into the synaptic gap and which bind to post-synaptic ionic channels. This yields a change in the post-synaptic membrane potential, either excitatory *(EPSP)* or inhibitory *(IPSP)*. In the case of an EPSP an action potential will be triggered in the effector cell if the membrane threshold is exceeded.

Neuroanatomy

This section is a short summary of basic neuroanatomical results and is intended to ease the readability of subsequent chapters. Further reference can be found in [Tre11].

The complete human nerval system contains roughly 10^{12} neurons and is subdivided into the central nerval system and the peripheral nerval system. The central nerval system is structured into white and grey matter. Grey matter is defined as those regions in which neuronal cell bodies predominate. It consists therefore of cell bodies, neuropil, glial cells and capillaries. White matter, in contrast, mainly contains myelinated axons. Nuclei and cortices are regions where grey matter can be primarily found.

Based on morphological, phylogenetic and functional aspects, the human brain can be subdivided in medulla oblongata, pons, mesencephalon, diencephalon, cerebellum and telencephalon, also known as cerebrum, cf. Fig. (5.4).

The cerebrum is the most differentiated and largest part of the brain and can only be found in such a way in the human organism. It consists, macroscopically, of two hemispheres, divided by the media longitudinal fissure *(fissura longitudinalis cerebri)* and connected by the colossal comissure *(corpus callosum)*. Each hemisphere consists of the frontal lobe *(lobus frontalis)*, the parietal lobe *(lobus parietalis)*, the temporal lobe *(lobus temporalis)* and the occipital lobe *(lobus occipitalis)*. Additional to this structural classification, further anatomical structures are the insular cortex *(lobus insularis)*, which is located between the temporal and the frontal lobe, and the cingulate cortex *(gyrus cinguli)*, situated above the corpus callosum. The surface of the cerebrum is folded with respect to a surface enlargement designated by ridges (so-called *gyri*) and depressions (so-called *sulci*) of the cerebral surface. With respect to cyto-architectonical aspects, the cerebrum has been classified by Korbinian Brod-

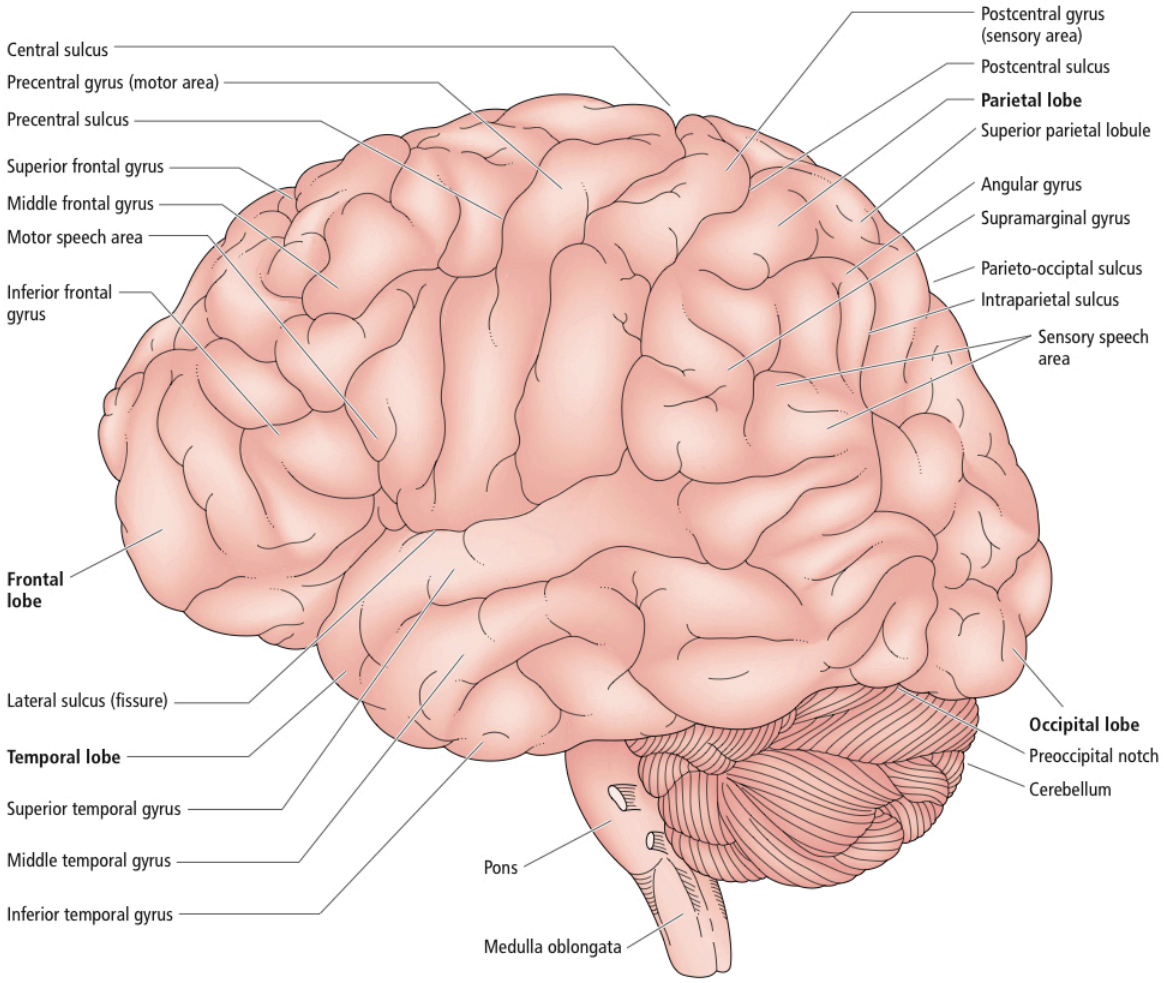

Fig. 5.5: Diagram of the brain from a lateral view. Copyright: Kandel et al. 2000, [KSJ00]

mann [Bro09] in more than 50 areas with beginning enumeration in the postcentral gyri (Brodmann's area: BA 1–3), cf. Fig. (5.5). Phylogenetically, it can be divided in the striatum, which consists of the caudate nucleus and the putamen (part of the basal ganglia), the paleocortex, which is the most ancient part of cerebrum, the archicortex and the neocortex, which appeared most recently in the phylogenesis of human brain.

The paleocortex comprises the rhinencephalon and parts of the olfactory system, as well as the amygdala, a complex of grey matter which is deeply located in the temporal lobe, and which is part of the limbic system. The limbic system is particularly associated with emotional functions. Several further functional aspects are assigned to the

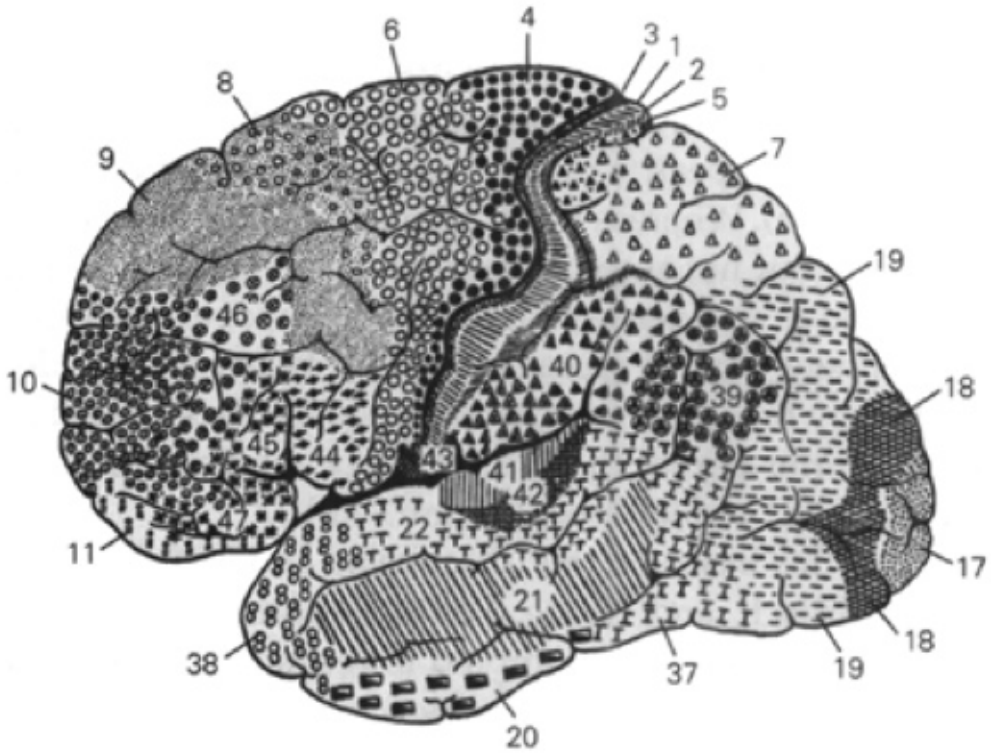

Fig. 5.6: Brodmann classification of the human cerebral cortex. Copyright: Kandel et al. 2000, [KSJ00]

amygdala. Besides modulating vegetative functions in the hypothalamus, transmitting fight-and-flight responses, the amgydala plays an important role in learning emotions and developping memory.

The archicortex mainly consists of the hippocampus as well as parts of the parahippocampal gyrus and cingulate gyrus. Located in the medial temporal lobe, the hippocampus constitutes a part of the limbic system and is relevant for vegetative and emotional processes, as well as recognition. It can be divided in the dentate gyrus, cornu ammonis, and subiculum. The cingulate gyrus, an important part of the limbic system, is located immediately above the corpus callosum and affects vegetative, psychomotoric and locomotive processes.

The neocortex or isocortex, which represents the largest part of cerebrum, is associated with higher mental functions and contains two types of neural cells: excitatory

pyramidal neurons (85 % of neocortical cells) mostly releasing the neurotransmitter glutamate, and inhibitory interneurons, transmitting GABA (gamma-Aminobutryc acid). It can be subdivided in the following functional coponents: primary fields, which receive sensoric afferent information from the thalamus, secondary fields, which enable first-processing of sensoric information in terms of perceiving and allocating sensoric information, and, thirdly, associative fields, which are connected afferently and efferently with several primary and secondary fields and coordinate delivered information.

The following structures can be found in the frontal lobe: (i) the primary motor cortex (M1) which is located in the gyrus precentral (equivalent to BA 4). It shows an somototopic arrangement and is supposed to be involved in the voluntary movement system. (ii) the premotor cortex and supplementary motor area (largely equivalent to BA 6 and parts of BA 8) which are located next to M1. These regions are supposed to be involved in modeling of motion-sequences and have a pre-processing function for M1. The motoric speech centre, including Broca's area, is located in the inferior frontal gyrus and surrounding regions. The prefrontal cortex embraces the neocortical regions in front of M1 and the premotor regions. It is associated to short-term memory and higher cognitive performances. It receives afferent information from nearly all regions of the cerebral cortex, from the medial nuclear group of the thalamus and the reticular formation. The prefrontal cortex is efferently connected with numerous cortical areas and the thalamus.

The parietal lobe is mainly engaged in the somatosensory system. An important cortical structure in the parietal lobe is the postcentral gyrus (equivalent to BA 1, 2 and 3). It is located next to the lateral sulcus (Sylvian fissure) and seems to be the primary terminal point of the somatosensitive pathway. In this region, sensory modalities like temperature, proprioception and nociception become aware without further interpretation. The secondary somatosensitive cortex (equivalent to BA 5 and 7) is located next to the postcentral gyrus and enables a first-processing of somatosensitive impulses. The angular gyrus (BA 39) lies near the boundary of the superior temporal sulcus and is the central switchpoint between the visual cortex and the sensoric speech centre in the secondary auditory cortex.

The occiptal lobe is the neocortical manifestation of the visual system. The primary visual cortex (V1) (equivalent to BA 27) is also known as the striate cortex, because of its macroscopically observable white band (band of Vicq d'Azyr). It can be found

in and around the calcarine fissure. The secondary visual cortex or prestriate cortex encircles V1 and comprises BA 18 and 19.

The temporal lobe is significatly involved in the auditory sensory system. The primary auditory cortex (BA 41) can be found, specifically in the human organism, in the transverse temporal gyrus, also called Heschl's gyrus, cf. [GS80] and [LPKL98]. The secondary auditory cortex (BA 22) is located lateral to A1. The brain functional lateralization yields that Wernicke's area is located in the dominant hemisphere, which, for the majority of human beings, can be found in the left hemisphere.

The thalamus is the largest and most important part of the diencephalon and surrounds the third ventricle. It consists of multiple nuclei groups with different functions, which are connected to each other via associative fibres. Almost all sensitive and sensoric pathways project into the thalamus, where information is re-diverted to the cerebral cortex. At this connection, many integrative processes occur, which are crucial for the selection of informational flow.

Memory and its age-related changes

Characterization of memory

Memory is the ability to store, preserve and recall information. William James (1842–1910) was among the first who described memory as to be "the knowledge of a former state of mind after it has already once dropped from consciousness; or rather it is the knowledge of an event, or fact, of which we have not been thinking, with the additional consciousness that we have thought or experienced it before", cf. [Jam90].

Memory can be differentiated into episodic and semantic memory, first proposed by Endel Tulving in 1972, cf. [Tul72]. Both together make up the declarative memory. Semantic memory is based on the knowledge which has been learned, whereas episodic memory is connected to experience in spatiotemporal context and is rather autobiographical in its nature, cf. [KG09] and [Con09]. However, the underlying processes of extracting and representing experience in episodic memory still remain unknown.

Another distinction of different memory types is based on the persistence of memory

and dates back to Hermann Ebbinghaus (1850-1909) and William James (1842-1910), cf. [KG09]. According to this characterization, memory is being subdivided into immediate memory (lasting seconds to minutes), short-term memory (lasting minutes to an hour) and long-term memory (lasting more than an hour). The storage of information in short-term memory for the purpose of further processing is also known under the notion "working memory", cf. [BB08].

Nota bene: In the course of this thesis, especially regarding the analysis of functional networks, we will not further distinguish between immediate memory and short-term memory and mostly using the latter notion unless otherwise specified. Analogously, and by abuse of notation, we will use the notions episodic memory and long-term memory interchangeably.

Knowledge about the anatomical location of brain regions, which are involved in the processing of memory, emerged in the 1950s for the first time. The examination of amnestic loss after lesions, mostly in surgical patients, boosted the understanding of memory localization, cf. [SM57], [GCC88], [ZMS85]. Furthermore, animal experiments contributed as well to the understanding of memory localization, e.g. also confirmed a diminuation of memory caused by bilateral lesions in the hippcampus, cf. [ZMS85] and [Mis78].

Cortical structures that play a crucial role in the formation of memory comprise the entorhinal, perirhinal and parahippocampal cortices, cf. [ZMSAS89], [ZMSCR93]. After memory has been acquired, the neocortex becomes more and more important regarding memory storage and retrieval, cf. [SB07] and [TPR$^+$06]. The activation of memory, i.e. the retrieval of information, primarily passes through the hippocampus, which acts as a hub for the perirhinal and parahippocampal cortex. There are three pathways for the information flow through the hippocampus: firstly, the entorhinal-hippocampal pathway (also known as the perforant pathway) from entorhinal cortex to the dentate gyrus, secondly, the mossy fiber pathway from granule cells of dentate gyrus to Cornu Ammonis area (=CA) 3 and thirdly, the Schaffer collateral pathway from CA3 to CA.

Memory comprises billions of so-called engrams, which are a hypothetical means by which memory traces are stored as permanent physiological changes in the brain in response to external stimuli. Engrams are built by long-term potentiation (LTP) giving

due regard to a more cellular level, cf. [BL73]. It is the LTP which causes an enhancement of synaptic transmission that underlies post-synaptically on a displacement of Mg^{2+}-ion plug from (NMDA)-receptor (N-methyl-d-aspartate). This entails a change in the activation status of the cell membrane: from hypopolarization to depolarization, cf. [BC93], whereas Ca^{2+}-ions flow into the cell. Protein kinases, Ca^{2+}-calmodulin and retrograde signal generators are activated, which lead to enhanced release of glutamate and trafficking of AMPA-receptors (α-amino-3-hydroxy-5-methyl-4-isoxazolepropionic acid receptor) to the membrane.

LTP can be sub-divided in an early (1–3 hrs.) and a late phase (beyond 24 hrs.), whereas the early LTP occurs because of the binding of glutamate to AMPA-receptors and adjacent depolarization. The late LTP, which is crucial for long-term memory, cf. [ANB+97], [BAB+98] and [PHP+02], needs an induction of genes, cf. [FHK93] and [QGC+93]. For the consolidation of short-term memory into long-term memory, the phosphorylation of transcription factors is necessary. This involves the second messenger cAMP[1]-dependent protein kinase, which modulates the expression of memory genes like CREB-1 (cAMP response element-binding protein), cf. [ABK98] and [DHK90].

Age-related changes

Ageing is a physiological process which is associated with the deterioration of sensoric and cognitive abilities, like the slowdown of information processing and the loss of memory, cf. [BOH89], [GDR00] and [SPAea00]. It is correlated with atrophy, loss of brain volume, increase in white matter hyper-intensities and vascular changes, cf. [GJC+99], [KTCea08] and [FF10].

The causes for the loss of volume seem to be multifactorial, examples of which include the loss of synaptic connections, cf. [Bar04], and the reduction of neuropil, cf. [PMS01]. In this regard, an age-related reduction in grey matter (12–14 %) and white matter (23–26 %) can be found, which is observed to be non-linear in time, cf. [SPT+03]. In particular, the regression of white matter seems to be a reason for an impairment of attentional and mental processes, specifically of deficits in memory, cf. [GDR00]. However, the age-related structural changes seem to be quite specific in the different brain areas. By means of Diffusion Tensor Imaging (DTI) it has been found that there

[1] cAMP = cyclic adenosine monophosphate

is an age-related reduction of synaptic connections in the prefrontal cortex that is associated with attentional deficits, cf. [SMM+95]. In addition to the prefrontal cortex, there has been found hyperintensities in MRI data of the medial temporal lobe and the cingulum that are also related to attentional deficits, cf. [NRY+06]. Apparently, an age-related loss of brain volume can primarily be found in the temporal and frontal lobe, i.e. in regions that are involved in attentional processes and in working memory, cf. [ABBD05], whereas the visual cortex seems not to be affected, cf. [RLR+05]. In particular, the frontal and temporal lobe seem to be vulnerable for structural changes during the life span, cf. [Gre07]. Because of its integrative function in cognition, the frontal lobe is assigned an important role in cognitive aging, which is referred to, in literature, as the ,,prefrontal cortex function theory to cognitive aging", cf. [Wes96]. A further aspect is that a loss of volume in the hippocampus seems to occur only at older age. Up to the age of 70 years there cannot be found any reduction of volume in hippocampus, cf. [SMM+95], whereas after the age of 85 years extensive reductions accumulate, cf. [MDM+96].

Although many processes can be observed and are assigned an important role in aging, the different findings are like pieces of an unsolved puzzle. It remains very much unclear to what extent the structural changes and cognitive functions, such as performance of memory, can be set in context, cf. [SKJ02] and [RR04]. However, examining the age-related changes of interaction between brain areas, could initiate relevant considerations. Grady et al. (2003) examined age-related changes in functional connectivity between hippocampus and cortical structures during recognition performance, cf. [GMC03]. In the group of young adults (mean age: 23 years), activity of hippocampus showed a correlation to activity of ventral prefrontal and extrastriate regions. At this, increased activity of these regions was associated with better recognition. In the group of older adults (mean age: 66 years) hippocampal activity was correlated with dorsolateral prefrontal and parietal regions. Similarly to the younger adults, increased activity in these regions was also connected to better memory performance. The results show that ageing and its effects on memory performance is associated with functional hippocampal interactions and a ventral/dorsal shift of involved functionally connected regions. However, it is difficult to separate physiological effects of aging from pathophysiological processes like Alzheimer's disease and dementia, whose prevalence increases with age, cf. [SPTea06].

Functional magnetic resonance imaging

This section of the chapter briefly summarizes the physical foundations of MRI (resp. fMRI). This technique has been used to measure the brain activity and, hence, yielded the raw data for our analysis. Some physiological aspects which are related to functional brain activation are highlighted. Further reference can be found in [SF06] and [GM10].

Physical background of fMRI

Functional magnetic resonance imaging (fMRI) is a non-invasive technique to measure and visualize the hemodynamic response (change in blood flow) related to neural activity in the brain. This method features a comparatively good spatial resolution (2–6mm) and abstains from using ionizing radiation. It was applied to the human brain for the first time in 1991, cf. [BKM$^+$91]. Moreover, fMRI allows for a precise localization of specifically stimulated brain areas. The spatial resolution exceeds the values that can be attained by other non-invasive techniques such as positron emission tomography (PET), magnetoencephalography (MEG) or electroencephalography (EEG), cf. [HF00]. However, the temporal resolution of roughly 5–8 seconds is relatively low compared to the other aforementioned techniques.

The physical phenomenon behind MRI is the effect of nuclear spin resonance, which was described in 1946 for the first time, cf. [Blo46] and [PTP46]. The nuclear spin is the total angular momentum of the nucleus, being composed of the orbital angular momentum and the intrinsic angular momentum. The rotating nucleus features an electrical charge which yields a dipole moment proportional to the angular (spin) momentum. The dipole moments in matter are lacking a structural organization, unless there is some external influence. By applying a strong external magnetic field, the nuclear spins and hence, also the dipole moments, orient toward the magnetic field lines. When applying a second external electromagnetic high-frequency field, the energetic configuration of the nuclei will change and, as a consequence, the spatial orientation of the dipole moments, accordingly. As soon as the second high-frequency field is turned off, the nuclei will revert to their preferential alignment according to the weaker main magnetic field. By doing so, the nuclei emit electromagnetic radiation which can be measured: the emitted radiation induces an electric potential in a receptor coil, which is then recorded as the *magnetic resonance signal (=MR-signal)*.

Random noise in the signal is assumed to be uniformly distributed and thus, can be minimized by averaging the signal from stimulation and resting (or control) phases, accordingly. Measuring the induced resonance signal always yields the sum signal for all nuclear spins in the testing range. The cubic or ashlar-formed three-dimensional measuring volume is sub-divided into smaller pieces, the so-called *voxels*.

Spatial encoding, such as slice selection, frequency or phase encoding, is used in order to calculate the individual contributions of each voxel to the sum signal, cf. [Lau73] or [MG73]. The spatially encoded MR-signal is henceforth recorded as a complex number, having a frequency part and a phase part. By applying an inverse Fourier transformation to these two-dimensional arrays of values one can reconstruct a phase image in the real position space, i.e. the usual sliced MR-picture having grey scale values and depicting different intensity values.

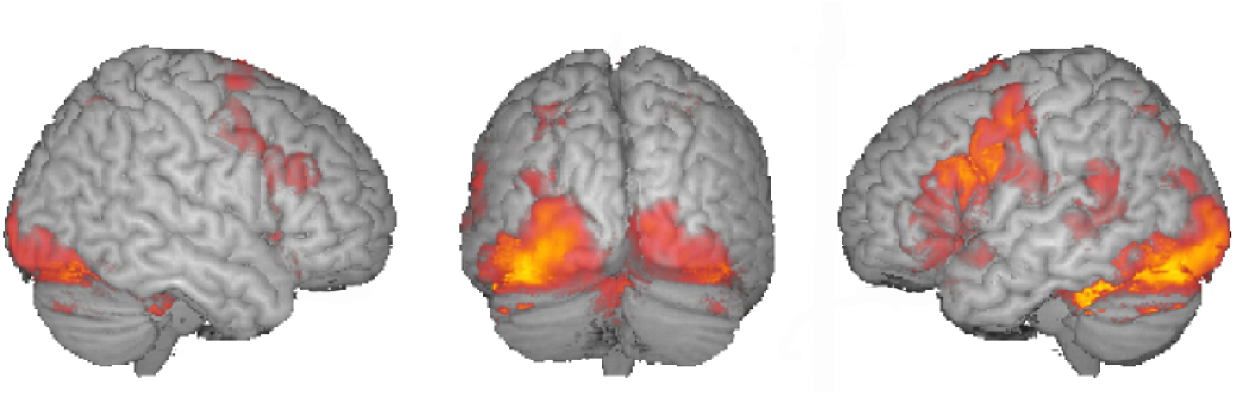

Fig. 5.7: Example of an fMRI picture. Copyright: `http://www.med.nyu.edu/thesenlab/group/images/fmri2.jpg`

Physiological background of fMRI

Hemoglobin enables the transport of oxygen and appears in two variants in the blood: oxyhemoglobin and de-oxyhemoglobin. Increased neuronal activity yields a local rise in the blood volume and also in the blood flow, thereby oxyhemoglobin is metabolized into de-oxyhemoglobin. This increase in the concentration of de-oxyhemoglobin is being over-compensated by a net increase in oxyhemoglobin, which is caused by the inflow of fresh, oxygenized blood. The diamagnetic oxyhemoglobin does not influence the magnetic field, whereas the paramagnetic de-oxyhemoglobin causes a change in the susceptibility parameters and, as a consequence, to a decrease of the measured signal strength. This change in the MR-signal is denoted by the term blood oxagenation level dependent (BOLD) contrast, cf. [SHT$^+$02].

The relaxation times for oxygenized (t= 181ms) and de-oxygenized (t=254ms) blood[1] are different. Basically, it is the difference of intensity in the BOLD contrast, and thus the different relaxation times between stimulation phases and control phases, that is being measured. The activation of brain regions correlates with an increase in the BOLD contrast in the corresponding areas and hence, yields a higher signal.

The hemodynamic response function, i.e. the hemodynamic impulse following a stimulus onset, has a periodic length of about $20s$ to $25s$ and is thus relatively long compared to the direct excitation transmission of the involved neurons, which in turn lasts only about 1 millisecond. However, a complete fMRI scan, which covers all brain slices, lasts about 2 seconds and is thus negligibly short compared to the period of the hemodynamic response function, cf. [HOD04] and [BWF98].

[1]The relaxation times mentioned here refer to a magnetic field strength of B = 1.5 Tesla.

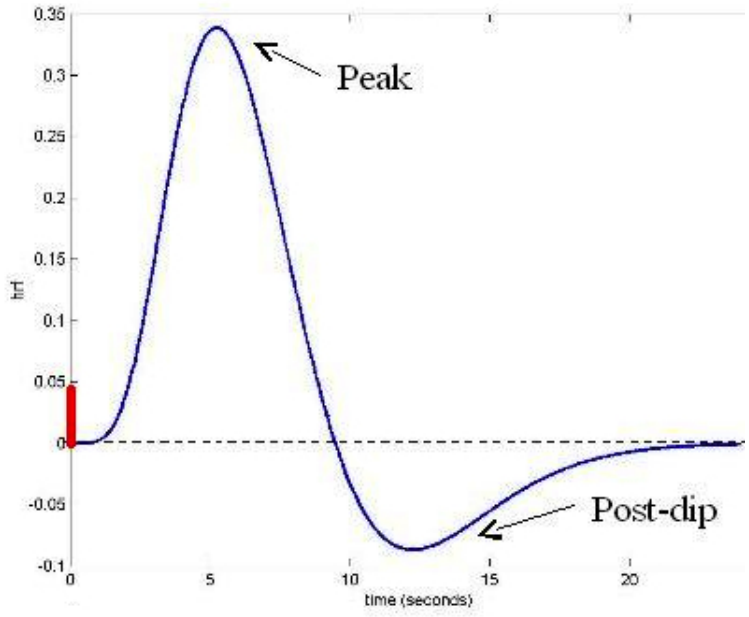

Fig. 5.8: Typical hemodynamic response function. The thick bar on the vertical axis denotes schematically the stimulus onset. Copyright: `http://www.unc.edu/~wenjiec/images/glover.jpg`

Abbreviations and Talairach atlas

Abbreviation	Anatomical structure
caud	caudate
a.cing	anterior cingulate
s.front	superior frontal gyrus
mi.front	middle frontal gyrus
i.front	inferior frontal gyrus
me.front	medial frontal gyrus
ins	insula
parahip	parahippocampal gyrus
s.temp	superior temporal gyrus
m.temp	middle temporal gyrus
cing	cingulate gyrus
postcen	postcentral gyrus
precen	precentral gyrus
i.parite	inferior parietal lobule
s.pariet	superior parietal lobule
precun	precuneus
cun	cuneus
ling	lingual gyrus
fusi	fusiform gyrus
i.occ	inferior occipital gyrus
m.occ	middle occipital gyrus
p.cing	posterior cingulate
unc	uncus
lenti	lentiform nucleus
thal	thalamus

	HEMISPHER	GROBSTRUI	LOBE	GYRUS	TISSUE	TISSUE TYPE
1	Right	Cerebrum	Limbic Lode	Inferior Semi-Lunar Lobule	Gray Matter	Brodmann area 1
2	Left	Cerebrellum	Occipital Lobe	Fusiform Gyrus		Brodmann area 2
3	Inter-Hemisperic	Brainstem	Frontal Lobe	Parahippocampal Gyrus		Brodmann area 3
4			Parietal lobe	Superior Occipital Gyrus		Brodmann area 4
5			Temporal Lobe	Uncus		Brodmann area 5
6			Midbrain	Subcallosal Gyrus		Brodmann area 6
7			Sub-lobar	Cerebellar Tonsil		Brodmann area 7
8			Posterior lobe	Cerebellar Lingual		Brodmann area 8
9			Anterior lobe	Sub-Gyral		Brodmann area 9
10				Anterior Cingulate		Brodmann area 10
11				Cuneus		Brodmann area 11
12				Precuneus		
13				Tuber of Vermis		Brodmann area 13
14				Superior Frontal Gyrus		
15				Middle Frontal Gyrus		
16				Inferior Frontal Gyrus		
17				Angular Gyrus		Brodmann area 17
18				Superior Parietal Lobule		Brodmann area 18
19				Declive of Vermis		Brodmann area 19
20				Thalamus		Brodmann area 20
21				Inferior Temporal Gyrus		Brodmann area 21
22				Uvula		Brodmann area 22
23				Lingual Gyrus		Brodmann area 23
24				Insula		Brodmann area 24
25				Lentiform Nucleus		Brodmann area 25
26				Transverse Temporal Gyrus		
27				Paracentral Lobule		Brodmann area 27
28				Uvula of Vermis		Brodmann area 28
29				Inferior Occipital Gyrus		Brodmann area 29
30				Rectal Gyrus		Brodmann area 30
31				Medial Frontal Gyrus		Brodmann area 31
32				Pyramis of Vermis		Brodmann area 32
33				Precentral Gyrus		Brodmann area 33
34				Posterior Cingulate		Brodmann area 34
35				Claustrum		Brodmann area 35
36				Inferior Parietal Lobule		Brodmann area 36
37				Pyramis		Brodmann area 37
38				Postcentral Gyrus		Brodmann area 38
39				Culmen of Vermis		Brodmann area 39
40				Culmen		Brodmann area 40
41				Supramarginal Gyrus		Brodmann area 41
42				Orbital Gyrus		Brodmann area 42
43				Middle Temporal Gyrus		Brodmann area 43
44				Declive		Brodmann area 44
45				Cingulate Gyrus		Brodmann area 45
46				Extra-Nuclear		Brodmann area 46
47				Middle Occipital Gyrus		Brodmann area 47
48				Superior Temporal Gyrus		
49				Nodule		
50				Fastigium		
51				Tuber		

Fig. 5.9: Talairach atlas, including lobe, Gyri and Brodmann level. Copyright: [TT08]

References

[AB02] R. Albert and A.-L. Barabasi, *Statistical mechanics of complex networks*, Rev. Mod. Phys. **74** (2002), 47–97.

[AB07] S. Achard and E. Bullmore, *Efficiency and cost of economical brain functional networks*, PloS Comp. Biol **3** (2007), e17.doc10.1371/journal/pcbi.0030017.

[ABBD05] J.S. Allen, J. Bruss, C.K. Brown, and H. Damasio, *Normal neuroanatomical variation due to age: the major lobes and a parcellation of the temporal region.*, Neurobiol Aging **26(9)** (2005), 1245–1260.

[ABJ06] F.M. Atay, T. Biyikoglu, and J. Jost, *Network synchronization: Spectral versus statistical properties*, Elsevier **224** (2006), 35–41.

[ABK98] T. Abel, K.C. Bartsch, and E.R. Kandel, *Memory suppressor genes: Inhibitory constraints on the storage of long-term memory.*, Science **279(5349)** (1998), 338–341.

[ADGPV06] A. Arenas, A. Diaz-Guilera, and C.J. Perez-Vicente, *Synchronization reveals topological scales in complex networks*, Phys. Rev. Letters **96** (2006), 114102.

[AGD94] L. Arnold, V. Gundlach, and L. Demetrius, *Evolutionary formalism for products of positive random matrices*, Annals of Probab. **4** (1994), 859–901.

[AJB00] R. Albert, H. Jeong, and A.L. Barabasi, *Error and attack tolerance of complex networks*, Nature **406** (2000), 378–381.

[AJW04] F.M. Atay, J., and A. Wende, *Delays, connection topology, and synchronization of coupled chaotic maps*, Phys. Rev. Letters **92** (2004), 144101.

[ANB+97] T. Abel, P.V. Nguyen, M. Barad, T.A. Deuel, E.R. Kandel, and R. Bourtchouladze, *Genetic demonstration of a role for pka in the late phase of ltp and in hippocampus-based long-term memory.*, Cell **88(5)** (1997), 615–626.

[AO04] L. Amaral and J. Ottino, *Complex networks: Augmenting the framework for the study of complex systems*, Eur.Phys. J. **38** (2004), 147–162.

[ASBS00] L.A.N. Amaral, A. Scala, M. Barthelemy, and H.E. Stanley, *Classes of small-world networks*, Proc Natl Acad Sci USA **97** (2000), 11149–11152.

[ASW+06] S. Achard, R. Salvador, B. Whitcher, J. Suckling, and E. Bullmore, *A resilient, low-frequency, small-world human brain functional network with highly connected association cortical hubs*, J Neuroscience **26** (2006), 63–72.

[BA99] L. Barabasi and R. Albert, *Emergence of scaling in random networks*, Science **286** (1999), 509–512.

[BAB+98] R. Bourtchouladze, T. Abel, N. Berman, R. Gordon, K. Lapidus, and E.R. Kandel, *Different training procedures recruit either one or two critical periods for contextual memory consolidation, each of which requires protein synthesis and pka.*, Memory **5(4-5)** (1998), 365–374.

[Bad10] A. Baddeley, *Working memory*, Curr Biol **20** (2010), 136–140.

[Ban08a] A. Banerjee, *The spectrum of the graph laplacian as a tool for analyzing structure and evolution of networks*, Universität Leipzig, Leipzig, 2008.

[Ban08b] ———, *Structural distance and evolutionary relationship of networks*, arXiv:0807.3185 (2008).

[Bar03] A.L. Barabasi, *Linked.*, London: Penguin. (2003).

[Bar04] G. Bartzokis, *Age-related myelin breakdown: a developmental model of cognitive decline and alzheimer's disease.*, Neurobiol. Aging **25(1)** (2004), 5–18.

[BB08] Ch. M. Bird and N. Burgess, *The hippocampus and memory: insights from spatial processing.*, Nature **9** (2008), 182–194.

[BBML08] D.S. Bassett, E. Bullmore, and A. Meyer-Lindenberg, *Hierarchical organization of human cortical networks in health and schizophrenia.*, J. Neuroscience **28(37)** (2008), 9239–9248.

[BC93] T.V. Bliss and G.L. Collinridge, *A synaptic model of memory: Long-term potentiation in the hippocampus.*, Nature **361(6407)** (1993), 31–39.

[Ber93] H.C. Berg, *Random walks in biology*, Princeton University Press, Princeton, 1993.

[BFM+04] E.T. Bullmore, M.J. Fadili, V. Maxim, L. Sendur, B. Whitcher, J. Suckling, and M. Bramer, *Wavelets and functional magnetic resonance imaging of the human brain.*, NeuroImage **23** (2004), 234–249.

[Bil65] P. Billingsley, *Ergodic theory and information*, Wiley, New York, 1965.

[BJa] A. Banerjee and J. Jost, *Graph spectra as a systematic tool in computational biology*, arXiv **0706.0113v1**.

[BJb] ———, *Laplacian spectrum and protein-protein interaction networks*, arXiv **0705.3373v1**.

[BJc] ———, *On the spectrum of the normalized graph laplacian*, arXiv **0705.3772v1**.

[BJ07] ———, *Spectral plots and the representation and interpretation of biological data*, Theory Biosc. **126** (2007), 15–21.

[BJ08] ———, *Spectral plot properties: Towards a qualitative classification of networks*, NHM **3** (2008), 395–411.

[BJ09] ———, *Spectral characterization of network structures and dynamics*, in: Dynamics on and of Complex Networks (2009), 117–132.

[BKM+91] J.W. Belliveau, D.N. Kennedy, RC. McKinstry, B.R. Buchbinder, R.M. Weisskoff, M.S. Cohen, J.M. Vevea, T.J. Brady, and B.R. Rosen, *Functional mapping of the human visual cortex by magnetic resonance imaging.*, Science **254** (1991), 716–719.

[BL73] T.V. Bliss and T. Lomo, *Long-lasting potentiation of synaptic transmission in the dentate area of the unanaestetized rabbit following stimulation of the perforant path.*, Journal of Physiology **232(2)** (1973), 331–356.

[BLM+06] S. Boccaletti, V. Latora, Y. Moreno, M. Chavez, and D.U. Hwang, *Complex networks: structure and dynamics*, Physics Reports **424** (2006), 175–308.

[Blo46] F. Bloch, *Nuclear interaction.*, Phys. Rev. **70** (1946), 460–474.

[BMLA+06] D.S. Bassett, A. Meyer-Lindberg, S. Achard, Th. Duke, and E. Bullmore, *Adaptive reconfiguration of fractal small-world human brain functional networks*, PNAS **103** (2006), 19518–19523.

[BOH89] T.R. Bashore, A. Osman, and E.F. Heffley, *Mental slowing in elderly persons: a cognitive psychophysiological analysis.*, Psychol. Aging. **4** (1989), 235–244.

[Bol01] B. Bollobas, *Random graphs*, Academic Press, New York **2nd edition** (2001).

[Bre95] S.L. Bressler, *Large-scale cortical networks and cognition*, Brain Res. Brain Res. Rev. **20** (1995), 288–304.

[Bre97] G.E. Bredon, *Topology and geometry*, Springer, New York, 1997.

[Bro09] K. Brodmann, *Vergleichende lokalisationslehre der großhirnrinde.*, Barth, Leipzig, 1909.

[BS09] E. Bullmore and O. Sporns, *Complex brain networks: graph theoretical analysis of structural and functional systems*, Nature **10** (2009), 186–198.

[BSHG07] L.M.A. Bettencourt, G.J. Stephens, M.I. Ham, and G.W. Gross, *Functional structure of cortical neuronal networks grown in vitro*, Phys. Rev. E. **75** (2007), 021915.

[BWF98] R.B. Buxton, E.C. Wong, and L.R. Frank, *Dynamics of blood flow and oxygenation changes during brain activation: the balloon model.*, Magn Reson Med **39** (1998), 855–864.

[Cal85] H. B. Callen, *Thermodynamics and an introduction to thermostatistics*, Wiley, New York, 1985.

[CCdS06] E. Carlsson, G. Carlsson, and V. de Silva, *An algebraic topological method for feature identification*, Int J Comp Geometry **16** (2006), 291–314.

[CCM08] R. Cabeza, E. Ciaramelli, and M. Moscovitch, *The parietal cortex and episodic memory: an attentional account*, Nature Reviews **9** (2008), 613–625.

[Chu97] F. Chung, *Spectral graph theory*, AMS, 1997.

[Con09] M.A. Conway, *Episodic memories.*, Neuropsychologia **47** (2009), 2305–2313.

[CSEH07] D. Cohen-Steiner, H. Edelsbrunner, and J. Harer, *Stability of persistence diagrams*, Discrete Comput. Geom. **37** (2007), 103–120.

[CW51] H.B. Callen and T.A. Welton, *Irreversibility and generalized noise*, Physical Review **83** (1951), 34–40.

[CZCG05] G. Carlsson, A. Zomorodian, A. Collins, and L. Guibas, *Persistence barcodes for shapes*, Int J Shape Modeling (2005), 149–187.

[DDC08] S.W. Davis, N.A. Dennis, and R. Cabeza, *Que pasa? the posterior-anterior shift in ageing*, Cerebral Cortex **18** (2008), 1201–1209.

[Dem97] L. Demetrius, *Directionality principles in thermodynamics andevolution*, PNAS **94** (1997), 3491–3498.

[DGO04] L. Demetrius, V.M. Gundlach, and G. Ochs, *Complexity and demographic stability in population models*, Theor. Popul. Biol. **65** (2004), 211–225.

[DHK90] P.K. Dash, B. Hochner, and E.R. Kandel, *Injection of the camp-responsive element into the nucleus of aplysia sensory neurons blocks long-term facilitation.*, Nature **345(6277)** (1990), 718–721.

[DHM05] L. Donetti, P.I Hurtado, and M.A. Munoz, *Entangled networks, synchronization, and optimal network topology*, Phys. Rev. Letters **95** (2005), 188701.

[DM03] S.N. Dorogovtsev and J.F.F. Mendes, *Evolution of networks. from biological nets to the internet and www*, Oxford University Press, 2003.

[DM04] L. Demetrius and T. Manke, *Robustness and network evolutionÑan entropic principle*, Physica A, Elsevier **346** (2004), 682–696.

[DMSM00] V. Della-Maggiore, A.B. Sekuler, and A.R. McIntosh, *Cortiolimbic interactions associated with performance on a short-term memory task are modified by age.*, J. Neuroscience **20(22)** (2000), 8410–8416.

[Dor09] S. Dorogovtsev, *Lectures on complex networks*, Oxford, Oxford, 2009.

[DSH05] P. Deetjen, E.-J. Speckmann, and J. Heschler, *Physiologie*, Elsevier, München, 2005.

[ECS+05] V.M Equiliuz, D.R. Chialvo, P. Skudlarski, J.C. Gore, and R.T. Constable, *Scale-free brain functional networks*, Phys. Rev. Lett. **94** (2005), Art.no.018102.

[ELZ02] H. Edelsbrunner, D. Letscher, and A. Zomorodian, *Topological persistence and simplification*, Discrete and Computational Geometry **28** (2002), 511–533.

[FF10] M. Folstein and S. Folstein, *Functional expressions of the aging brain.*, Nutr. Rev. **68** (2010), 70–73.

[FHK93] U. Frey, Y.Y. Huang, and E.R. Kandel, *Effects of camp simulate a late stage of ltp in hippocampal ca1 neurons.*, Science **260(5114)** (1993), 1661–1664.

[GCC88] J.D. Gabrieli, N.J. Cohen, and S. Corkin, *The impaired learning of semantic knowledge following bilateral medial temporal-lobe resection.*, Brain and Cognition **7(2)** (1988), 157–177.

[GCG02] M. Grossmann, A. Cooke, and J. Gee, *Age-related changes in working memory during sentence comprehension: an fmri study*, NeuoImage **15** (2002), 302–317.

[GDR00] F.M. Gunnin-Dixon and N. Raz, *The cognitive correlates of white matter abnormalities in normal aging: a quantitative review.*, Neuropsychology **14** (2000), 224–232.

[GJC+99] J.N. Giedd, N.O. Jeffries, F.X. Castellanos, H. Liu, A. Zijdenbos, and et al., *Brain development during childhood and adolescence: a longitudinal mri study.*, Nat Neurosci. **2(10)** (1999), 861–863.

[GKM03] M.D. Greicius, B. Krasnow, and V. Menon, *Functional connectivity in the resting brain: a network analysis of the default mode hypthesis*, PNAS **100(1)** (2003), 253–258.

[GM10] C. Gerthsen and D. Meschede, *Gerthsen physik*, Springer, Berlin, 2010.

[GMC03] C.L. Grady, A.R. McIntosh, and F.I. Craik, *Age-related differences in the functional connectivity of the hippocampus during memory encoding.*, Hippocampus **13(5)** (2003), 572–586.

[GR01] C. Godsil and G. Royle, *Algebraic graph theory*, Springer, Heidelberg, 2001.

[Gra08] C.L. Grady, *Cognitive neuroscience of aging.*, Ann N Y Acad Sci **1124** (2008), 127–144.

[Gre07] P.M. Greenwood, *Functional plasticity in cognitive aging: review and hypothesis.*, Neuropsychology **21(6)** (2007), 657–673.

[GS80] A. Galaburda and F. Sanides, *Cytoarchitectonic organization of human auditory cortex.*, J Comp Neurol. **190** (1980), 597–610.

[GSM04] M.D. Greicius, G. Srivastava, and V. Menon, *Default-model network activity distinguishes alzheimer's disease from healthy ageing: evidence from functional mri*, PNAS **101(3)** (2004), 4637–4642.

[Har69] F. Harary, *Graph theory*, Perseus Reading, Massachusetts, 1969.

[Hat02] A. Hatcher, *Algebraic topology*, Cambridge University Press, Cambridge, 2002.

[HBO+00] C.C. Hilgetag, G.A. Burns, M.A. O'Neill, J.W. Scannell, and M.P. Young, *Anatomical connectivity defines the organization of clusters of cortical areas in the macaque monkey and the cat*, Phil. Trans. R. Soc. Lond. B. **355** (2000), 91–110.

[HCE07] Y. He, Z. Chen, and A. Evans, *Small-world anatomical networks in the human brain revealed by cortical thickness from mri*, Cereb. Cortex **17(10)** (2007), 2407–2419.

[HDC06] M. Hampson, N.R. Driesen, and R.T. Constable, *Brain connectivity related to working memory performance*, J. Neuroscience **26(51)** (2006), 13338–13343.

[HF00] B. Horwitz and K.J. Friston, *Neural modeling and functional brain imaging: an overview.*, Neural Netw. **13** (2000), 829–846.

[HG08] M.D. Humphries and K. Gurney, *Network 'small-worldness': A quantitative method for determining canonical network equivalence*, PLoS ONE **3(4)** (2008), e0002051.

[HGP05] M.D. Humphries, K. Gurney, and T.J. Prescott, *Small-world and scale-free properties of the brainstem reticular formation.*, Proc R Soc Lond B Biol Sci **in press** (2005).

[HMR09] D. Horak, S. Maletic, and M. Rajkovic, *Persistent homology of complex networks*, J Stat. Mechanics (2009), P03034.

[HOD04] D.A. Handwerker, J.M. Ollinger, and M. D'Esposito, *Variation of bold hemodynamic responses across subjects and brain regions and their effects on statistical analyses.*, Neuroimage **21** (2004), 1639–1651.

[Hor03] B. Horwitz, *The elusive concept of brain connectivity.*, NeuroImage **19** (2003), 466–470.

[IM02] M. Ipsen and A.S. Mikhailovic, *Evolutionary reconstruction of networks*, Phys. Rev. E **66** (2002).

[Jam90] W. James, *Principles of psychology.*, Henry Holt and Co., New York, 1890.

[JJ02] J. Jost and M.P. Joy, *Spectral properties and synchronization in coupled map lattices*, Phys. Rev. E **65** (2002).

[Jon07] J. Jonsson, *Simplicial complexes of graphs*, Springer, Heidelberg, 2007.

[Jos05] J. Jost, *Dynamical systems. examples of complex behaviour.*, Springer, Heidelberg, 2005.

[Jos07] ———, *Dynamical networks, in networks: From biology to theory*, Springer Lecture Notes in Computer Science, Heidelberg, 2007.

[JTA+00] H. Jeong, B. Tombor, R. Albert, Z.N. Oltvai, and L.A. Barabasi, *The large-scale organization of metabolic networks*, Nature **407** (2000), 651–654.

[JW94] D. Johnston and S. Miao-Sin Wu, *Foundations of cellular neurophysiology*, MIT Press, Boston, 1994.

[KG09] J. Koppel and T. Goldberg, *The genetics of episodic memory.*, Cogn. Neuropsychiatry **14** (2009), 356–376.

[KH04] M. Kaiser and C.C. Hilgetag, *Spatial growth of real-world networks.*, Phys Rev E **69** (2004), 036103.

[KSea09] R. Klinke, S. Silbernagl, and et al., *Physiologie*, Thieme-Verlag, Stuttgart, 2009.

[KSJ00] E.R. Kandel, J.H. Schwartz, and T.M. Jessell, *Principles of neural science.*, Mcgraw-Hill Professional, 2000.

[KTCea08] P. Kochunov, P.M. Thompson, T.R. Coyle, and et al., *Relationship among neuroimaging indices of cerebral health during normal aging.*, Hum Brain Mapp. **20** (2008).

[LAJ07] W. Lu, F.M. Atay, and J. Jost, *Synchronization of discrete-time dynamical networks with time-varying couplings*, SIAM J. Math. Anal. **39** (2007), 1231–1259.

[Lau73] P. Lauterbur, *Image formation by induced local interactions: Examples employing nuclear magnetic resonance.*, Nature **242** (1973), 190–191.

[Lee05] D.S. Lee, *Synchronization transition in scale-free networks: clusters of synchrony.*, Phys. Rev. Letters **72** (2005), 026208.

[LFR08] A. Lancichinetti, S. Fortunato, and F. Radicchi, *Benchmark graphs for testing community detection algorithms*, arXiv **0805.4770v4** (2008).

[LHNPI01] K. Linkenkaer-Hansen, V.V. Nikouline, J.M. Palva, and R.J. Ilmoniemi, *Long-range temporal correlations and scaling behaviour in human brain oscillations*, J Neurosci **21** (2001), 1370–1377.

[LPKL98] C.M. Leonard, C. Puranik, J.M. Kuldau, and L.J. Lombardino, *Normal variation in the frequency and location of human auditory cortex landmarks. heschl's gyrus: Where is it?*, Cereb. Cortex **8** (1998), 397–406.

[LS03] S.B. Laughlin and T.J. Sejnowski, *Communication in neuronal networks.*, Science **301** (2003), 1870–1873.

[LWP+97] J.L. Lancaster, M.G. Woldorff, L.M. Parsons, M. Liotti, C.S. Freitas, L. Rainey, P.V. Kochunov, D. Nickerson, S.A. Mikiten, and P.T. Fox, *Automated talairach atlas labels for functional brain mapping*, Human Brain Mapping **10** (1997), 120–131.

[MAB09] D. Meunier, S. Achard, and E. Bullmore, *Age-related changes in modular organization of human brain functional networks*, NeuroImage **44** (2009), 715–723.

[May92] J.P. May, *Simplicial objects in algebraic topology*, University of Chicago Press, Chicago, 1992.

[MDM+96] D.G. Murphy, C. DeCarli, A.R. McIntosh, E. Daly, M.J. Mentis, P. Pietrini, and et al., *Sex differences in human brain morphometry and metabolism: an in vivo quantitative magnetic resonance imaging and positron emission tomography study on the effect of aging.*, Arch Gen Psychiatry **53(7)** (1996), 585–594.

[MDV04] T. Manke, L. Demetrius, and M. Vingron, *An entropic characterization of protein interaction networks and cellular robustness*, J. R. Soc. Interface **3** (2004), 843–850.

[Mes00] M.M. Mesulam, *Principles of behavioural and cognitive neurology.*, Oxford University Press, New York (2000).

[MG73] P. Mansfield and P.K. Granell, *Nmr 'diffraction' in solids?*, J Phys C **6** (1973), 422–426.

[Mil67] S. Milgram, *The small-world problem.*, Psychol. Today **1** (1967), 17–61.

[Mis78] M. Mishkin, *Memory in monkeys severely impaired by combined but not by separate removal of amygdala and hippocampus.*, Nature **273(5660)** (1978), 297–298.

[MSB+12] F. Matthäus, J.P. Schmidt, A. Banerjee, T. Schulze, T. Demirakca, and C. Diener, *Effects of age on the structure of functional connectivity networks during episodic and working memory demand*, Brain Connectivity *(under review)* (2012).

[MSOI+02] R. Milo, S. Shen-Orr, S. Itzkovitz, N. Kashtan, D. Chklovskii, and U. Alon, *Network motifs: simple building blocks of complex networks*, Science **298** (2002), 824–827.

[MVT+09] S. Micheloyannis, M. Vourkas, V. Tsirka, E. Karakonstantaki, K. Kanatsouli, and C.J. Stam, *The influence of ageing on complex brain networks: a graph theoretical analysis*, Human Brain Mapping **30(1)** (2009), 200–208.

[New03] M.E.J. Newman, *The structure and function of complex networks*, SIAM Rev. **45(2)** (2003), 167–256.

[Nie11] F. Nielsen, *A family of statistical symmetric divergences based on jensen's inequality*, arXiv:1009.4004v2 (2011).

[NMH03] T. Nishikawa, A.E. Motter, and F.C. Hoppensteadt, *Heterogeneity in oscillator networks: are smaller worlds easier to synchronize?*, Phys. Rev. E **93** (2003), 014101.

[NMW00] M. Newman, C. Moore, and D.J. Watts, *Mean-field solution of the small-world network model*, Phys Rev Letters **84** (2000), 3201–3204.

[NRY+06] C.W. Nordahl, C. Ranganath, A.P. Yonelinas, C. Decarli, E. Fletcher, and W.J. Jagust, *White matter changes compromise prefrontal cortex function in healthy elderly individuals.*, Cogn Neurosci **18(3)** (2006), 418–429.

[NSW01] M.E. Newman, S.H. Strogatz, and D.J. Watts, *Random graphs with arbitrary degree distributions and their applications*, Phys. Rev. **64** (2001), 026118.

[PHP+02] C. Pittenger, Y.Y. Huang, R.F. Paletzki, R. Bourtchouladze, H. Scanlin, S. Vronskaya, and et al., *Reversible inhibition of creb/atf transcription factors in region ca1 of the dorsal hippocampus disrupts hippocampus-dependent spatial memory.*, Neuron **34(3)** (2002), 447–462.

[PMKP10] J.M. Palva, S. Monto, S. Kulashekhar, and S. Palva, *Neuronal synchrony reveals working memory networks and predicts individual memory capacity*, PNAS **107** (2010), 7580–7585.

[PMS01] A. Peters, M.B. Moss, and C. Sethares, *The effects of aging on layer 1 of primary visual cortex in the rhesus monkey.*, Cereb Cortex **11(2)** (2001), 93–103.

[PNL+06] J. Persson, L. Nyberg, J. Lind, A. Larsson, L.G. Nilsson, M. Ingvar, and et al., *Structure-function correlates of cognitive decline in aging.*, Cereb Cortex **16** (2006), 907–915.

[PRK01] A. Pikovsky, M. Rosenblum, and J. Kurths, *Synchronization - a universal concept in nonlinear science*, Cambridge University Press, Cambridge, 2001.

[PTP46] E. Purcell, H. Torrey, and R. Pound, *Resonance absorption by nuclear magnetic moments in a solid.*, Phys. Rev. **69** (1946), 37–48.

[QGC+93] Z. Qian, M.E. Gilbert, M.A. Colicos, E.R. Kandel, and D. Kuhl, *Tissue-plasminogen activator is induced as an immediate-early gene during seizure, kindling and long-term potentiation.*, Nature **361(6411)** (1993), 453–457.

[RLR+05] N. Raz, U. Lindenberger, K.M. Rodrigue, K.M. Kennedy, D. Head, A. Williamson, and et al., *Regional brain changes in aging healthy adults: general trends, individual differences and modifiers.*, Cereb Cortex **15(11)** (2005), 1676–1689.

[RR04] K.M. Rodrigue and N. Raz, *Shrinkage of the entorhinal cortex over five years predicts memory performance in healthy adults.*, J Neuroscience **24(4)** (2004), 956–963.

[RS10] M. Rubinov and O. Sporns, *Complex network measures of brain connectivity: uses and interpretations*, NeuroImage **52** (2010), 1059–1069.

[SB04] C.J. Stam and E.A. Bruin, *Scale-free dynamics of global functional connectivity in the human brain*, Hum Brain Mapp **22** (2004), 97–109.

[SB07] L.R. Squire and P.J. Bayley, *The neuroscience of remote memory.*, Current Opinion in Neurobiology **17(2)** (2007), 185–196.

[SF06] F. Schneider and G. Fink, *Funktionelle mrt in psychiatrie und neurologie*, Springer, Berlin, 2006.

[SGS09] J. Steffener, Y. Gazes, and Y. Stern, *The impact of age-related changes on working memory functional activity*, Brain Imaging and Behaviour **3** (2009), 142–153.

[SHR12] J.P. Schmidt, D. Horak, and M. Rajkovic, *Persistent homology analysis of functional brain networks, in preparation* (2012).

[SHT+02] C. Stippich, S. Heiland, V. Tronnier, A. Mohr, and K. Sartor, *Klinische funktionelle magnetresonanztomographie (fmrt): Physiologische grundlagen, technische aspekte und anforderungen für die klinische anwendung.*, Rofo **174** (2002), 43–49.

[SJS06] C.J. Stam, B.F. Jones, and Ph. Sheltens, *Small-world networks and functional connectivity in alzheimer's disease*, Cerebral Cortex **17** (2006), 92–99.

[SKJ02] D.H. Salat, J.A. Kaye, and J.S. Janowsky, *Greater orbital prefrontal volumeselectively predicts worse working memory performance in older adults.*, Cereb. Cortex **12(5)** (2002), 494–505.

[SM57] W.B. Scoville and B. Miner, *Loss of recent memory after bilateral hippocampal lesions. journal of neurology.*, Journal of Neurology, Neurosurgery and Psychiatry. **20(1)** (1957), 11–21.

[SMG08] K. Supekar, V. Menon, and M.D. Greicius, *Network analysis of intrinsic functional brain connectivity in alzheimer's disease*, PLOS Comp. Biol. **4** (2008), e1000100.

[SMM+95] E.V. Sullivan, L. Marsh, D.H. Mathalon, K.O. Lim, and A. Pfefferbaum, *Agerelated decline in mri volumes of temporal lobe gray matter but not hippocampus.*, Neurobiol Aging **16(4)** (1995), 591–606.

[SPAea00] D. Schretlen, G.D. Pearlson, J.C. Anthony, and et al., *Elucidating the contributions of processing speed, executive ability, and frontal lobe volume*

to normal age-related differences in fluid intelligence., J Int Neuropsychol Soc. (2000).

[Spo06] O. Sporns, *Small-world connectivity, motif composition and complexity of fractal neuronal connections.*, Biosystems **85** (2006), 55–64.

[SPT+03] E.R. Sowell, B.S. Peterson, P.M. Thompson, S.E. Welcome, A.L. Henkenius, and A.W. Toga, *Mapping cortical change across the human life span.*, Nat Neurosci **6(3)** (2003), 309–315.

[SPTea06] T.M. Scott, I. Peter, K.L. Tucker, and et al., *The nutrition, aging, and memory in elders (name) study: design and methods for a study of micronutrients and cognitive function in a homebound elderly population.*, Int J Geriatr Psychiatry. **21** (2006), 519–528.

[SR07] C.J. Stam and J.C. Reijneveld, *Graph theoretical analysis of complex networks in the brain*, Nonlin. Biomed. Phys. (2007).

[SSC+05] R. Salvador, J. Suckling, M.R. Coleman, J.D. Pickard, D. Menon, and E. Bullmore, *Neurophysiological architecture of functional magnetic resonance images of human brain*, Cereb Cortex. **15** (2005), 1332–1342.

[STE00] O. Sporns, G. Tononi, and G.M. Edelmann, *Connectivity and complexity: the relationship between neuroanatomy and brain dynamics*, Neural Netw. (2000).

[Str01] S.H. Strogatz, *Exploring complex networks.*, Nature **410** (2001), 268–276.

[SZ04] O. Sporns and J.D. Zwi, *The small-world of the cerebral cortex*, Neuroinformatics **2** (2004), 145–162.

[TPR+06] A. Takashima, K.M. Petersson, F. Rutters, I. Tendolkar, O. Jenson, M.J. Zwarts, and et al., *Declarative memory consolidation in humans: A prospective functional magnetic resonance imaging study.*, Proceedings of the National Academy of Science of the United States of America **103(3)** (2006), 756–761.

[Tre11] M. Trepel, *Neuroanatomie: Struktur und funktion.*, Elsevier, 2011.

[TSE94] G. Tononi, O. Sporns, and G.M. Edelman, *A measure for brain complexity: Relating functional segregation and integration in the nervous system.*, Proc. Natl. Sci. USA **91** (1994), 5033–5037.

[TT08] J. Talairach and P. Tournoux, *Co-planar stereotaxic atlas of the human brain*, Thieme, Stuttgart, 2008.

[Tul72] E. Tulving, *Episodic and semantic memory.*, Academic Press, Inc., New York, 1972.

[US06] P.J. Uhlhaas and W. Singer, *Neural synchrony in brain disorders: relevance for cognitive dysfunctions and pathophysiology*, Neuron **52** (2006), 155–168.

[VCS02] S. Valverde, R. Ferrer Cancho, and R.V. Sole, *Scale-free networks from optimal design*, Europhys Lett **60** (2002), 512–517.

[Wag01] A. Wagner, *The yeast protein interaction network evolves rapidly and contains few redundant duplicate genes*, Mol. Biol. Evol. **18** (2001), 1283–1292.

[Wat99] D.J. Watts, *The dynamics of networks between order and randomness*, Princeton University Press, 1999.

[Wes96] D.B. West, *Introduction to graph theory*, Prentice Hall, Upper Saddle River, NJ, 1996.

[WF94] S. Wasserman and K. Faust, *Social network analysis: Methods and applications*, Cambridge University Press, Cambridge, 1994.

[WS98] D.J. Watts and S.H. Strogatz, *Collective dynamics of "small-world" networks*, Nature **393** (1998), 440–442.

[ZC05] A. Zomorodian and G. Carlsson, *Computing persistent homology*, Discrete and Computational Geometry **33** (2005), 247–274.

[ZMS85] S. Zola-Morgan and L.R. Squire, *Medial temporal lesions in monkeys impair memory on a variety of tasks sensitive to human amnesia.*, Behavioral Neuroscience **99(1)** (1985), 22–34.

[ZMSAS89] S. Zola-Morgan, L.R. Squire, D.G. Amaral, and W.A. Suzuki, *Lesions of perirhinal and parahippocampal cortex that spare the amygdala and hippocampal formation produce severe memory impairment.*, Journal of Neuroscience **9(12)** (1989), 4355–4370.

[ZMSCR93] S. Zola-Morgan, L.R. Squire, R.P. Clower, and N.L. Rempel, *Damage to the perirhinal cortex exacerbates memory impairment following lesions to the hippocampal formation.*, Journal of Neuroscience **13(1)** (1993), 251–265.

[ZZK06] L. Zemanova, Ch. Zhou, and J. Kurths, *Structural and functional clusters of complex brain networks*, Physica D **224** (2006), 202–212.